

**DETECTION OF TRACE AMOUNT OF NO₂ IN THE ATMOSPHERE USING
BLUE LASER DIODE**

BY

SAMEH M. A. ALTANANY

A Thesis Presented to the
DEANSHIP OF GRADUATE STUDIES

KING FAHD UNIVERSITY OF PETROLEUM & MINERALS

DHAHRAN, SAUDI ARABIA

In Partial Fulfillment of the
Requirements for the Degree of

MASTER OF SCIENCE

In

PHYSICS


MAY, 2017

KING FAHD UNIVERSITY OF PETROLEUM & MINERALS

DHAHRAN- 31261, SAUDI ARABIA

DEANSHIP OF GRADUATE STUDIES

This thesis, written by **SAMEH M. A. ALTANANY** under the direction of his thesis advisor and approved by his thesis committee, has been presented and accepted by the Dean of Graduate Studies, in partial fulfillment of the requirements for the degree of **MASTER IN PHYSICS**.



Dr. Abdulaziz M. Aljalal
(Advisor)



Dr. Abdullah A. Al-Sunaidi
Department Chairman



Dr. Mohammad A. Gondal
(Member)



Dr. Salam A. Zummo
Dean of Graduate Studies



Dr. Khaled Gasmri
(Member)

8/8/2017
Date

© SAMEH M. A. ALTANANY

2017

[Dedication]

I dedicate this research to the nation of “read”; the nation of Islam, to my mother land “Palestine”. I dedicate this research to the heroes of Palestine who stand against the Israeli persecution defending their simplest rights of having a decent life.

ACKNOWLEDGMENTS

First and above all, I praise Allah, the almighty, the merciful who guided me to the real path of knowledge.

I would like to express my deep thankfulness to my supervisor Dr. Abdulaziz M. Aljalal for his continuous guiding, collegiality and limitless support throughout my research work. I would like to extend my sincere thanks to the members of my thesis defense committee, Prof. Mohammad A. Gondal and Dr. Khaled Gasmi for their direction, dedication and invaluable advices.

My heartfelt thanks also go to my lovely parents, brothers and sisters for their prayers, endless sacrifices, supports, love and vast patience to make me reach this stage of qualification and success.

TABLE OF CONTENTS

ACKNOWLEDGMENTS	V
TABLE OF CONTENTS.....	VI
LIST OF TABLES.....	VIII
LIST OF FIGURES.....	IX
LIST OF ABBREVIATIONS.....	XII
ABSTRACT.....	XIII
ملخص الرسالة	XIV
CHAPTER 1 INTRODUCTION.....	15
CHAPTER 2 LITERATURE REVIEW	17
2.1 Formation of NO ₂ in the atmosphere.....	17
2.2 Optical techniques for NO ₂ detection in the atmosphere	19
2.2.1 Theoretical background	23
CHAPTER 3 EXPERIMENT	27
3.1 Measurement of the laser spectrum	27
3.1.1 The laser diode	28
3.1.2 The spectrometer	29
3.1.3 Data acquisition for measuring laser spectra	31
3.2 Measurement of NO ₂ transmittance.....	33
3.2.1 The setup for measuring NO ₂ transmittance	33
3.2.2 Data acquisition for measuring NO ₂ transmittance.....	36

CHAPTER 4 RESULTS AND CONCLUSION	39
4.1 Transmittance estimation by simulation	39
4.2 Effect of NO₂ adsorption on the transmittance	47
4.3 Results of the transmittance calculation.....	50
4.4 Detection Limit	57
CHAPTER 5 CONCLUSION.....	59
APPENDIX A LABVIEW BLOCK DIAGRAMS AND FRONT PANELS DEVELOPED FOR EXPERIMENTAL MEASUREMENTS.....	60
APPENDIX B MATHEMATICA CODES FOR DATA ANALYSIS	72
APPENDIX C FORMATS OF MEASUREMENT DATA FILES	82
REFERENCES.....	85
VITAE.....	88

LIST OF TABLES

Table 3.1 Spectral lines of krypton lamp and their pixel locations.	30
--	----

LIST OF FIGURES

Figure 2.1	Absorption Spectroscopy of monochromatic beam.	23
Figure 2.2	A Fabry-Perot blue diode laser spectrum. λ_{\min} and λ_{\max} are the minimum and maximum laser emission limits.	25
Figure 2.3	Incident and transmitted laser intensities.	26
Figure 3.1	A schematic diagram for measuring the laser spectrum.....	28
Figure 3.2	Relative intensity vs pixel locations on the CCD camera.	30
Figure 3.3	The calibration line we obtained.	31
Figure 3.4	LabVIEW front panel for measuring laser spectra.....	32
Figure 3.5	Schematic diagram of measuring the laser spectra; BDL, blue diode laser, BS, beam splitter, M, mirror, ND, neutral density filter; DAQ, data acquisition system, PD, photodiode detector, PC, personal computer.	34
Figure 3.6	Photo of the experimental setup.	35
Figure 3.7	LabVIEW Front Panel for controlling the flow rate of the gas and reading the flow rate and pressure.	35
Figure 3.8	LabVIEW Program Front Panel for measuring NO ₂ transmittance: Signal -to-noise ratio vs time.	35
Figure 3.9	LabVIEW Program Front Panel for measuring NO ₂ transmittance: Signal -to-noise ratio vs current.....	35
Figure 4.1	A plot of NO ₂ absorption cross section versus wavelength[9]. The shadowed rectangle marks the spectral area of interest.....	40
Figure 4.2	Laser spectra for the TOPTICA diode laser at T= 10°C and different currents from 30 mA up to 160 mA with a step current of 10 mA.	42
Figure 4.3	The effect of the temperature on the emission range of the TOPTICA laser.	43
Figure 4.4	The effect of the temperature on the emission range of the ROITHNER laser.....	44

Figure 4.5	The calculated NO ₂ transmittance versus the laser injection current at the diode temperature T= 20 °C for the TOPTICA laser.	45
Figure 4.6	The calculated NO ₂ transmittance versus the laser injection current at different diode temperatures for the TOPTICA laser.	46
Figure 4.7	The calculated NO ₂ transmittance versus the laser injection current at different diode temperatures for the ROITHNER laser.	46
Figure 4.8	Transmittance vs time for different flow rates: 50, 100, 200, 400, 600, and 800 ml/min.	49
Figure 4.9	Transmittance vs time for flow rates: 400, 600, and 800 ml/min.	50
Figure 4.10	Simulation vs experiment of the transmittance curve at T=10 °C for the TOPTICA laser. The curve with circles joined by straight lines is the simulation curve.	51
Figure 4.11	Simulation vs experiment of the transmittance curve at T=20 °C for the TOPTICA laser. The curve with circles joined by straight lines is the simulation curve.	52
Figure 4.12	Simulation vs experiment of the transmittance curve at T=30 °C for the TOPTICA laser. The curve with circles joined by straight lines is the simulation curve.	52
Figure 4.13	Simulation vs experiment of the transmittance curve at T=40 °C for the TOPTICA laser. The curve with circles joined by straight lines is the simulation curve.	53
Figure 4.14	Simulation vs experiment of the transmittance curve at T=50 °C for the TOPTICA laser. The curve with circles joined by straight lines is the simulation curve.	53
Figure 4.15	Simulation vs experiment of the transmittance curve at T=60 °C for the TOPTICA laser. The curve with circles joined by straight lines is the simulation curve.	54
Figure 4.16	Simulation vs experiment of the transmittance curve at T=10 °C for the ROITHNER laser. The curve with circles joined by straight lines is the simulation curve.	54

Figure 4.17	Simulation vs experiment of the transmittance curve at $T=20\text{ }^{\circ}\text{C}$ for the ROITHNER laser. The curve with circles joined by straight lines is the simulation curve.	55
Figure 4.18	Simulation vs experiment of the transmittance curve at $T=30\text{ }^{\circ}\text{C}$ for the ROITHNER laser. The curve with circles joined by straight lines is the simulation curve.	55
Figure 4.19	Simulation vs experiment of the transmittance curve at $T=40\text{ }^{\circ}\text{C}$ for the ROITHNER laser. The curve with circles joined by straight lines is the simulation curve.	56
Figure 4.20	Simulation vs experiment of the transmittance curve at $T=50\text{ }^{\circ}\text{C}$ for the ROITHNER laser. The curve with circles joined by straight lines is the simulation curve.	56
Figure 4.21	Simulation vs experiment of the transmittance curve at $T=60\text{ }^{\circ}\text{C}$ for the ROITHNER laser. The curve with circles joined by straight lines is the simulation curve.	57
Figure 4.22	Voltage ratio of the signal and reference detectors as a function of the laser injection current.	58

LIST OF ABBREVIATIONS

Limit Of Detection: LOD

Nitrogen Dioxide: NO₂

part per million: ppm

part per billion: ppb

part per trillion: ppt

Tunable Diode Laser Absorption Spectroscopy: TDLAS

|

ABSTRACT

Full Name : [SAMEH M. A. ALTANANY]

Thesis Title : [DETECTION OF TRACE AMOUNT OF NO₂ IN THE
ATMOSPHERE USING BLUE LASER DIODE]

Major Field : [Physics]

Date of Degree : [May, 2017]

|

A direct tunable diode laser absorption spectroscopy setup has been developed for detecting trace amounts of nitrogen dioxide (NO₂) at atmospheric pressure and room temperature. Two different Fabry-Perot blue diode lasers have been evaluated in the setup as light sources. One of the lasers is from TOPTICA Photonics Inc., model LD-0445-0050-1 and the other is from Roithner LaserTechnick GmbH, model LD-445-50PD. Both lasers do have multi-longitudinal modes with emission wavelengths at around 445 nm. The laser transmittances as a function of laser injection current at fixed temperatures have been simulated and experimentally measured with very good agreements. A detection limit of 4 ppm in a gas cell of length 40 cm has be attained for both lasers |

ملخص الرسالة

الاسم الكامل: سامح معين عاشور الطناني

عنوان الرسالة: كشف كميات ضئيلة من ثاني أكسيد النيتروجين في الهواء بواسطة ليزر الدايدود الأزرق

التخصص: فيزياء

تاريخ الدرجة العلمية: مايو, 2017

تم بناء تقنية تحليل الطيفي لامتصاص ليزر دايدود قابل للضبط بهدف الكشف عن كمية ضئيلة من ثاني أكسيد النيتروجين في الهواء تحت تأثير الضغط الجوي و درجة حرارة الغرفة. لقد تمت مقارنة ليزري Fabry-Perot أزرقين ناتجين من ديودين مختلفين كمصدرين ضوء في التقنية. أحد الليزين من انتاج: TOPTICA Photonics ,Inc, موديل: LD-0445-0050-1 , و الآخر من انتاج: Roithner LaserTechnick GmbH , موديل: LD-445-50PD. الليزران ذوا أنماط متعددة الطولية و لكل منهما أطوال انبعاث موجية تقارب 445 نانومتر. نفاذ الليزر كدالة في تيار الديود عند درجة حرارة ديود ثابتة تم تقديره بالمحاكاة من جهة و كذلك حسابه تجاريا من جهة أخرى مع ملاحظة توافقات جيدة جدا بين الحالتين. تم التوصل الى أقل حد ممكن من الكشف بمقدار يقارب 4 أجزاء من المليون من وحدة الحجم عبر اسطوانة غاز طولها 40 سم لكل من الليزين.

CHAPTER 1

INTRODUCTION

One of the major topics of concern is the pollution of the atmosphere by trace gases that result in changing the oxidizing capacity of the atmosphere and therefore harm the human health.

Nitrogen dioxide (NO_2), one of several oxides of nitrogen, is one of the major air pollutants [1]. At very high concentrations, NO_2 is an oxidizing, corrosive, reddish-brown gas with a characteristic pungent odor [2]. Trace amounts of NO_2 are known to be responsible for photochemical smog that takes place in the urban areas but also spread to more rural zones by transport of polluted air masses [3]. The concentration of NO_2 goes up to hundreds of parts in 10^9 by volume (ppbv) in high traffic urban areas, however, it may go down to below 100 parts in 10^{12} (pptv) in rural areas [4]. Many organizations across the world like the World Health Organization (WHO), the US Environmental Protection Agency (EPA), and the European Union (EU) have provided two air quality standards for safe exposure to NO_2 gas in the ambient air, one is for short-term exposure over one hour and the other is for long-term exposure over one year [5]. The hourly and annually allowed maximum concentrations given by both WHO and EU are about 100 ppb and 20 ppb, respectively, while an annual standard of about 50 ppb is given by EPA [5]. Exceeding these limits probably will cause several health problems such as reducing the immunity to lung infections and therefore causing wheezing, coughing, colds, and bronchitis.

Accordingly, monitoring the atmospheric NO₂ gas is always a subject of great interest. This can be achieved either by optical or chemical methods [6]. NO₂ shows a strong and broadband absorption in the spectral range (250-650 nm) with a absorption cross-section of about 6×10^{-19} cm²/molecule within the blue region [7]. Many optical techniques with light sources have been used to detect trace amounts of the atmospheric NO₂ with different detection limits. Recently, blue laser diodes became commercially available having advantages like their short wavelengths, long lifetimes and low power consumption and therefore are suitable for wide applications including the detection of trace amounts of the atmospheric NO₂ gas [8].

In the present study, a tunable blue diode laser absorption spectroscopy technique has been developed to detect trace amount of atmospheric NO₂ gas. Moreover, two blue laser diodes of emission wavelengths of about 450 nm from two different companies have been employed in the technique as light sources.

This thesis includes three more chapters: Chapter 2 (BACKGOURND) briefly reviews some common optical techniques that have been used to detect trace amount of NO₂ gas including techniques employing blue diode lasers. Also, it discusses the theoretical basis of our technique. Chapter 3 (EXPERIMENT) discusses the experimental setup, the operation procedure of the developed setup, and the software used for collecting and analyzing data. Chapter 4 (RESULTS AND CONCLUSIONS) presents simulation for NO₂ transmittance through the setup, NO₂ loss within the cell, measurements of NO₂ transmittance as a function of laser injection current, and the NO₂ detection limit of the setup.]

CHAPTER 2

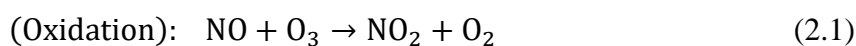
LITERATURE REVIEW

In this chapter, we briefly discuss the formation of NO₂ gas in the atmosphere, some typical optical techniques to measure trace amounts of NO₂ including those using blue diode lasers, and theoretical basis of the technique used in this thesis.

2.1 Formation of NO₂ in the atmosphere

NO₂ is produced naturally and anthropogenically (by human activities) [9]. Natural sources, like lightning, soil emissions, biomass burning and they, are responsible for about half of the total production of nitrogen oxides [10]. The human activities are responsible for the rest of NO₂ production and include mainly fossil fuel combustion in electrical utilities and operation of on-road and off-road vehicles [3][11]. The nitrogen oxides resulting from fossil fuel combustion mostly consists of nitric oxide (NO) which is converted into NO₂ by photochemical oxidization reaction.

In the atmosphere NO reacts with ozone and produce NO₂ through the dominant pathway [3][12]:



The formation of NO₂ can also be achieved through the oxidization of NO by hydroperoxyl radical HO₂ or peroxy radical RO₂ through the following reactions [2][13]:

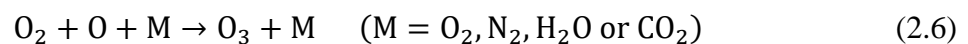
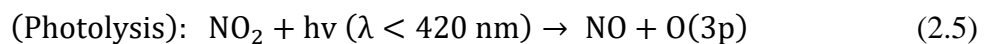


Moreover, NO₂ is formed through the following reaction of NO with O₂ [14]:



However, the rate of this reaction strongly depends on the NO concentration and under most tropospheric condition this reaction is insignificant [12]. This reaction is only significant when the NO concentration is higher than one ppm [2].

NO_x (NO + NO₂) contributes to the photochemical air pollution through photolysis of NO₂ to give NO, and O(3p) and therefore forming ozone through the following reactions [13] [15]:



In addition to the NO produced by combustion processes and other sources, the NO produced in this reaction will react through reaction [1] and hence a cyclic process is formed driven continuously by sunlight and ozone.

It is worth mentioning here that NO₂ is a precursor for nitric acid (HNO₃), which contributes substantially to acidic rains during the daytime through the reaction [16]:



while at night the following reactions take place [17]:



2.2 Optical techniques for NO₂ detection in the atmosphere

In the following various optical techniques used to detect trace amounts of NO₂ gas in the atmosphere are briefly discussed. These are based on Chemiluminescence (CL), Differential Optical Absorption Spectroscopy (DOAS), Differential Absorption Lidar (DIAL), Cavity Ring Down Spectroscopy (CRDS), and Cavity Enhanced Absorption Spectroscopy (CEAS),

Laser-induced-fluorescence (LIF), PhotoAcoustic Spectroscopy (PAS) and Tunable Diode Laser Absorption Spectroscopy (TDLAS).

Chemiluminescence (CL) is an indirect and standard method for measurement of the ambient NO_2 . This technique is based on the usage of a catalytic converters, which includes conversion of NO_2 into NO using a heated molybdenum catalyst. And then, the CL reaction of NO in excess O_3 takes place and being detected. In this method the concentration of NO_2 gas can be measured by subtraction of the NO signal observed before exposing the sample air to the hot catalyst. By using techniques based on chemiluminescence for NO_2 detection, a sensitivity of 1ppbv has been reached [8].

Differential optical absorption spectroscopy (DOAS) technique has been used for detecting NO_2 at ppb or even ppt levels [18]. DOAS techniques are classified into two types, namely, active and passive DOAS. Active DOAS are those in which lamp lights are used whereas passive DOAS rely on the solar light. The principle of DOAS is well described by the Lambert-Beer's Law that relates the absorption of the incoming light with specific wavelength to the concentration of species within a path length. The DOAS method is mainly based on the idea of mathematically separating the absorption cross section into two parts: one varies slowly while the other varies rapidly with the wavelength. The part that varies rapidly is responsible for molecular absorption, and the one that varies slowly is responsible for broadband absorption such as that caused by Rayleigh scattering [19].

Differential Absorption Lidar (DIAL) has been employed for remote measurements over path lengths of more than 2000 m and a precision of ± 5 ppbv of NO₂ [20]. The base of this technique is to find the difference in absorption cross section of NO₂ gas at two or more adjacent wavelengths.

Cavity Ring Down Spectroscopy (CRDS) detects NO₂ within an optical cavity with low loss and high reflectivity ($\sim 100\%$) concave mirrors [21]. A radiation is injected into the cavity through one of the mirrors. Hence, multiple reflections occur inside the cavity and lead to radiation leakage from the cavity recorded by an appropriate photodetector. NO₂ has been detected in the atmosphere using blue diode laser based CRDS at 404 nm with limit of detection (LOD) of 22 pptv [22].

A variant of the CRDS technique is the Cavity Enhanced Absorption Spectroscopy (CEAS) in which the cavity is injected with a light pulse at a very small angle with respect to the cavity axes which forms a dense structure of weak optical axial modes that makes the whole system durable against instability in the laser spectrum and the cavity [21]. A sensitivity of sub-parts-per-billion of nitrogen dioxide has been reached by CEAS sensors [4]. Using CEAS, a blue-violet lasers (395-440 nm) have been used to detect NO₂ with 1ppbv sensitivity [23]. Furthermore, Optical Feedback Cavity Enhanced Absorption Spectroscopy (OF-CEAS) technique has been employed to detect NO₂ using extended cavity blue diode laser (411 nm) in the ambient air with detection limits with minimum LOD of 200 pptv [4].

Laser-induced-fluorescence (LIF) uses high power lasers and compact diode lasers for detecting NO_2 [24]. When a light of short wavelength is absorbed by a molecule, it undergoes vibrational and electronic transitions at high energy levels, and then emits light of longer wavelengths as it returns to lower energy levels. A very low detection limit from ppbv to sub pptv mixing ratios have been attained.

Photoacoustic (PAS) spectroscopy technique has been used to determine NO_2 concentration to part per trillion level [25]. When laser pulses are absorbed by a gas sample, heat pulses are generated within a cell containing the sample. These heat pulses create pressure pulses in the cell which can be detected by a microphone or ultrasonic detector. The signal is amplified by matching the modulation frequency with one of the acoustic resonances of the gas cell. A high power blue laser diode (444 nm) has been used in PA technique to detect NO_2 in N_2 at atmospheric pressure with LOD of 200 pptv [26].

Tunable Diode Laser Absorption Spectroscopy (TDLAS) technique is one of the leading techniques for the atmospheric detection of trace gases with concentrations down to ppb levels [27]. The sensitivity of TDLAS is increased by using modulation techniques such as frequency modulation and wavelength modulation techniques. A detection limit of 5 ppbv of NO_2 was obtained using TDLAS technique in lasers in the visible range [28]. Moreover, an in situ TDLAS detection at the level 400-700 pptv has been achieved using tunable infrared diode laser [29]. NO_2 has also been detected by external modulation and correlation detection based technique using a blue diode laser centered at 445 nm with a sensitivity of 5 ppmv [30].

2.2.1 Theoretical background

The fundamental principle for absorption spectroscopy is based on Lambert-Beer's law [31][32], which relates the intensities of an incident and transmitted light beams through a sample. According to Lambert-Beer's law, when an incident light beam of wavelength λ and intensity $I_0(\lambda)$ passes through an absorbing gas sample of length l and number density c , as shown in Figure 2.1, the intensity of the transmitted light beam $I_T(\lambda)$ is given by

$$I_T(\lambda) = I_0(\lambda)e^{-cl\sigma(\lambda)} \quad (2.11)$$

Here, $\sigma(\lambda)$ is the molecular absorption cross section of the gas molecules as a function of wavelength.

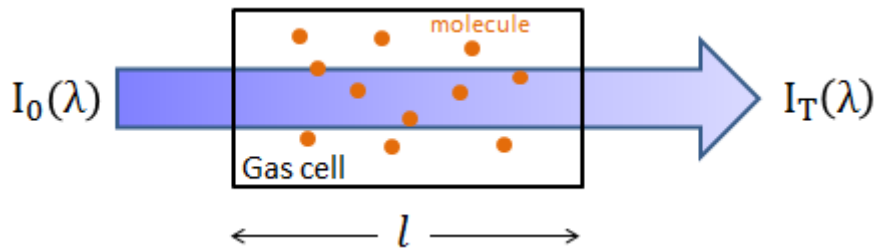


Figure 2.1 Absorption Spectroscopy of monochromatic beam.

The gas absorbance $a(\lambda)$ as a function of wavelength is a unitless quantity and is defined by

$$a(\lambda) \equiv -\ln\left(\frac{I_T(\lambda)}{I_0(\lambda)}\right) = cl\sigma(\lambda) \quad (2.12)$$

For small absorbance, $a \ll 1$, Lambert-Beer's law can be approximated by

$$I_T(\lambda) \approx I_0(\lambda)(1 - cl\sigma(\lambda)) \quad (2.13)$$

Or the absorbed intensity $I_{abs}(\lambda)$ is

$$I_{abs}(\lambda) \equiv I_0(\lambda) - I_T(\lambda) \approx I_0(\lambda) cl\sigma(\lambda) \quad (2.14)$$

In our experiment, we use a Fabry-Perot blue diode laser which has many longitudinal modes. An example of a measured spectrum of our lasers is shown in Figure 2.2. The spectrum of the laser can be tuned either by changing the laser injection current or by changing the laser temperature. Since tuning the laser with temperature is a relatively slow process, in our transmission measurements, the laser temperature is fixed while the laser current is tuned. The laser intensity is measured directly by a photo-diode and hence the

voltage measured by the photo-diode V is proportional to the integrated spectrum of the laser over its wavelength range, λ_{min} to λ_{max} ,

$$V \propto \int_{\lambda_{min}}^{\lambda_{max}} I(\lambda) d\lambda. \quad (2.15)$$

In the above equation, it is assumed that the response of the photodiode is constant over the laser emission wavelength range. This is a good assumption since the laser emission range of few nanometers is much smaller than the smooth response curve of the photodiode.

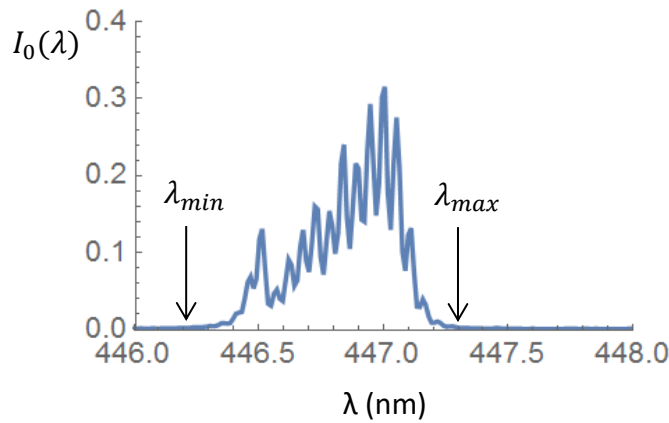


Figure 2.2 A Fabry-Perot blue diode laser spectrum. λ_{min} and λ_{max} are the minimum and maximum laser emission limits.

As shown in Figure 2.3, the intensity of the incident laser beam is proportional to

$$\int_{\lambda_{min}}^{\lambda_{max}} I_0(\lambda) d\lambda$$

and the intensity of the transmitted beam is proportional to $\int_{\lambda_{min}}^{\lambda_{max}} I_T(\lambda) d\lambda$.

Hence, the transmission curve of the diode laser $T(i)$ as a function of the laser injection current i at a fixed temperature can be calculated using

$$T(i) \equiv \frac{V_{sig}}{V_{ref}} = \frac{\int_{\lambda_{min}}^{\lambda_{max}} I_T(\lambda) d\lambda}{\int_{\lambda_{min}}^{\lambda_{max}} I_0(\lambda) d\lambda} = \frac{\int_{\lambda_{min}}^{\lambda_{max}} I_0(\lambda) e^{-cI\sigma(\lambda)} d\lambda}{\int_{\lambda_{min}}^{\lambda_{max}} I_0(\lambda) d\lambda} \quad (2.16)$$

Where V_{sig} , and V_{ref} are the voltages of the signal and reference photo-diode detectors.

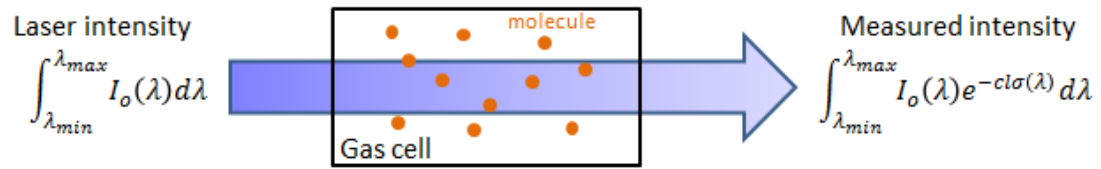


Figure 2.3 Incident and transmitted laser intensities.

CHAPTER 3

EXPERIMENT

Our experiment has two main objectives: one is to measure the laser spectrum at different temperatures and injection currents, and the other objective is to measure the transmittance of the NO₂ gas as a function of the injection current at specific diode temperature. These two objectives will be discussed in the following two sections.

3.1 Measurement of the laser spectrum

The laser spectra will be used to calculate the expected transmittance of an NO₂ sample as a function of laser injection current at specific laser temperature. Figure 3.1 shows a schematic diagram for the setup of measuring the laser spectra. It includes a blue laser diode with a temperature and current controllers, a data acquisition card (DAQ), a neutral density filter to control laser intensity, a spectrometer consisting of a monochromator and a line CCD camera, and a pc. In the following subsections, the laser diode, the spectrometer, and the data acquisition will be discussed.

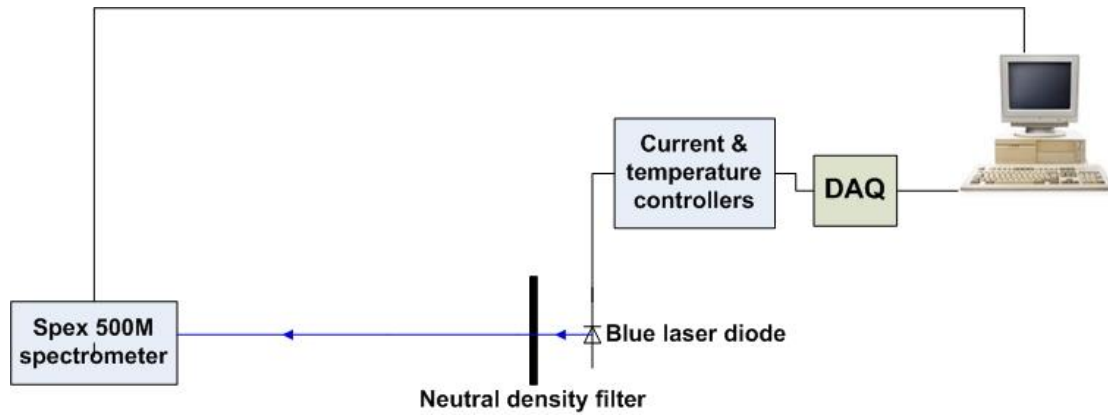


Figure 3.1 A schematic diagram for measuring the laser spectrum.

3.1.1 The laser diode

We study the spectra of two different blue laser diodes. One is from TOPTICA Photonics Inc., model LD-0445-0050-1 and the other is from Roithner LaserTechnick GmbH, model LD-445-50PD. From here on, we will refer to them as TOPTICA laser diode and Roithner laser diode, respectively. The laser diode is hosted in Thorlabs TCLDM9-TE- cooled mount and it is collimated by aspherical lens, Thorlabs C230TMD-A. Both laser emit around 450 nm. They have a threshold current of about 30 mA and a maximum allowable injection current of 160 mA. They can be operated within a temperature range from -10°C to 60°C . The laser diode temperature is controlled by a temperature controller, Thorlabs, model TED200C and the laser injection current is controlled by a current controller, Thorlabs, model LDC205C, 500 Ma. The temperature and current setting of the controllers can be either changed manually or through the data acquisition card.

3.1.2 The spectrometer

The spectrometer used to record the laser spectra consists of a SPEX 500M monochromator and line camera, Thorlabs, model LC1-USB. The SPEX 500M monochromator has a resolution of 0.02 nm and a linear dispersion of 1.6 nm/mm. The line CCD camera has 3000 pixels, each pixel has a width of 7 μm and length of 120 μm . The total width of the line camera is therefore $3000 \times 7 \mu\text{m} = 21 \text{ mm}$, which corresponds to $21 \text{ mm} \times 1.6 \text{ nm/mm} = 33.6 \text{ nm}$. On pixel corresponds to $7 \mu\text{m} \times 1.6 \text{ nm/mm} = 0.011 \text{ nm}$, which is smaller than the resolution of the monochromator.

The spectrometer is calibrated using a krypton discharge lamp, Cenco Instruments Corporation, Catalog No. 87262-3. A convex lens is used to image the lamp onto the entrance of the spectrometer. The slit width of the spectrometer is adjusted to be 6 μm .

Figure 3.2 shows the measured relative intensity of Kr spectral lines as a function of line CCD camera pixels. The Figure also shows the wavelength of each spectral line. The wavelengths are obtained from [34]. Table 3.1 shows the wavelength of spectral lines of the krypton lamp against their pixel locations.

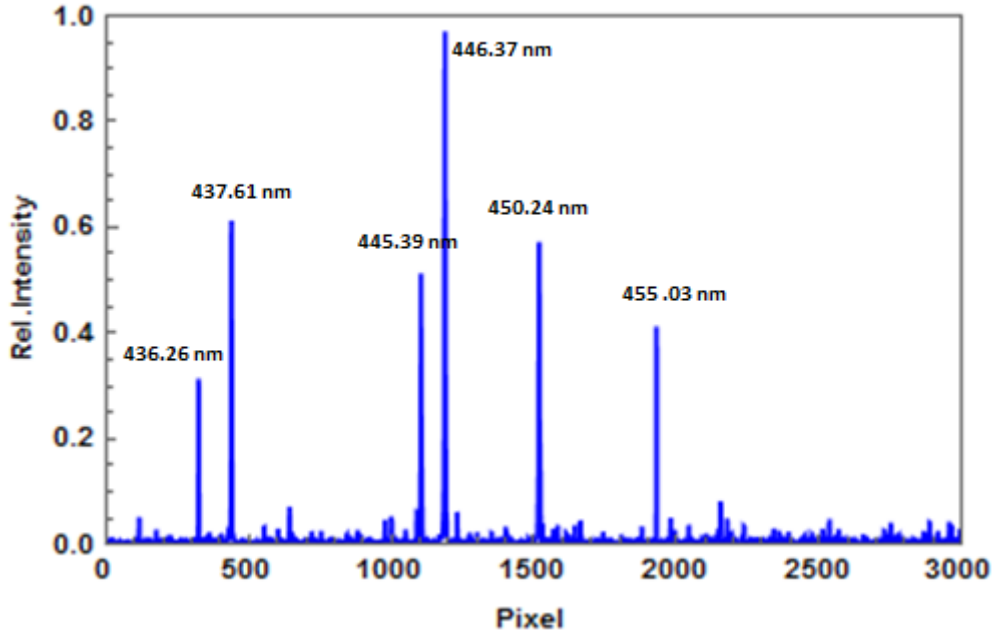


Figure 3.2 Relative intensity vs pixel locations on the CCD camera.

Table 3.1 Spectral lines of krypton lamp and their pixel locations.

λ (nm)	Pixel
436.26	324
437.61	439
440	642
442.52	858
445.39	1103.5
446.37	1187
450.24	1518

Figure 3.3 shows a plot of the wavelength of spectral lines of krypton lamp versus their pixel locations on the CCD camera. An excellent linear fitting is obtained for the calibration line.

The wavelength λ is related to the pixel location p as follows

$$\lambda(\text{nm}) = 432.473 + 0.011706 p$$

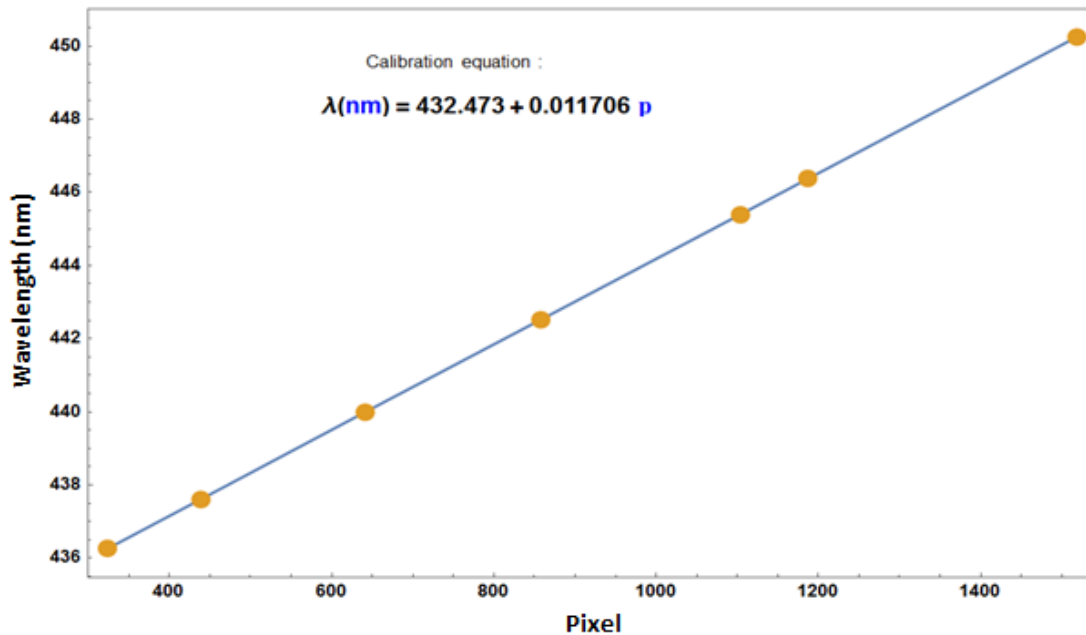


Figure 3.3 The calibration line we obtained.

3.1.3 Data acquisition for measuring laser spectra

A LabVIEW virtual instrument has been developed to record the laser spectra as a function of laser diode temperature and current.

Figure 3.4 shows the front panel of the LabVIEW virtual instrument for measuring the laser spectra. The panel contains a plot of the measured spectrum (intensity versus pixel) of the CCD camera. This spectrum is a result of averaging many identical spectra. The panel also contains input boxes to enter the exposure time and number of accumulations. The exposure time is the time over which the CCD camera measure one spectrum and the number of accumulations is the number of spectra used to obtain the average spectrum shown in the panel. The switch “save to file” gives an option to save the average spectrum to the computer in a form of a text file that contains the average intensity for each pixel. The comment input textbox is used to enter comments that are saved before the data in the text file. The “LC1

array” is an array to display the average intensity values of each pixel. The “LC1 handle” is the USB address of the CCD camera in the computer.

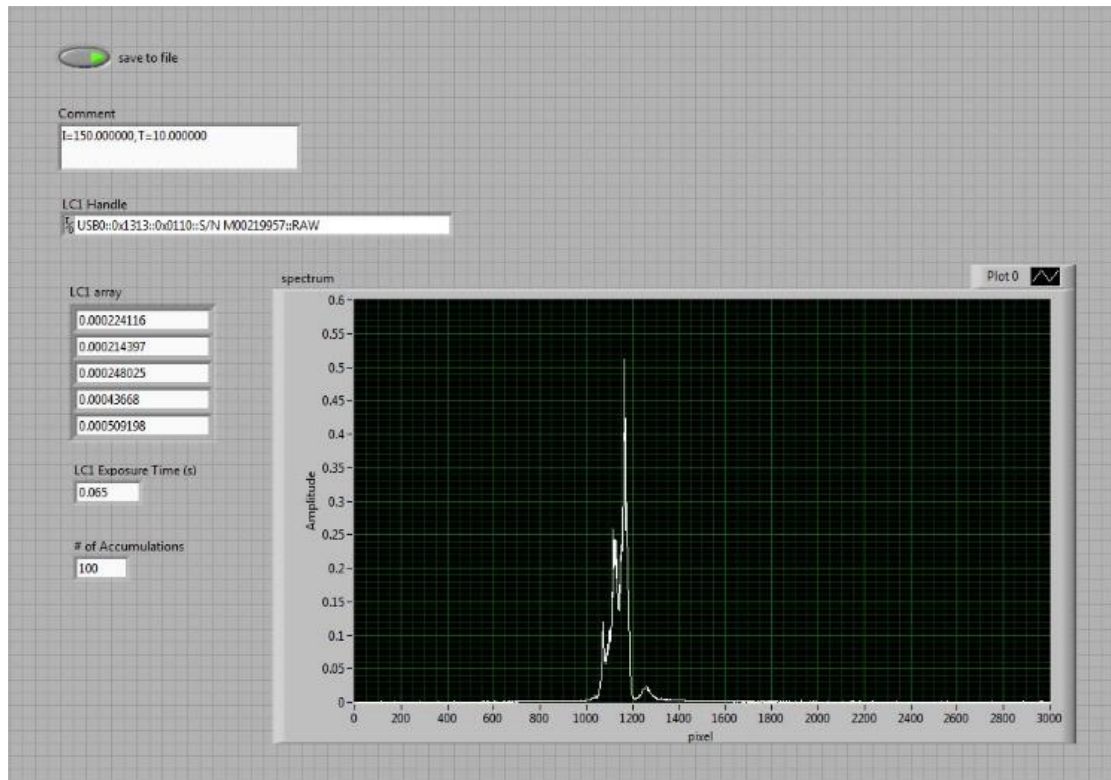


Figure 3.4 LabVIEW front panel for measuring laser spectra.

The LabVIEW block diagrams associated with the front panel of Figure 3.4 are presented in Appendix A.

3.2 Measurement of NO₂ transmittance

In this section, we discuss the setup developed to measure NO₂ transmittance and the minimum detectable limit. Figure 3.5 shows a schematic diagram of the setup.

3.2.1 The setup for measuring NO₂ transmittance

The blue laser diode **BLD** emits a beam which is split by a 50-50 beam splitter **BS** into two beams. One is called the reference beam, which is forwarded by a mirror **M** to one of the photodiode detectors **PD** in the Thorlabs balanced photodetector, model PDB210A/M. The second beam is called the signal beam, which travels through the absorption cell to the other photodiode detector in PDB210A/M. Neutral density filters **ND** made from white printing paper are used to reduce the intensity of the laser beams to prevent detector saturation.

The absorption cell is made from stainless steel and has two BK7 glass windows. It has a length of 40 cm and a diameter of 2.54 cm. The windows are tilted by an angle of about 45° to minimize interference between the incident beam and the reflected beams from the surfaces of the windows. The cell has a gas inlet and outlet. A pressurized pure N₂ gas cylinder or pressurized 200 ppm NO₂/N₂ gas mixture cylinder is used to supply gas to the cell with a flow rate regulated by a mass flow controller, Omega FMASS14ST. The maximum flow rate of the mass flow controller is 1000 mL/min. The labVIEW front panel for controlling the flow rate of NO₂ gas inside the cell is shown in Figure 3.7. The flow textbox is for controlling the flow rate while the data array is to read the pressure and the flow rate. The associated block diagram is presented in Appendix A. The pressure

in the cell is adjusted to atmospheric pressure by a needle valve and a vacuum pump and the pressure is measured by an absolute capacitance manometer, MKS 690A. The DAQ card is used to adjusted the flow rate of the mass flow controller and read the pressure of the pressure gauge.

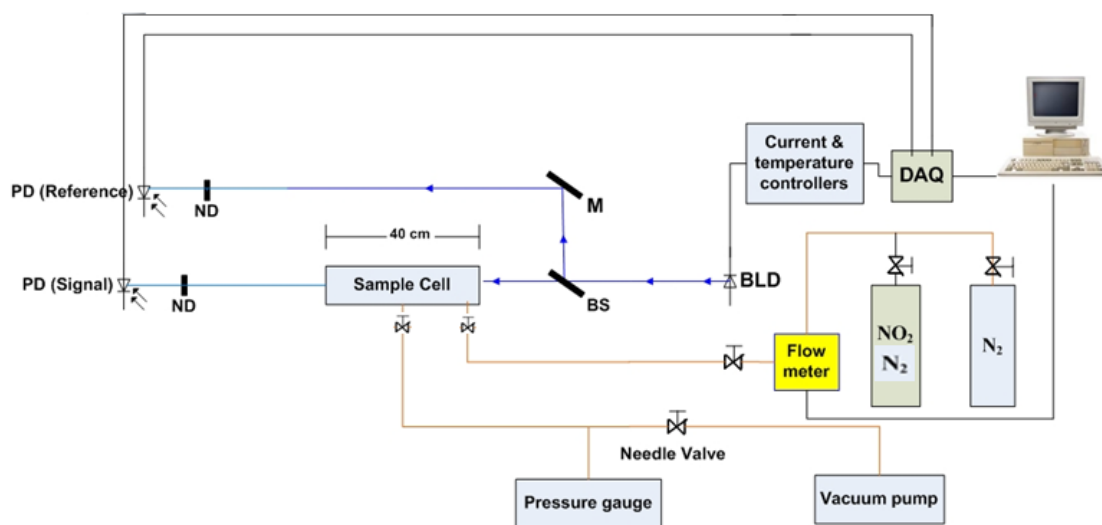


Figure 3.5 Schematic diagram of measuring the laser spectra; BDL, blue diode laser, BS, beam splitter, M, mirror, ND, neutral density filter; DAQ, data acquisition system, PD, photodiode detector, PC, personal computer.

Figure 3.6 shows a photo of the experimental setup developed for measuring the NO_2 transmittance.

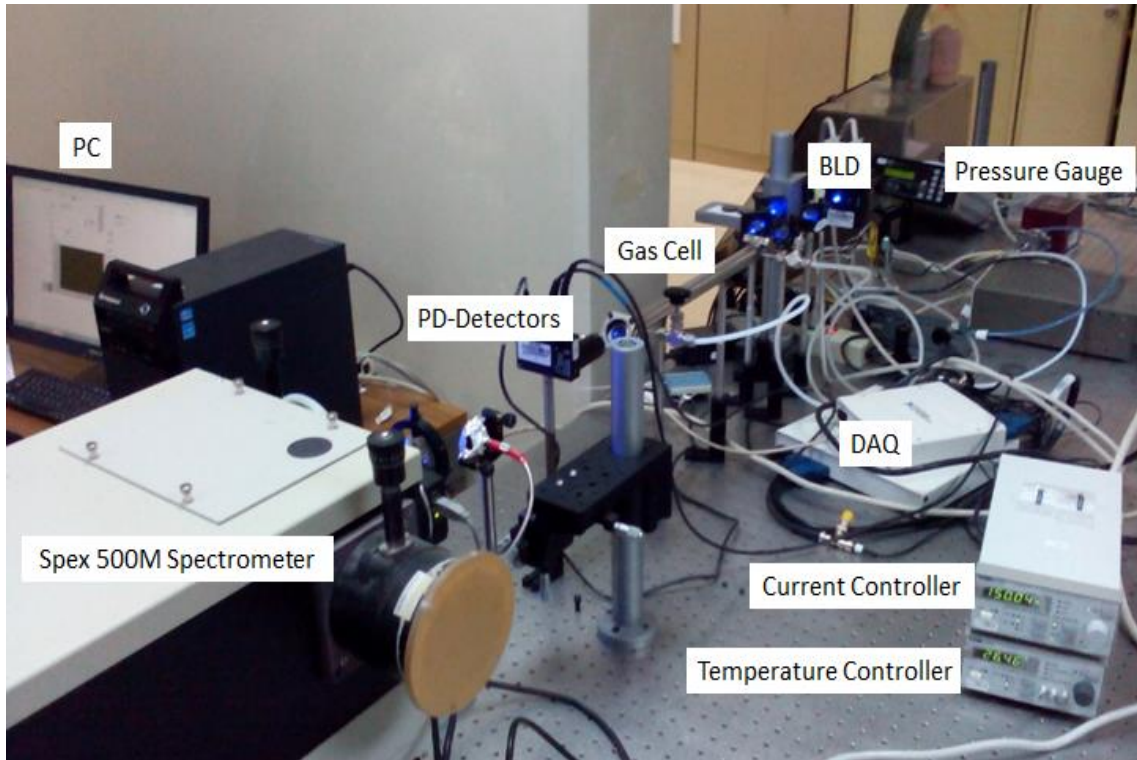


Figure 3.6 Photo of the experimental setup.

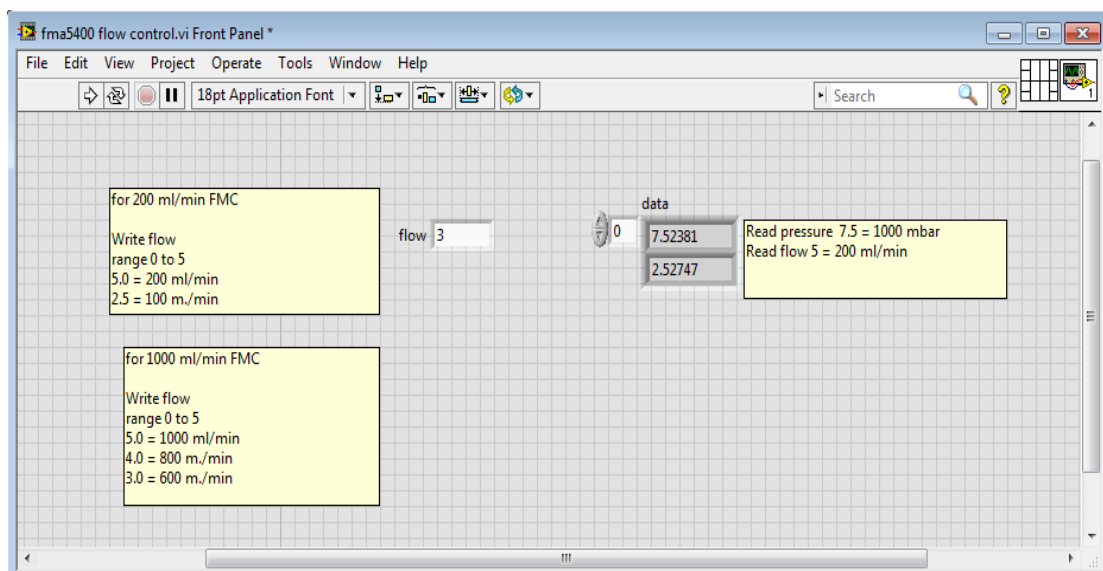


Figure 3.7 LabVIEW Front Panel for controlling the flow rate of the gas and reading the flow rate and pressure.

3.2.2 Data acquisition for measuring NO₂ transmittance

A LabVIEW virtual instrument has been developed to control and acquire data for the measurement of NO₂ transmittance.

Figures 3.8 and 3.9 show the labVIEW front panel of the virtual instrument for measuring the NO₂ transmittance. Transmittance measurement can be displayed either as a function of laser current or as a function of time using the “I or t” toggle switch shown on the bottom right side the plot. The plot contains three curves: the white curve is for the signal intensity, the red curve is for the reference intensity, and the green curve is for the signal-to-reference intensity ratio. The panel contains input boxes to enter the laser temperature, the minimum current, the maximum current and the step current of the laser. The current is stepped continuously between the minimum and the maximum limits. The panel also contains input boxes to enter the sampling rate and the number of samples. The sampling rate is the rate at which DAQ card reads the analog signal and converts it into digital form. The number of samples is the number over which each data point in the plot is averaged. The collected data can be saved to a data file by turning on the “write to file?” switch. The name of the file can be specified in the “file name to write” textbox and its directory path can be specified in the “directory” textbox. The “comments” input textbox is used to enter comments that are saved before the data in the text file. The current, the time, and the signal-to-reference ratio for the last data point are shown in the “I”, “time(s)”, “x/y” textboxes, respectively. The “stop” button is used to stop the data collection and turn off the experiment.

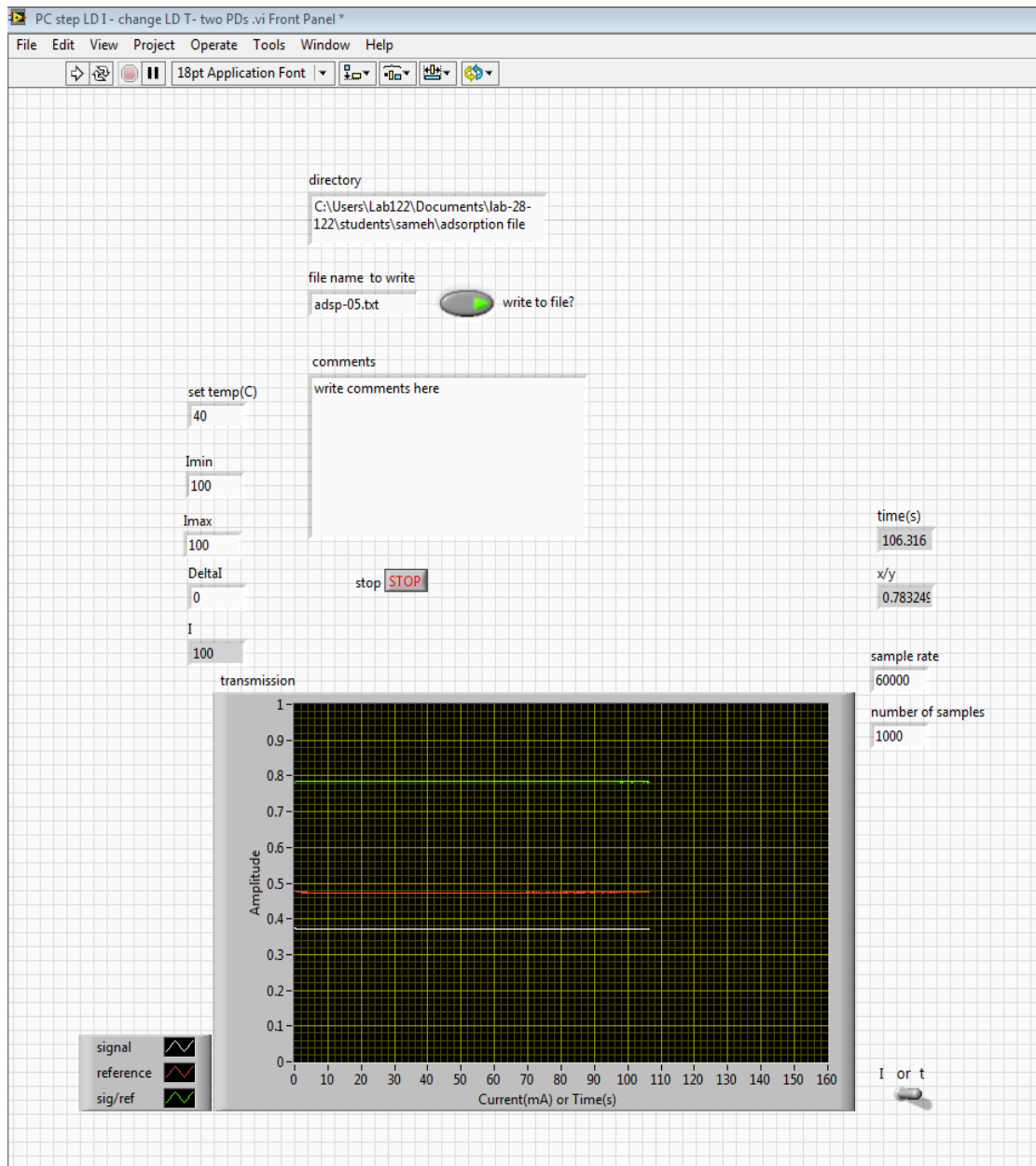


Figure 3.8 LabVIEW Program Front Panel for measuring NO₂ transmittance: Signal-to-noise ratio vs time.

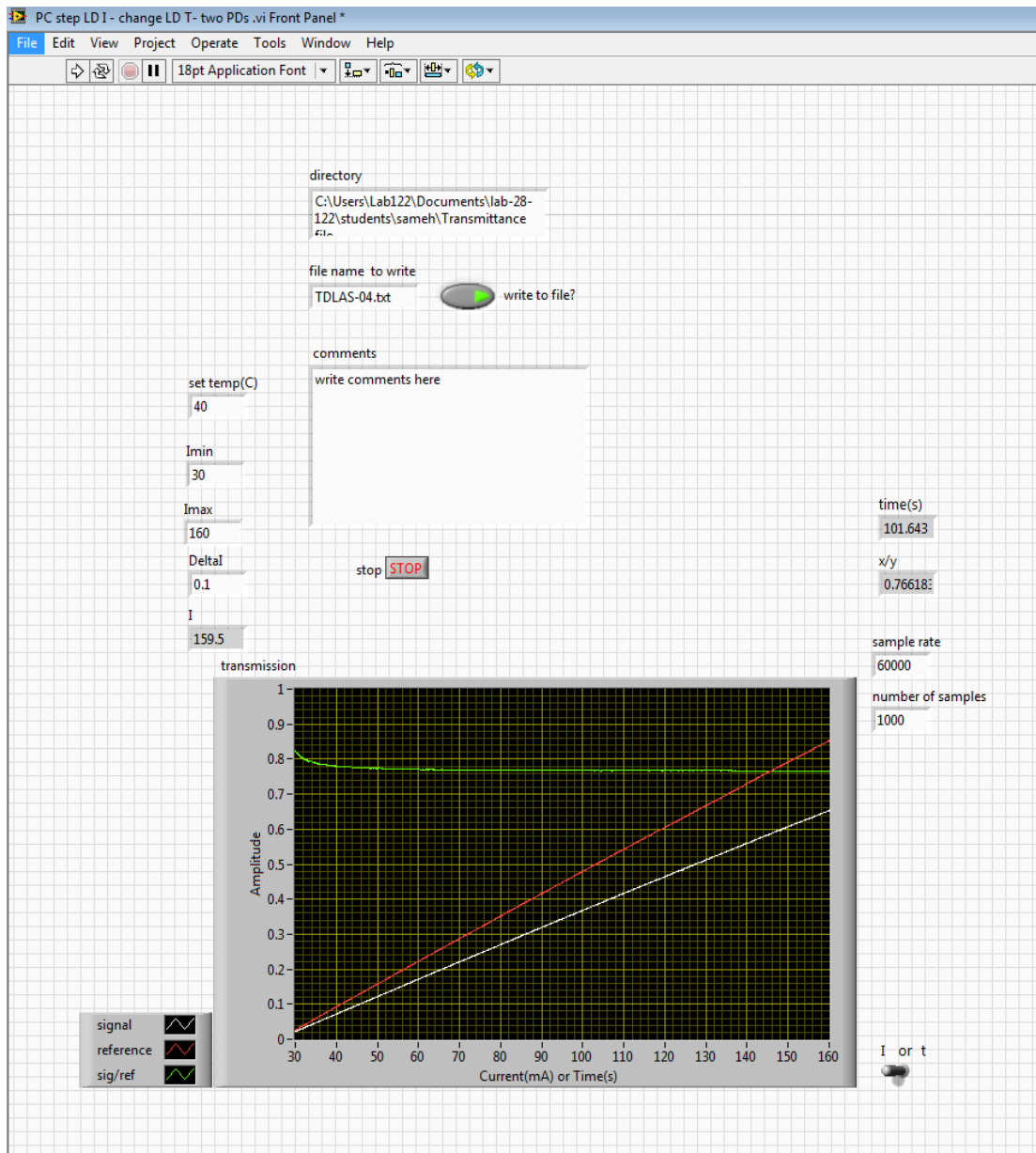


Figure 3.9 LabVIEW Program Front Panel for measuring NO₂ transmittance: Signal-to-noise ratio vs current.

The block diagrams associated with the front panels of Figures 3.8 and 3.9 are presented in Appendix A.

CHAPTER 4

RESULTS AND CONCLUSION

This chapter is comprised of four sections. In section 4.1, the simulation of the NO₂ gas transmittance as a function of the laser injection current is discussed. Section 4.2 discusses the effect of the NO₂ adsorption onto the cell walls upon the transmittance. In section 4.3, the experimental results for the NO₂ transmittance as a function of the laser injection current are shown and discussed. In section 4.4, the limit of detection of the developed setup for detecting trace amount of the atmospheric NO₂ gas is obtained.

4.1 Transmittance estimation by simulation

In this section, the results of a computer simulation of the blue diode laser transmittance through NO₂ gas under atmospheric pressure and room temperature conditions are presented. As discussed in chapter 2, the laser transmittance $T(I)$ as a function of the injection current I at certain laser diode temperature can be calculated from equation 2.15:

$$T(I) = \frac{\int_{\lambda_{\min}}^{\lambda_{\max}} I_T(\lambda) d\lambda}{\int_{\lambda_{\min}}^{\lambda_{\max}} I_o(\lambda) d\lambda} = \frac{\int_{\lambda_{\min}}^{\lambda_{\max}} I_o(\lambda) e^{-\sigma(\lambda)cl} d\lambda}{\int_{\lambda_{\min}}^{\lambda_{\max}} I_o(\lambda) d\lambda} \quad (2.15)$$

where $I_T(\lambda)$ is the intensity of the signal as a function of wavelength λ transmitted through an open path or a filled cell containing an absorber, $I_o(\lambda)$ is the intensity of the transmitted

signal with no absorber present, c is the concentration of the trace gas in molecules per unit volume, l is the path length of the cell, and σ is the NO_2 absorption cross section as a function of wavelength.

To use equation 2.15 to simulate the transmittance of NO_2 through our cell that has a length of $l = 40 \text{ cm}$, the absorption cross sections of NO_2 molecule $\sigma(\lambda)$ and the laser spectra $I_0(\lambda)$ are needed. For our measurements, the absorption cross section of the NO_2 molecule as a function of wavelength is obtained from ref.[33] and a plot of which shown in Figure 4.1. The rectangle indicates the part of the cross section that is used in our experiment.

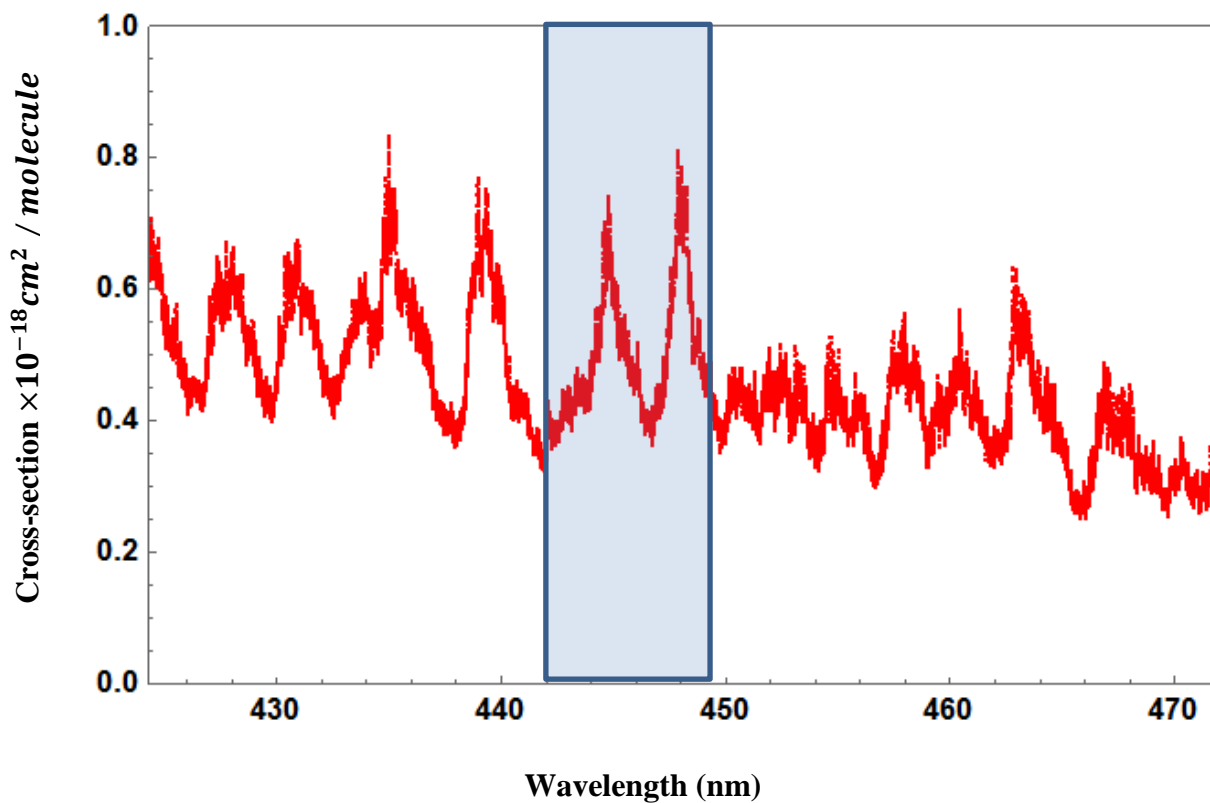
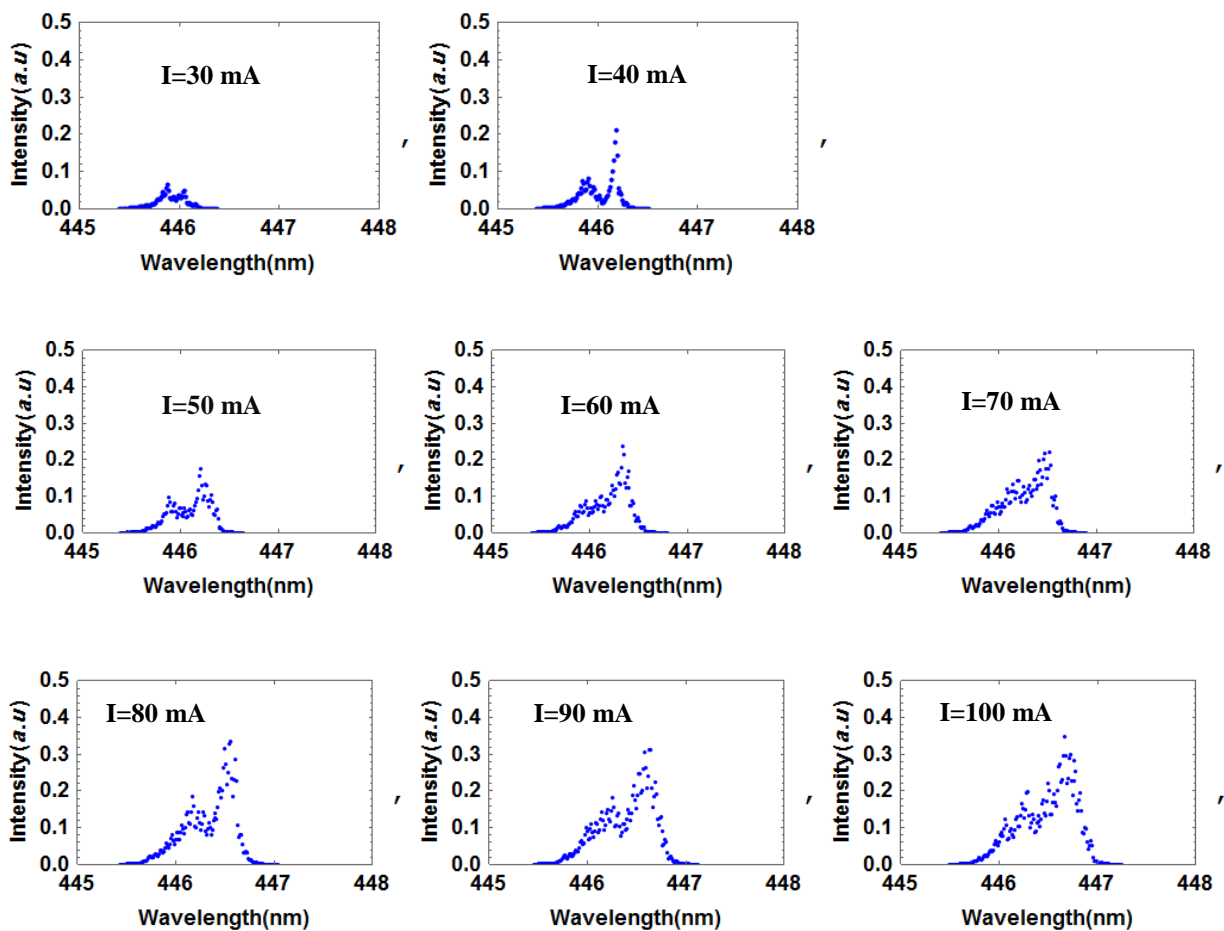


Figure 4.1 A plot of NO_2 absorption cross section versus wavelength[9]. The shadowed rectangle marks the spectral area of interest.

We measure the laser spectra $I_o(\lambda)$ using SPEX 500M monochromator for the two lasers at difference laser temperature and injection currents. Figure 4.2 shows some of the spectra for the TOPTICA laser at $T= 10^\circ\text{C}$ with different injection currents within the range between 30 and 160 mA with a step current of 10 mA. As evident from the measured spectra, the laser spectra change and shift clearly to higher wavelength ranges as the current increases. The laser threshold occurs at 30 mA with a laser emission at around 446 nm. The spectrum emission wavelength range starts at roughly 0.5 nm around threshold and increases with current up to a range of 2 nm at 160 mA. Each spectrum consists of many longitudinal modes, up to 20 modes, which are not well-resolved because of limited resolution of the monochromator.



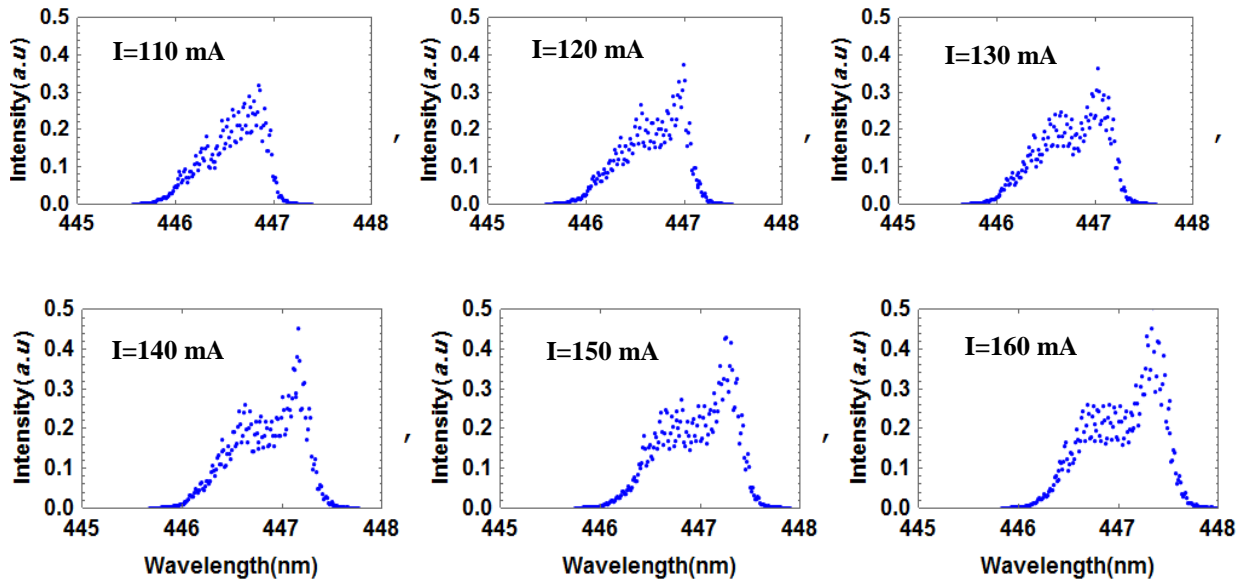


Figure 4.2 Laser spectra for the TOPTICA diode laser at $T = 10^{\circ}\text{C}$ and different currents from 30 mA up to 160 mA with a step current of 10 mA.

For the spectra shown in Figure 4.2 for which $T = 10^{\circ}\text{C}$, the laser emission covers the range from 445.4 to 448 nm as the injection current changes from 30 mA to 160 mA. The start of this range, 445.4 nm, is the start of the spectrum at 30 mA while the end, 448 nm, is the end of the spectrum at 160 mA. This range is displayed as a line in the bottom of Figure 4.3. The other lines represent the emission ranges for other temperatures for the TOPTICA diode laser. The width of the emission ranges at different temperatures are roughly the same, about 2.5 nm, but the ranges shift by about 0.5 nm for a step temperature of 10°C . Moreover, the NO_2 absorption cross section is displayed in the same figure. It can be noted that the emission ranges are wide enough to cover one of the largest pronounced features of the cross section. Hence, it is expected to observe big variations in transmittance as the laser is scanned through one of the emission ranges by scanning its injection current while fixing its temperature.

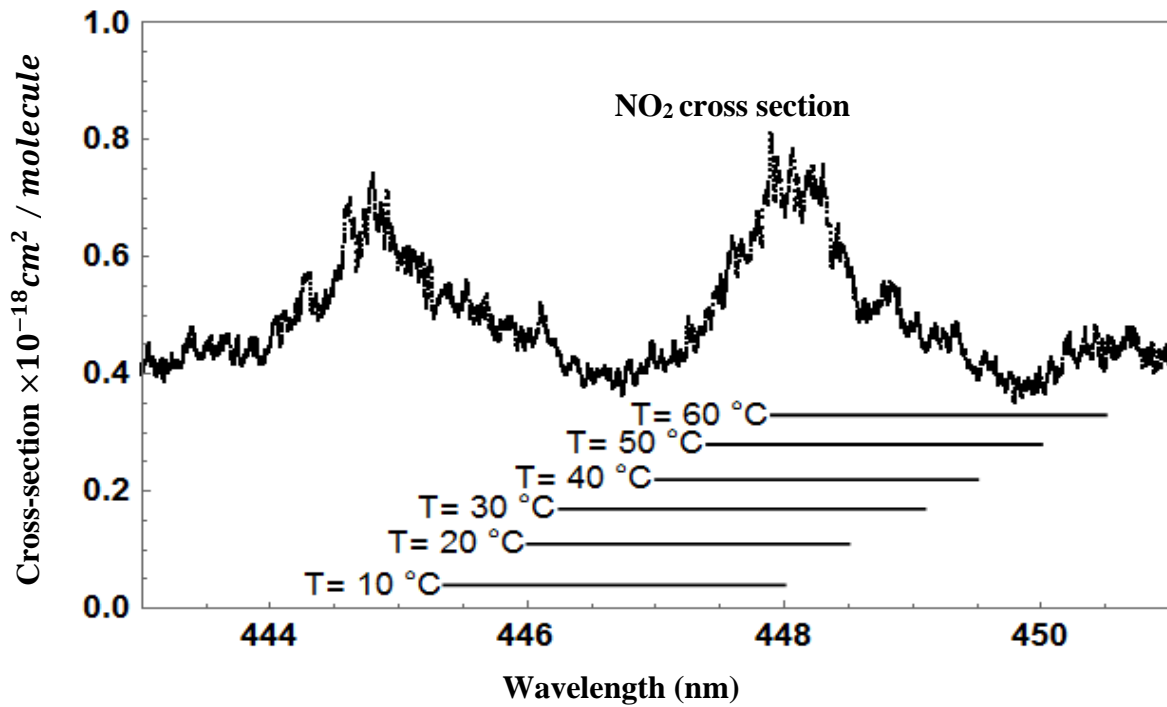


Figure 4.3 The effect of the temperature on the emission range of the TOPTICA laser.

Figure 4.4 is similar to Figure 4.3 and illustrates the effect of varying the ROITHNER diode temperature on its emission wavelength range as a function of the injection current. Here the width of the emission ranges at different temperatures are roughly the same, about 3 nm which is wider than 2.5 nm of the TOPTICA laser. The shift in the emission range per each 10°C is roughly the same for both lasers. However, the emission range of the ROITHNER laser at specific temperature is shifted by 2 nm below that of the TOPICA laser.

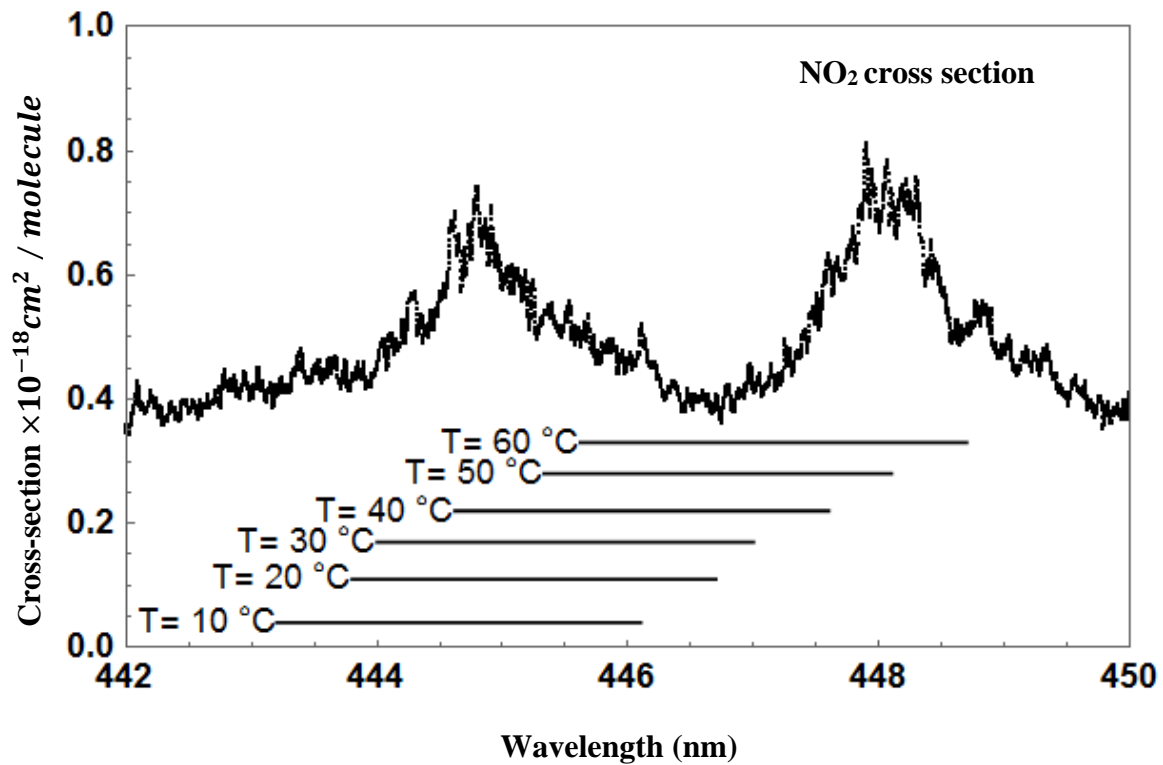


Figure 4.4 The effect of the temperature on the emission range of the ROITHNER laser.

Figure (4.5) shows the calculated NO₂ transmittance at the diode temperature T= 20 °C with different injection currents ranging from 30 -160 mA in steps of 10 mA. As indicated by Eq. 2.15, each dot in the figure results from the integration of the spectra similar to those shown in Figure 4.2 with the cross section shown in Figure 4.1.

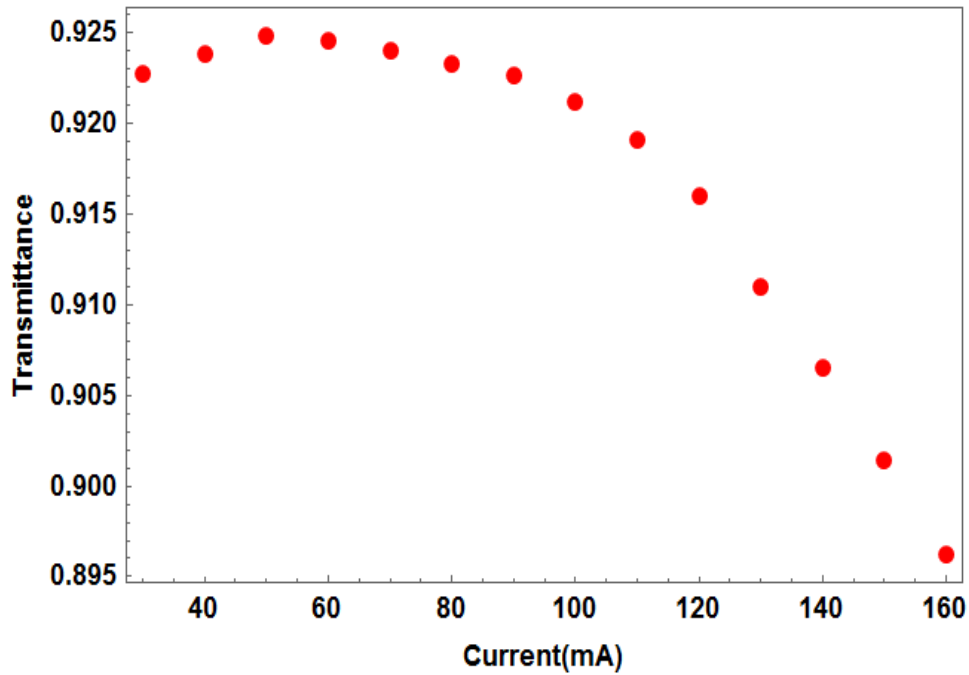


Figure 4.5 The calculated NO₂ transmittance versus the laser injection current at the diode temperature T= 20 °C for the TOPTICA laser.

Likewise, we can perform the transmittance calculation at any other laser diode temperature. Figures (4.6) and (4.7) exhibit the laser transmittance of NO₂ gas against the diode injection current at six different temperatures for the TOPITCA and ROITHNER lasers, respectively. It is worth mentioning that for the temperatures T=60 °C for the TOPTICA laser diode and T= 40, 50 and 60 °C for the ROITHNER laser diode, there is no transmittance observed for injection current 30 mA since at these diode temperatures the laser injection current is below the threshold current and the laser intensity is extremely weak.

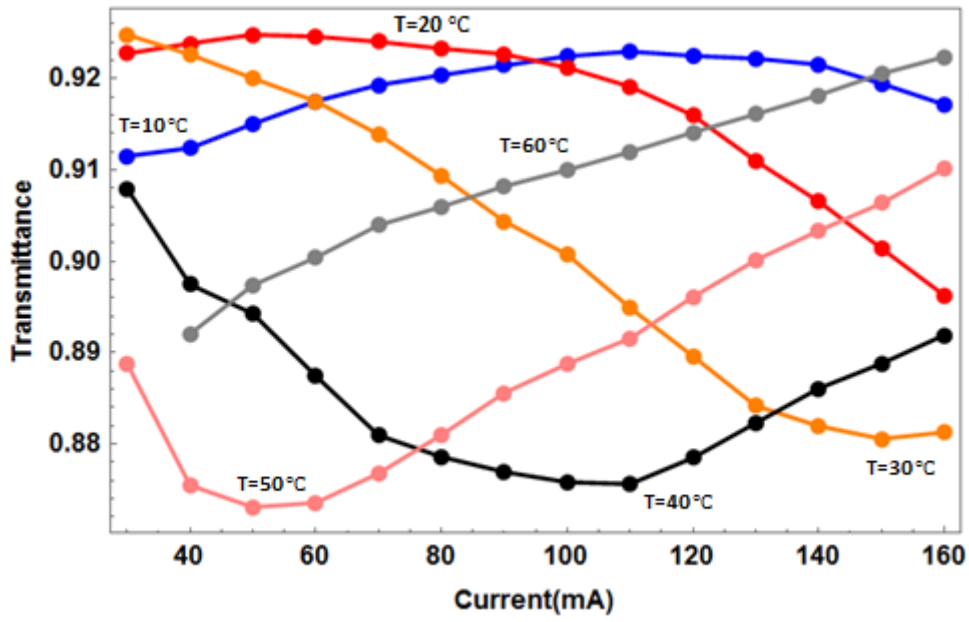


Figure 4.6 The calculated NO₂ transmittance versus the laser injection current at different diode temperatures for the TOPTICA laser.

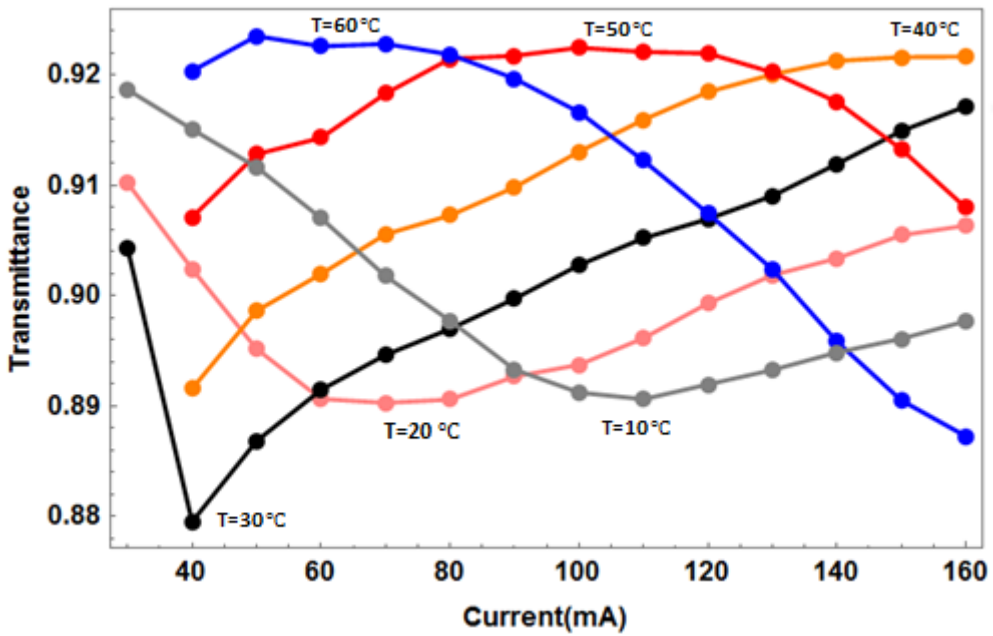


Figure 4.7 The calculated NO₂ transmittance versus the laser injection current at different diode temperatures for the ROITHNER laser.

4.2 Effect of NO₂ adsorption on the transmittance

It is observed that if the NO₂ gas mixture inside the absorption cell is not flowing, the transmittance due to NO₂ increases with time. This indicates that some of NO₂ gas is slowly lost with time. Since there is no leakage in our cell, the loss might be due to adsorption of NO₂ onto the walls of the cell or due to chemical reaction of NO₂ with the cell or with itself to form N₂O₄ dimer. To reduce the effect of this loss on our measurements, NO₂ gas mixture is flowed through the cell. We need to determine the minimum flow rate for which the variation in transmission due to NO₂ loss in the cell is almost eliminated. Higher flow rates serve the same purpose but consume valuable NO₂ gas mixture quickly.

In the following, the NO₂ number density C in the absorption cell as a function of time t is modeled. This simple model helps in determining roughly the steady state concentration in the cell and the time for NO₂ number density to reach the steady state. Assume that at time zero, NO₂/N₂ gas mixture with NO₂ number density C_0 and flow rate R starts to flow into a cell of volume V initially filled with pure N₂ gas. Assuming instant mixing time within the cell, the change in NO₂ number density ΔC during time interval Δt is given by

$$\Delta C = \frac{C_0 R \Delta t - CR \Delta t - Cr \Delta t}{V}$$

Here, the number of NO₂ molecules enters the cell is $C_0 R \Delta t$, the number exits is $CR \Delta t$, and the number lost due to adsorption or reaction is $Cr \Delta t$, where r is the rate of loss. For differential time interval, the above equation can be written as

$$\frac{dC}{dt} = \frac{(C_0 - C)R}{V} - \frac{Cr}{V} \equiv \frac{(C_0 - C)}{\tau} - \frac{C}{\tau_L}$$

Here $\tau \equiv V/R$ is the time constant without loss, and $\tau_L \equiv V/r$. The steady state solution C_{ss} is given by

$$C_{ss} = \frac{C_0}{1 + \frac{\tau}{\tau_L}}$$

For high flow rates $\tau \ll \tau_L$, $C_{ss} \approx C_0$. The time to reach steady state is roughly few times of the time constant τ . For a flow rate of 100 ml/min, the time constant for our setup is roughly

$$\tau \equiv \frac{V}{R} = \frac{40 \times \pi \times (2.54/2)^2}{100} = 2 \text{ min}$$

To determine experimentally the minimum flow to almost eliminate loss, transmittance at specific wavelength for different flow rates is observed as a function of time. At atmospheric pressure and specific flow rate, pure N_2 gas is flowed into the cell for a long time, about an hour, to clean up the cell then the N_2 valve is closed and simultaneously the NO_2 valve is opened.

Figures 4.8 shows the NO_2 transmittance at specific wavelength for six different flow rates, 50, 100, 200, 400, 600, and 800 ml/min. It is expected that the steady state takes some time to reach. For the 50 ml/min flow rate, the flow rate is relatively small to the extent that the steady state is not reached after more than two hours. For the 100 and 200 ml/min, the steady state is reached after 20 and 10 minutes, respectively. However, two different steady states are observed for the two flow rates indicating that these flow rates are not sufficiently large. In addition, the steady state value is less than the calculated value. For 400, 600, and 800 ml/min, the steady state is reached within about 5 minutes and their steady state transmittance are almost the same and in agreement with our prediction. To check repeatability, the transmittance at 400 ml/min flow rate is checked four times and the results along with the

transmittance at flow rates of 600 and 800 ml/min are shown in Figure 4.9. Within the measurement uncertainty, the steady state transmittance for flow rates higher than 400 ml/min are almost the same and therefore the flow rate of 600 ml/min, which reduces the consumption of NO₂ gas mixture, is used in the upcoming investigations.

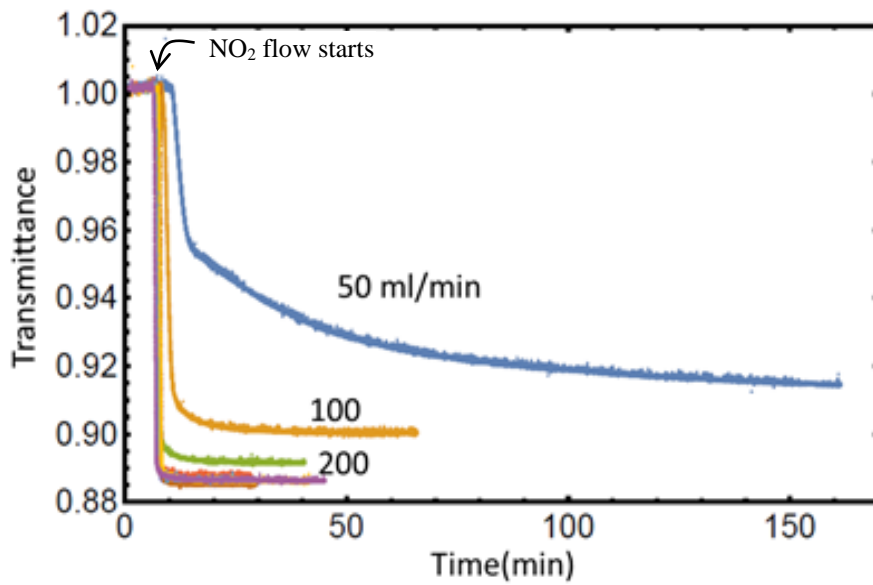


Figure 4.8 Transmittance vs time for different flow rates: 50, 100, 200, 400, 600, and 800 ml/min.

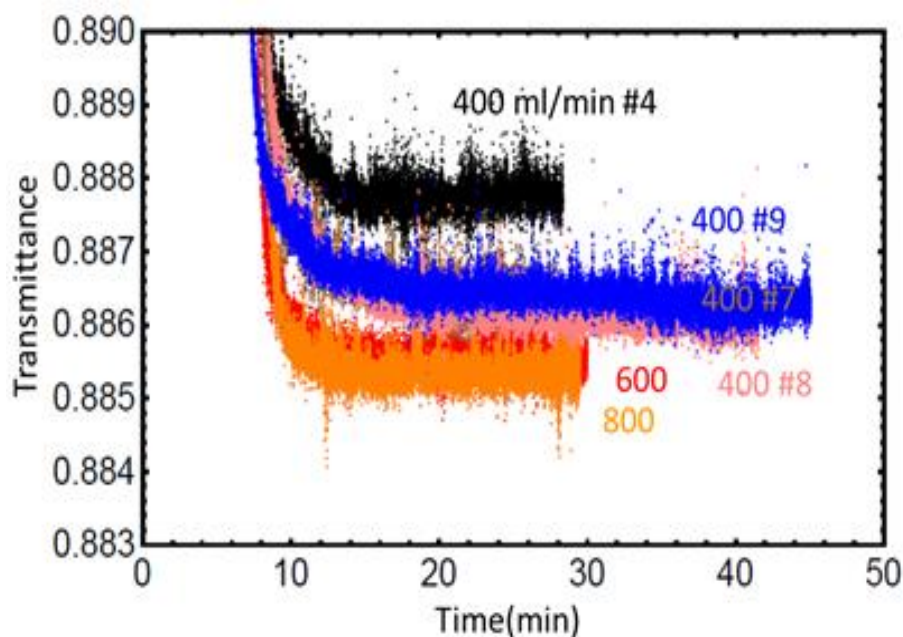


Figure 4.9 Transmittance vs time for flow rates: 400, 600, and 800 ml/min.

4.3 Results of the transmittance calculation

Figures 4.10-4.15 show the simulated and the experimental NO₂ transmittance as a function of the injection current for the TOPTICA laser for different fixed temperatures. Moreover, Figures 4.16-4.21 show similar curves for the ROITHNER laser.

In general, the experimental transmittance curves are in a good agreement with those obtained by simulation. The little discrepancy is most probably due to using laser spectra with limited resolution in the simulation. The resolution of the measured laser spectra is limited by the resolution of our SPEX 500 M monochromator. In addition, other causes that might affect the transmittance results are the variations in some of the experimental conditions while collecting data such as the absorption cell pressure and temperature.

We want to use the We have obtained the transmittance curves at various diode temperatures since we seek for the curve that shows the biggest variation in the transmittance over the current range, the variation that provides the highest measurement accuracy.

Eventually, we want to use the laser temperature that provides the biggest variation in the transmittance curve over the scanning current range. This maximizes the signal-to-noise ratio and results in the smallest minimum detectable level. For the TOPTICA laser, maximum variation in the transmittance curve of about 4% occurs at $T = 30$ or $T = 50$ °C. While for the ROITHNER laser, maximum variation in the transmittance curve of about 4% occurs at $T = 30$ or $T = 60$ °C.

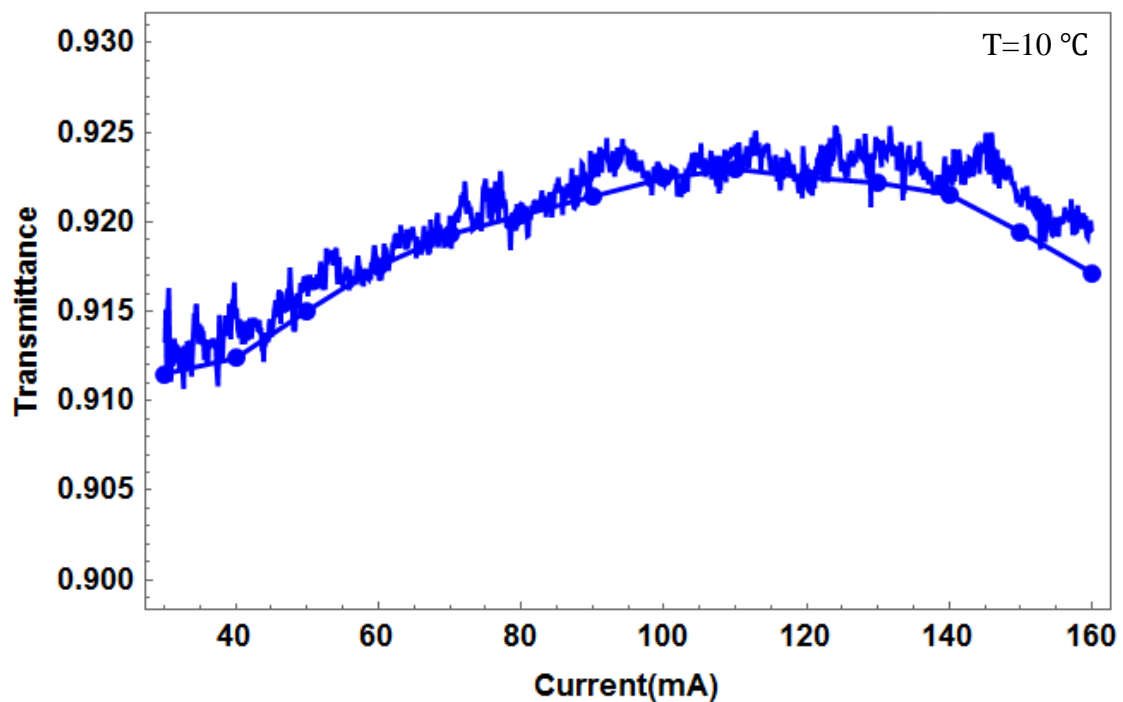


Figure 4.10 Simulation vs experiment of the transmittance curve at $T=10$ °C for the TOPTICA laser. The curve with circles joined by straight lines is the simulation curve.

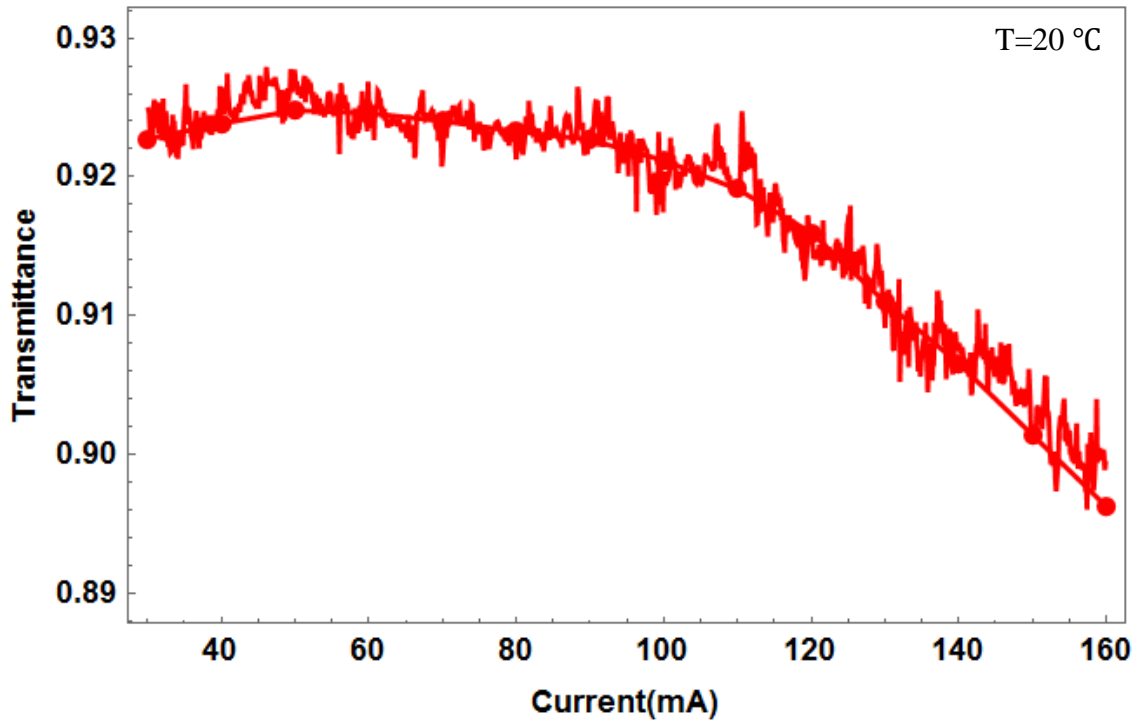


Figure 4.11 Simulation vs experiment of the transmittance curve at T=20 °C for the TOPTICA laser. The curve with circles joined by straight lines is the simulation curve.

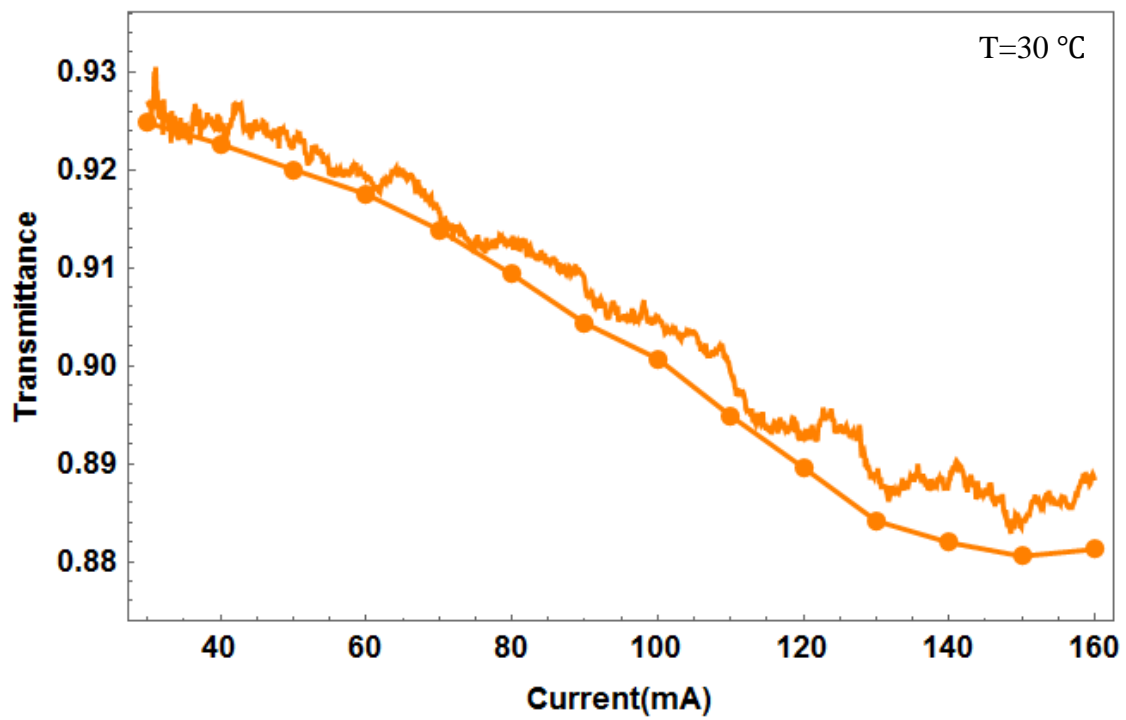


Figure 4.12 Simulation vs experiment of the transmittance curve at T=30 °C for the TOPTICA laser. The curve with circles joined by straight lines is the simulation curve.

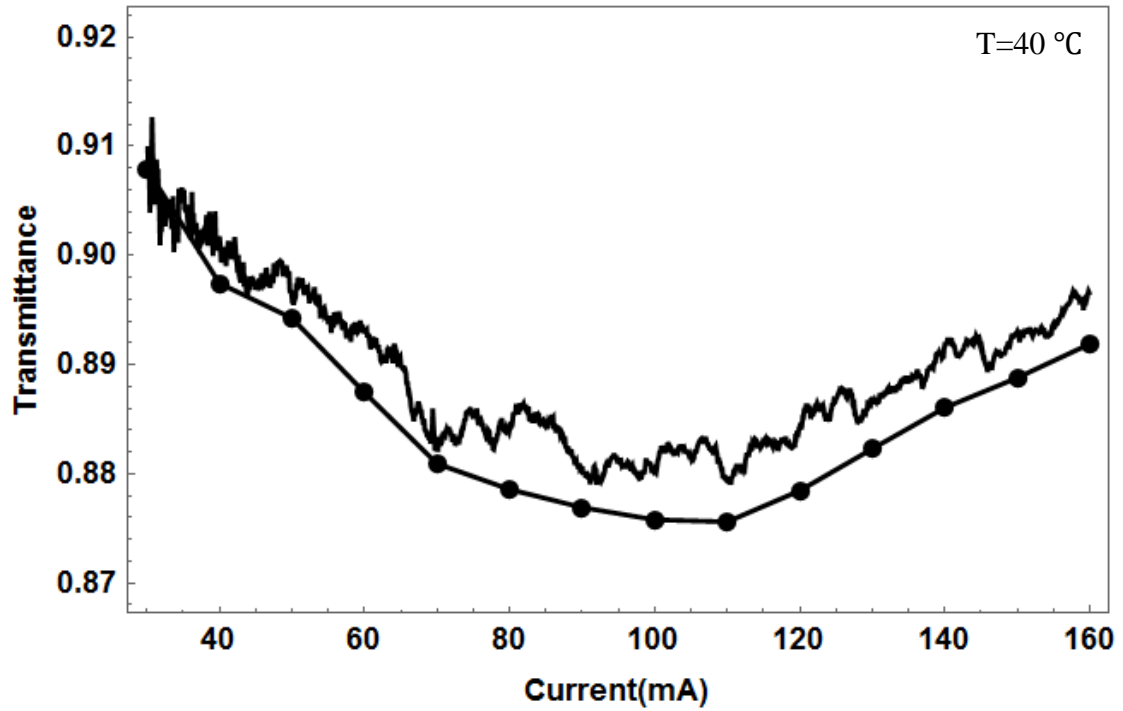


Figure 4.13 Simulation vs experiment of the transmittance curve at $T=40\text{ }^{\circ}\text{C}$ for the TOPTICA laser. The curve with circles joined by straight lines is the simulation curve.

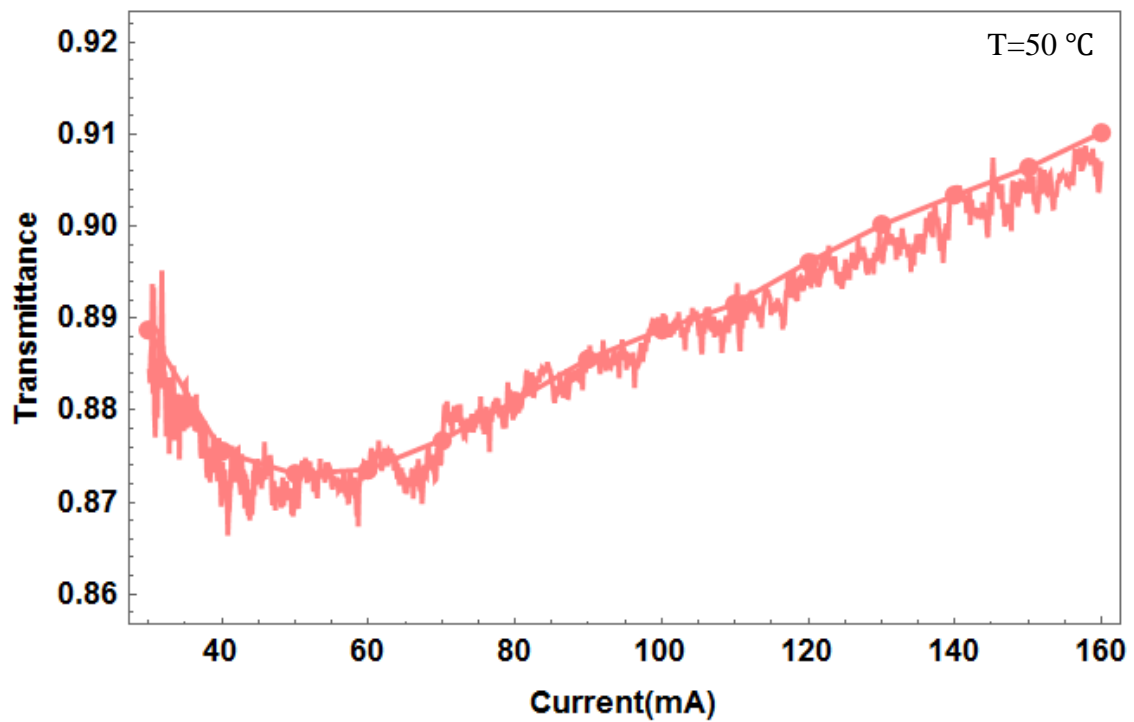


Figure 4.14 Simulation vs experiment of the transmittance curve at $T=50\text{ }^{\circ}\text{C}$ for the TOPTICA laser. The curve with circles joined by straight lines is the simulation curve.

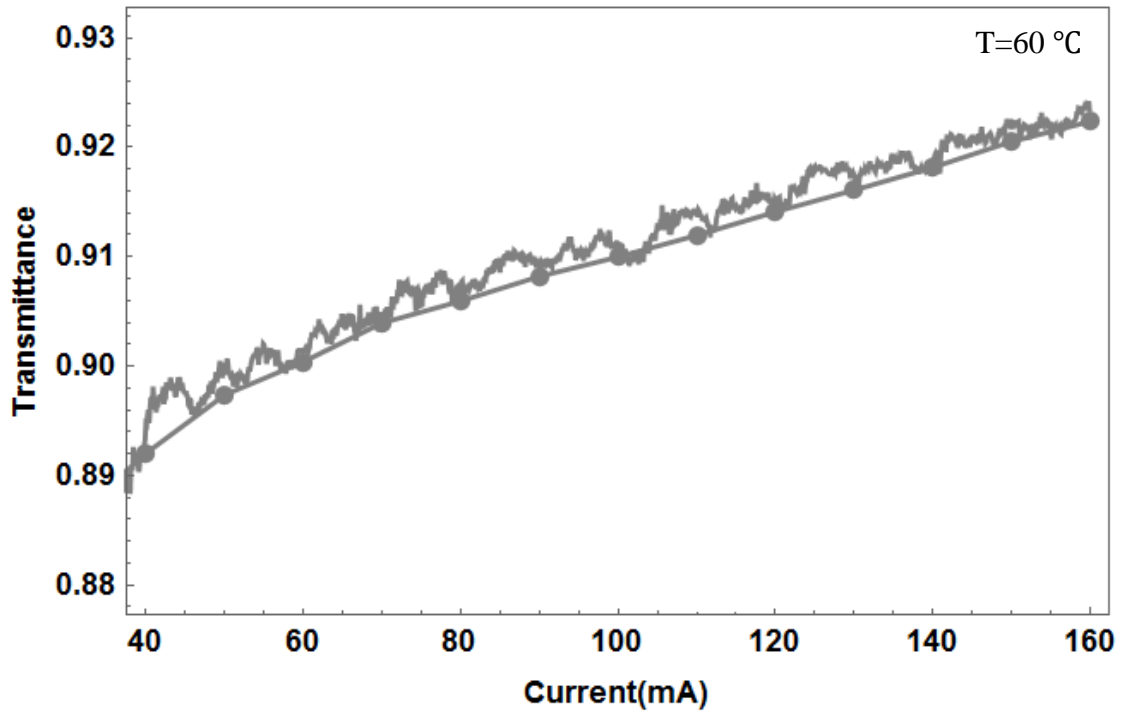


Figure 4.15 Simulation vs experiment of the transmittance curve at $T=60\text{ }^{\circ}\text{C}$ for the TOPTICA laser. The curve with circles joined by straight lines is the simulation curve.

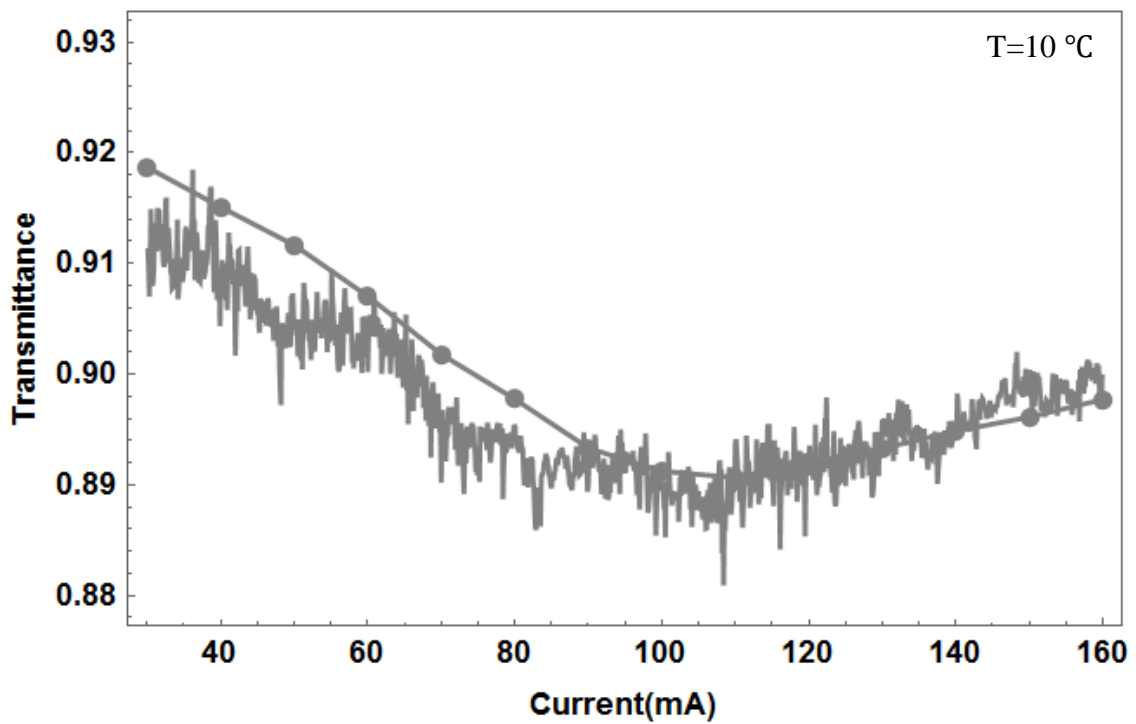


Figure 4.16 Simulation vs experiment of the transmittance curve at $T=10\text{ }^{\circ}\text{C}$ for the ROITHNER laser. The curve with circles joined by straight lines is the simulation curve.

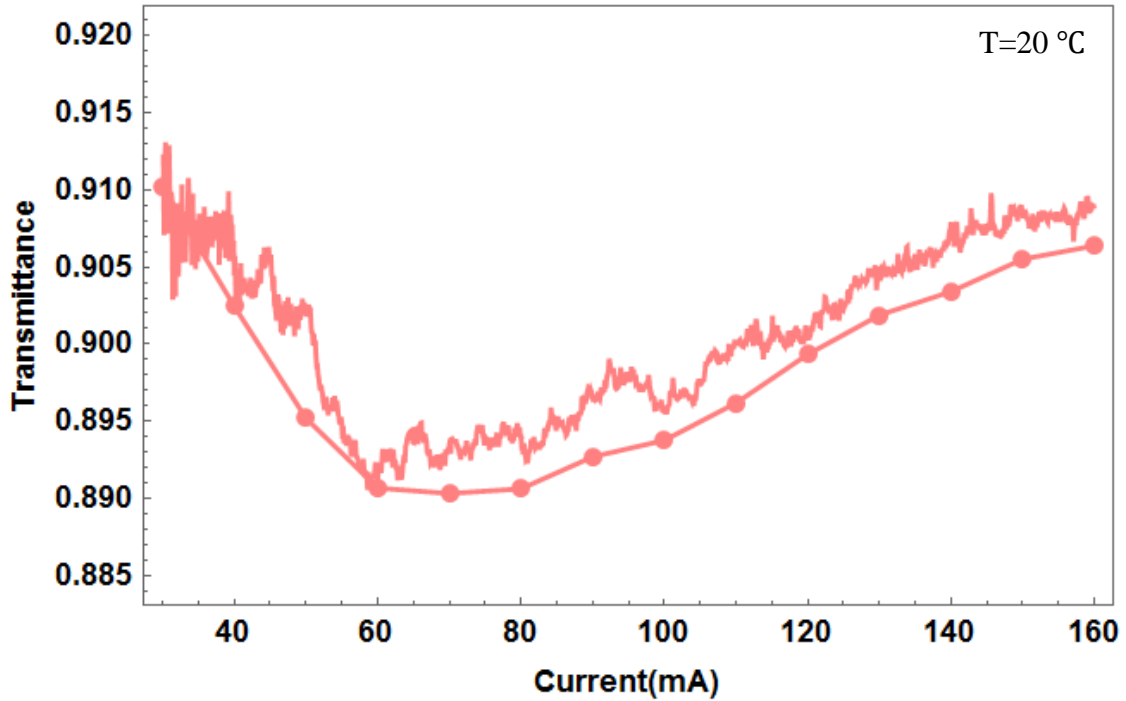


Figure 4.17 Simulation vs experiment of the transmittance curve at T=20 °C for the ROITHNER laser. The curve with circles joined by straight lines is the simulation curve.

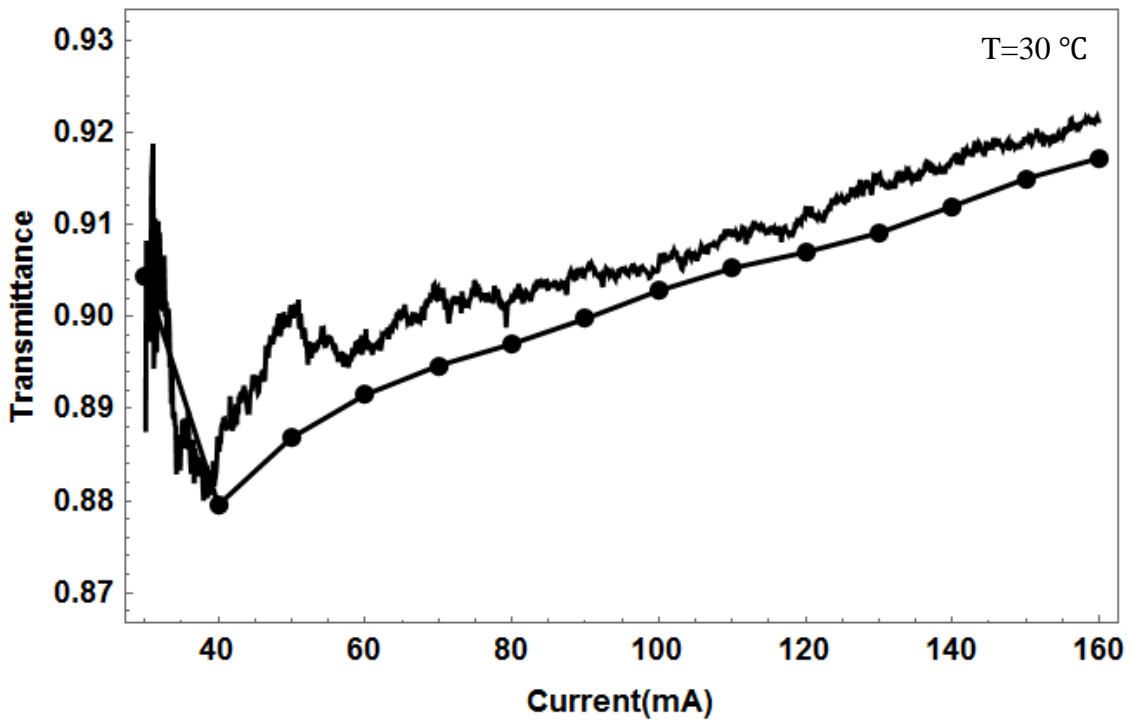


Figure 4.18 Simulation vs experiment of the transmittance curve at T=30 °C for the ROITHNER laser. The curve with circles joined by straight lines is the simulation curve.

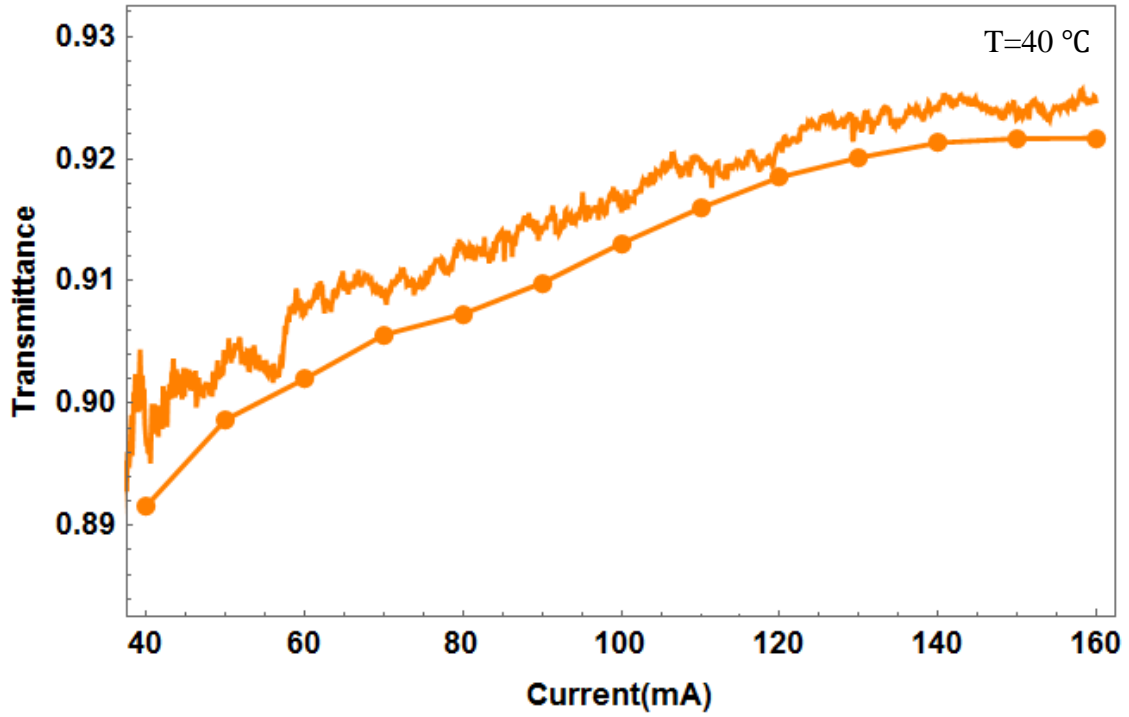


Figure 4.19 Simulation vs experiment of the transmittance curve at $T=40\text{ }^{\circ}\text{C}$ for the ROITHNER laser. The curve with circles joined by straight lines is the simulation curve.

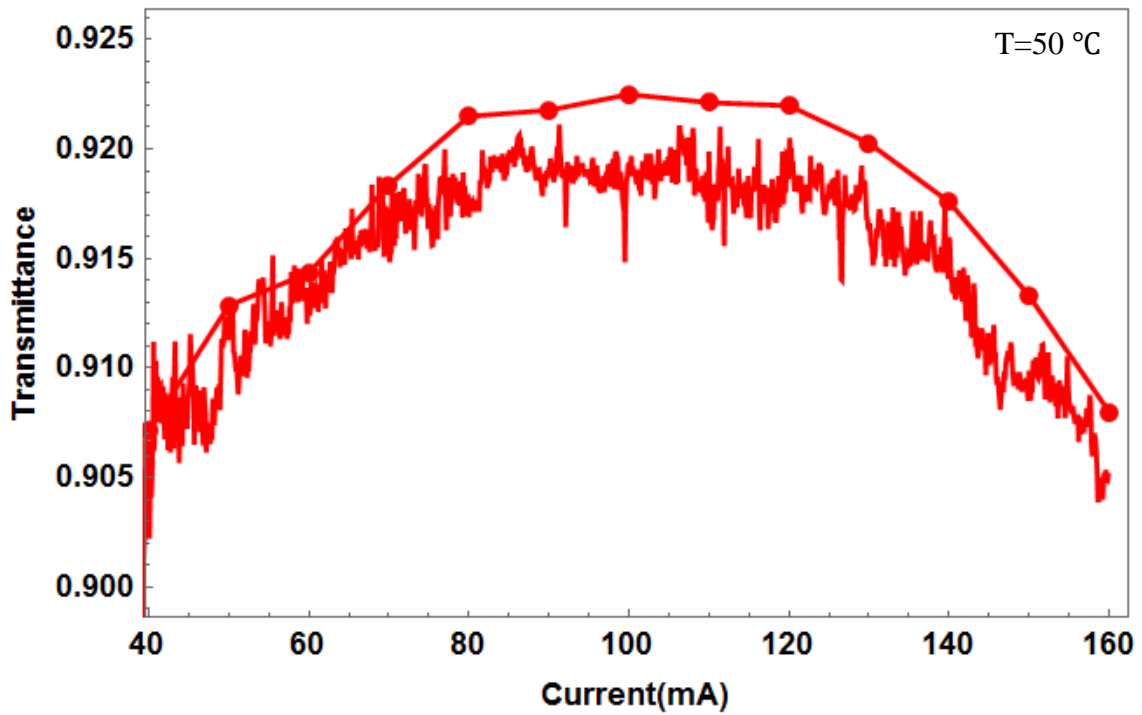


Figure 4.20 Simulation vs experiment of the transmittance curve at $T=50\text{ }^{\circ}\text{C}$ for the ROITHNER laser. The curve with circles joined by straight lines is the simulation curve.

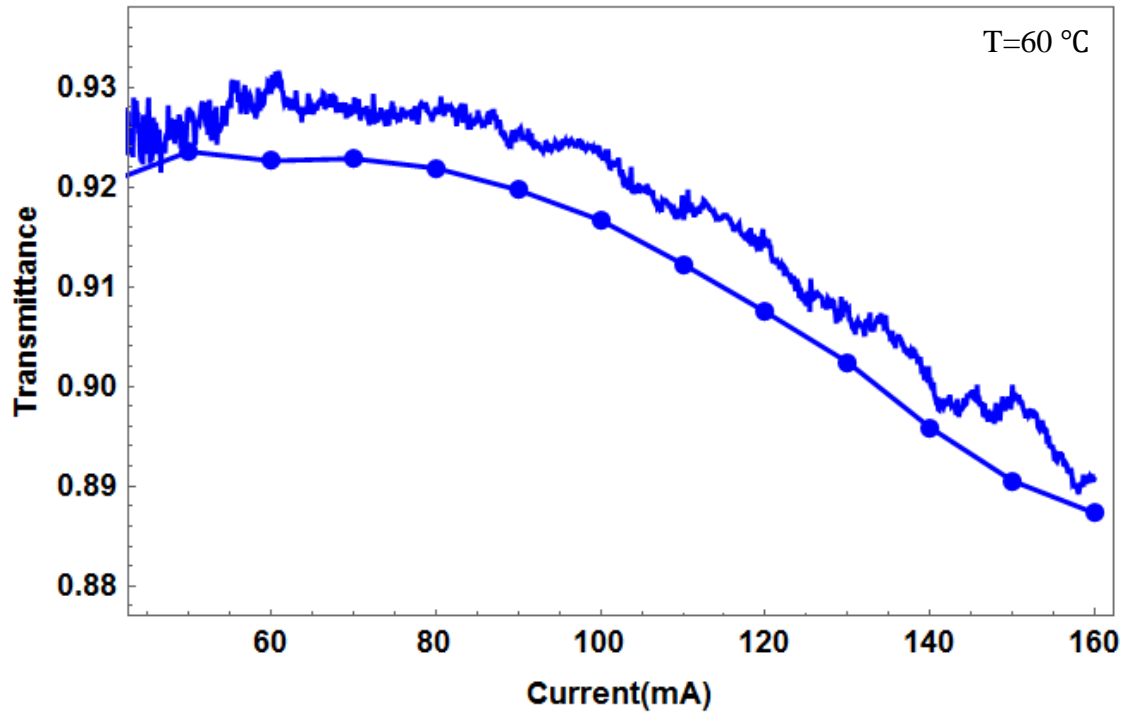


Figure 4.21 Simulation vs experiment of the transmittance curve at T=60 °C for the ROITHNER laser. The curve with circles joined by straight lines is the simulation curve.

4.4 Detection Limit

In The minimum detectable limit is estimated to be the amount of NO₂ that produces an absorption signal equal roughly to twice the noise level of the absorption signal. The noise level is estimated using the measurement for the case of pure N₂ since the curve obtained is straight and horizontal as shown in Figure 4.22, which shows the voltage ratio of the signal and reference detectors as a function of the laser current. The standard deviation, and the average of the voltage ratio are calculated to be 2.2×10^{-4} , and 0.86, respectively. Since the absorption curve is obtained from the ratio of the NO₂ voltage ratio to the N₂ voltage ratio, the noise level of the absorption signal is approximately $\sqrt{2} \times 2.2 \times 10^{-4} / 0.86 = 3.6 \times 10^{-4}$.

As discussed in the previous section, 200 ppm causes absorption up to about 0.40 in a cell of length 40 cm, the minimum detectable limit is

$$2 \times 3.6 \times 10^{-4} \times \left(\frac{200 \text{ ppm}}{0.40} \right) \approx 4 \text{ ppm}.$$

Hence, for a path length of 1000 m, the minimum detectable limit is

$$4 \text{ ppm} \times \left(\frac{0.4 \text{ m}}{1000 \text{ m}} \right) = 1.6 \text{ ppb}.$$

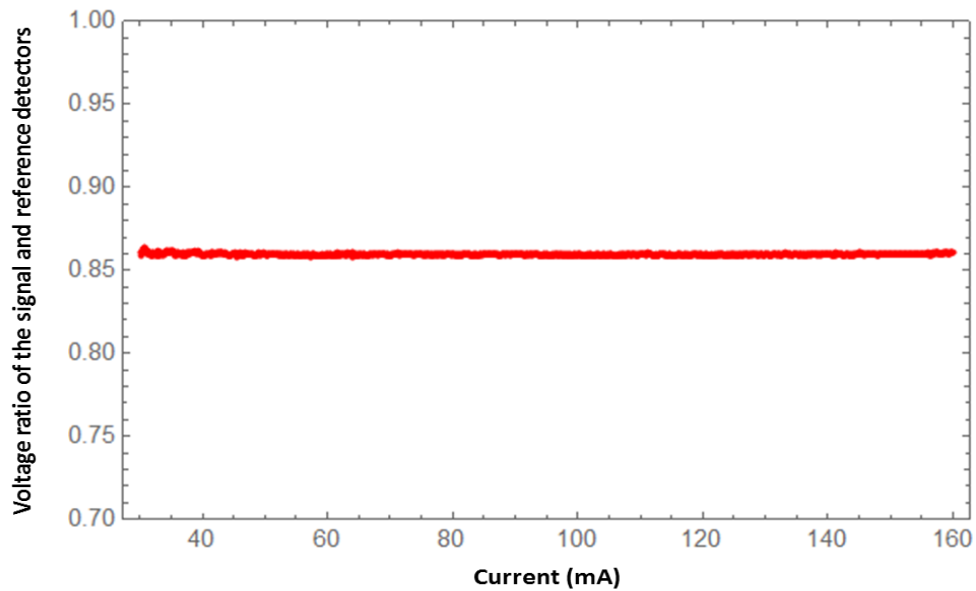


Figure 4.22 Voltage ratio of the signal and reference detectors as a function of the laser injection current.

CHAPTER 5

CONCLUSION

An experimental setup based on tunable diode laser absorption spectroscopy technique has been successfully developed for the detection of trace amounts of NO₂ gas at atmospheric pressure. Two multi-longitudinal mode blue diode lasers with emission wavelength of about 445 nm have been used separately in the setup: TOPTICA Photonics Inc., model LD-0445-0050-1 and Roithner LaserTechnick GmbH, model LD-445-50PD. To obtain the NO₂ concentrations experimentally, transmittance curves as a function of laser injection current at fixed temperatures have been measured using a gas cell of length 40 cm and NO₂/N₂ gas mixture with mixing ratio of 200 ppm. Also, these transmittance curves have been simulated using a reference NO₂ absorption cross section and measured laser spectra. Very good agreements have been found between the measured and simulated transmittance curves. A detection limit of 4 ppm in a gas cell of length 40 cm has been achieved for both lasers. This corresponds to a detection limit of 1.6 ppb for a length of 1km making the setup appropriate for monitoring atmospheric NO₂ pollution.

Appendix A

LabVIEW block diagrams and front panels developed for experimental measurements

Block diagrams and front panels for measuring laser spectra and NO₂ gas transmittance are shown below.

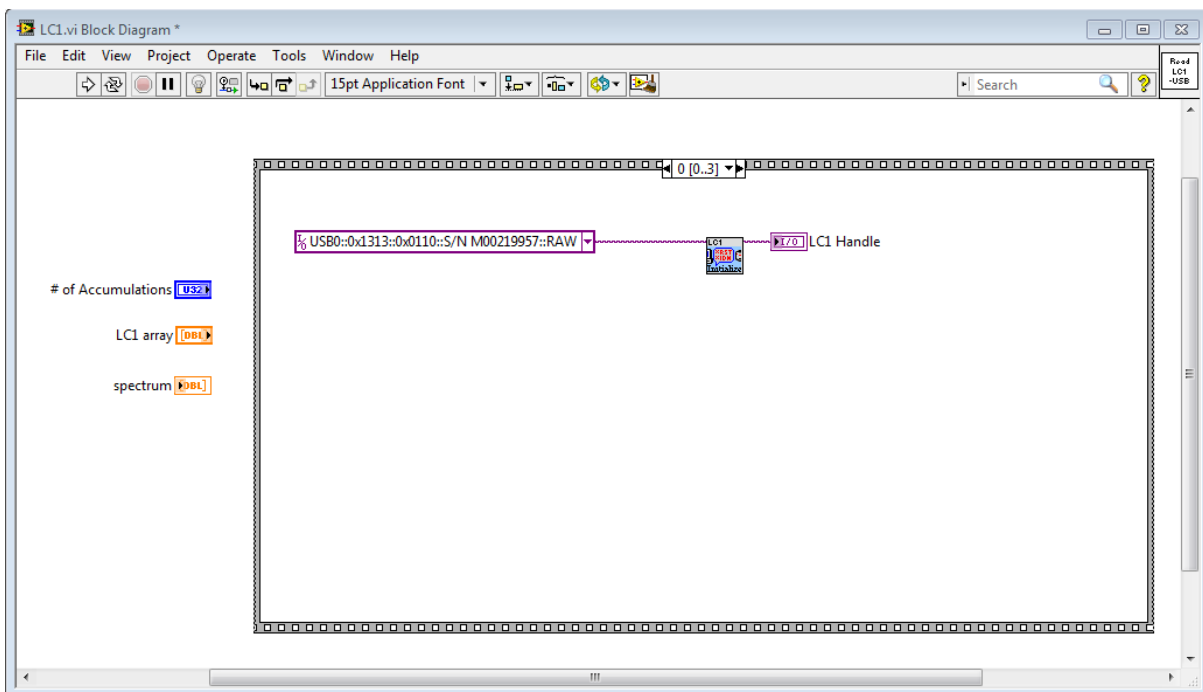


Figure A.1 The first portion of the block diagram associated with the front panel of Figure 3.4. The LC1 “Initialize.vi” virtual instrument is provided by the supplier of the LC1 camera, Thorlabs, Inc.

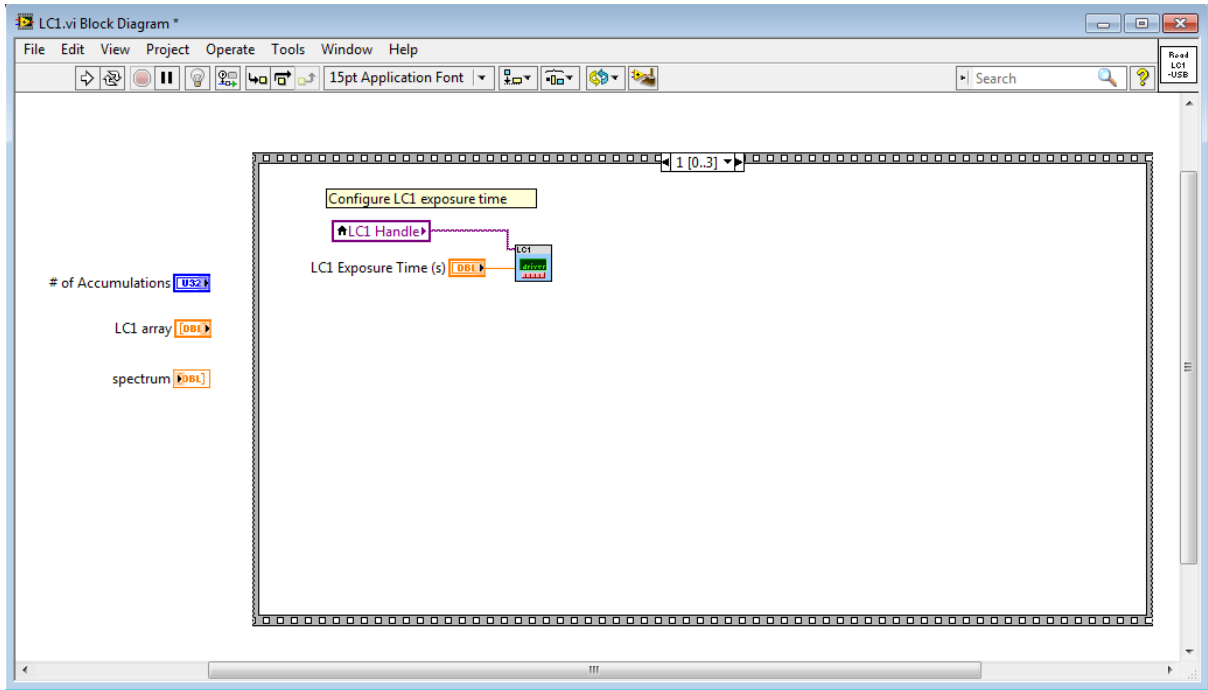


Figure A.2 The second portion of the block diagram associated with the front panel of Figure 3.4. The LC1 “Set Integration Time.vi” virtual instrument is provided by the supplier of the LC1 camera, Thorlabs, Inc.

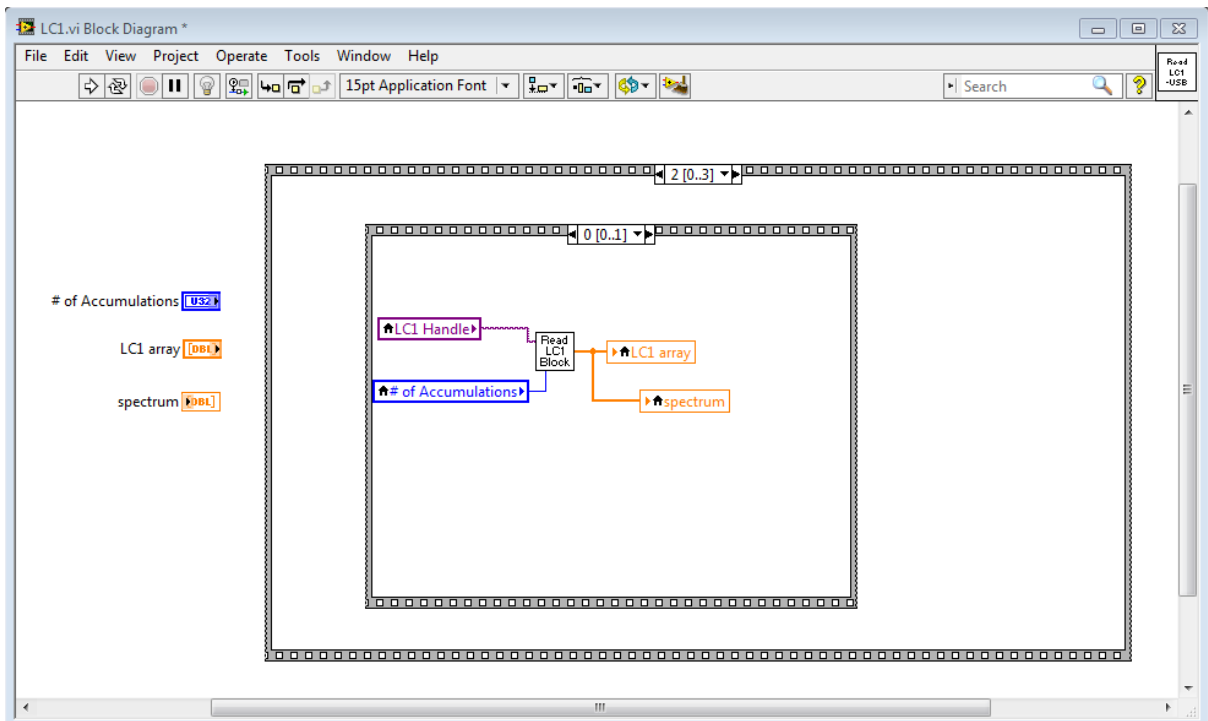


Figure A.3 The third portion-1 of the block diagram associated with the front panel of Figure 3.4 . The front panel of the “Read LC1 Block” virtual instrument is shown in Figure A.6. The portions of the associated block diagram are shown in Figures A.7, A.8 and A.9.

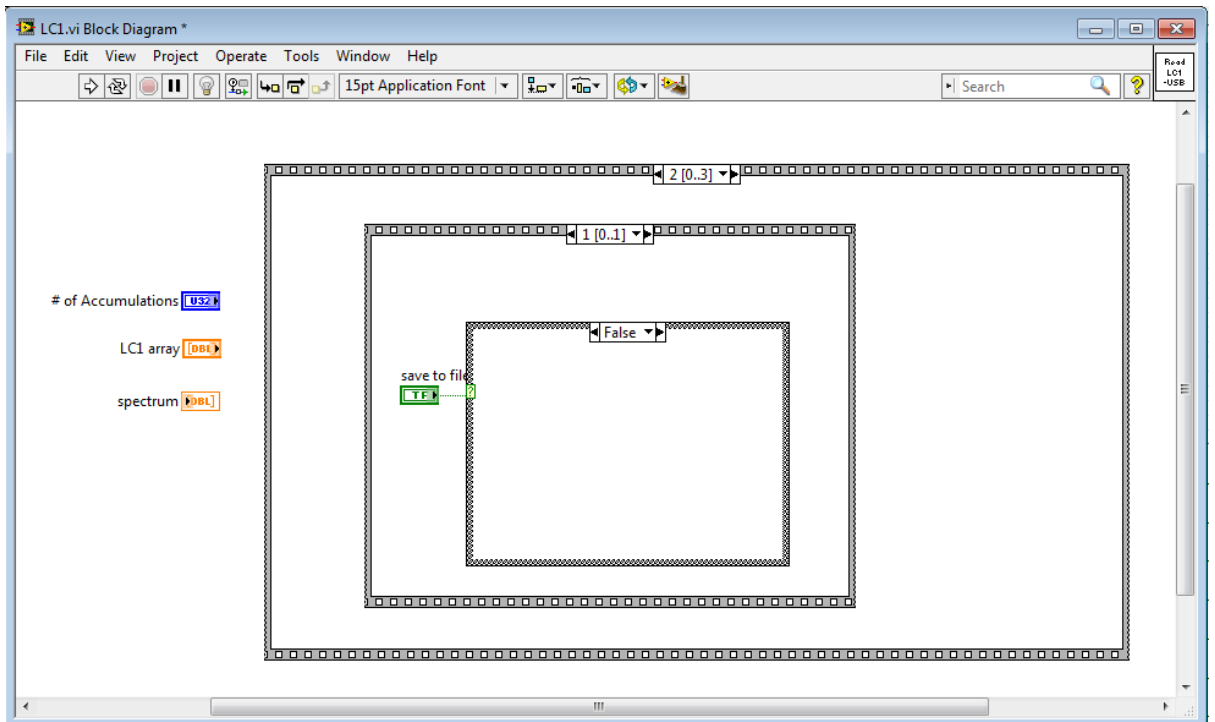
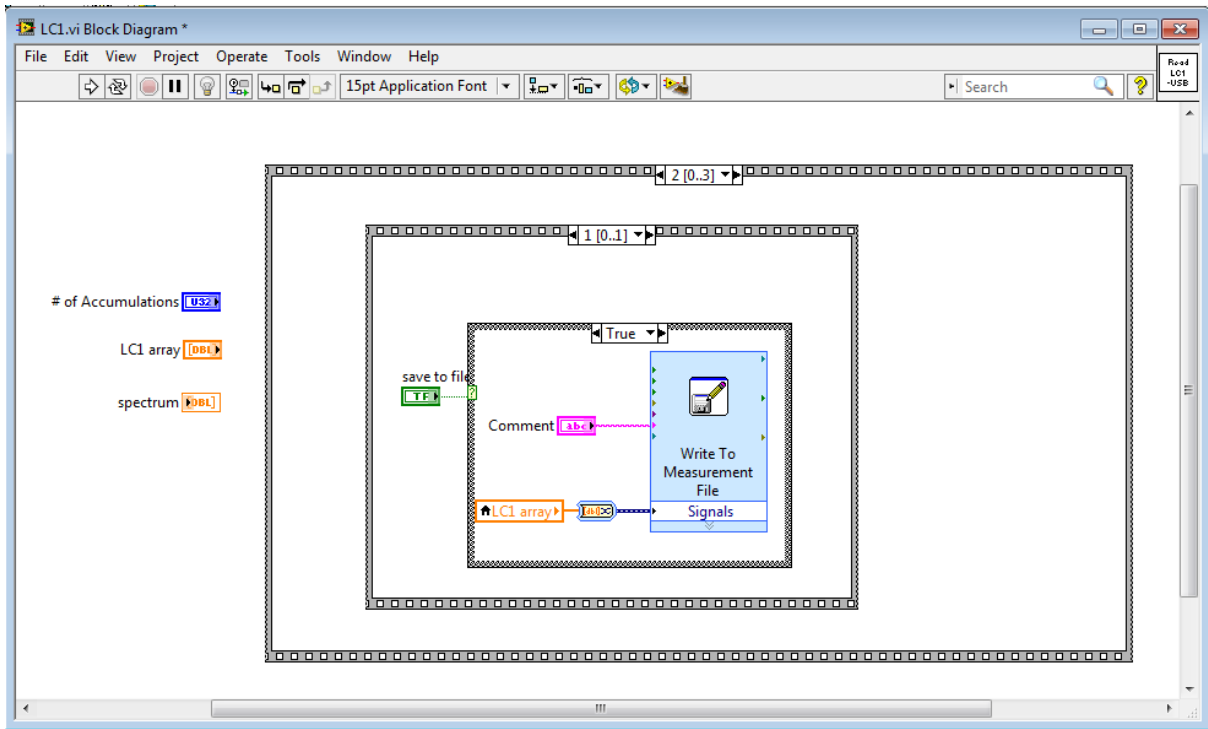


Figure A.4 The third portion-2 of the block diagram associated with the front panel of Figure 3.4 with different options of the case structures.

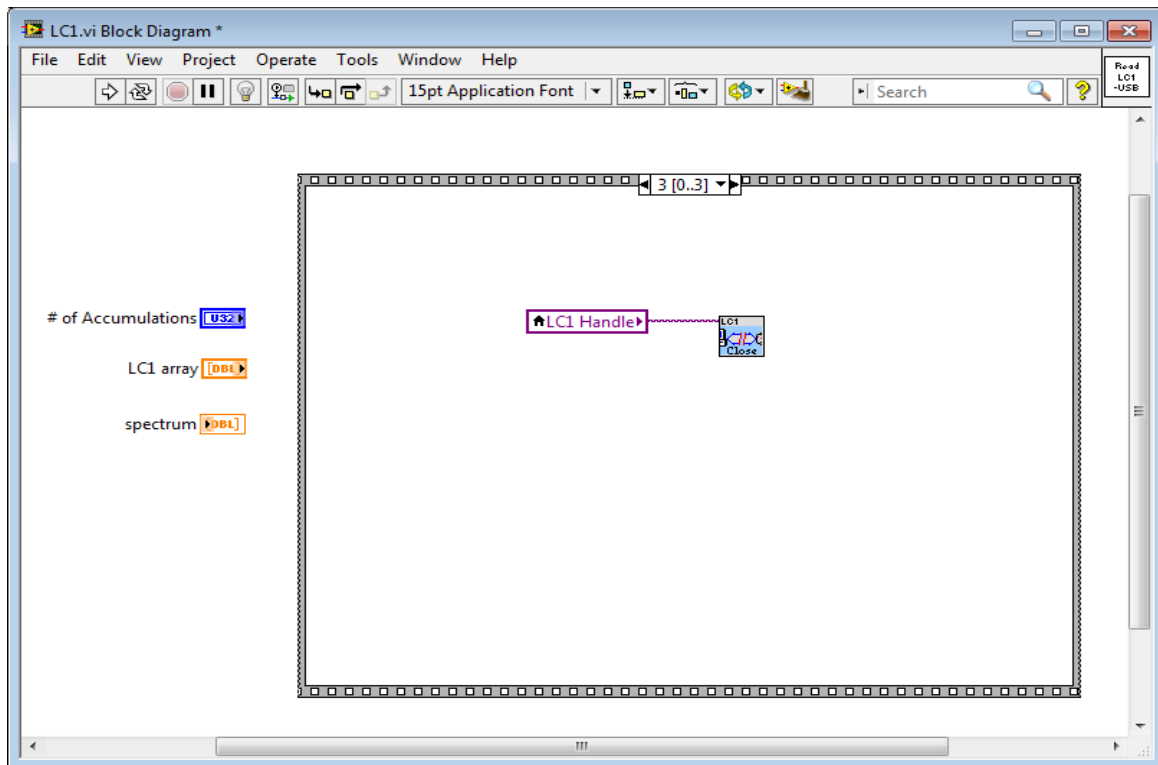


Figure A.5 The fourth portion of the block diagram associated with the front panel of Figure 3.4 .The LC1 “Close.vi” virtual instrument is provided by the supplier of the LC1 camera, Thorlabs, Inc.

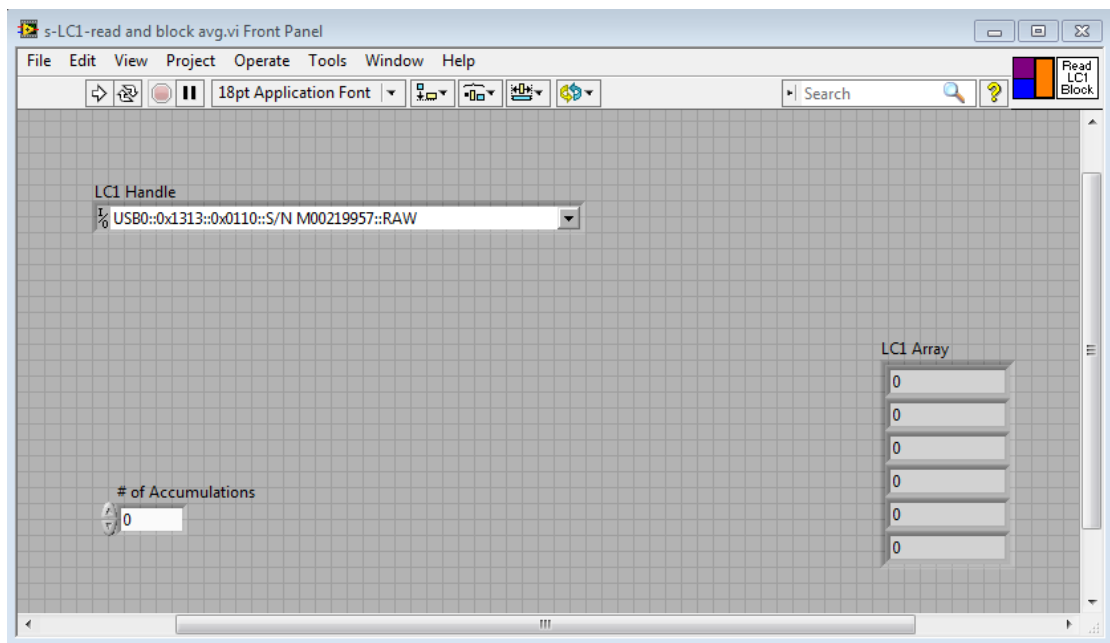


Figure A.6 The front panel of the “Read LC1 Block” virtual instrument used in Figure A.3. The portions of the block diagram associated with the front panel are shown in Figures A.7, A.8 and A.9.

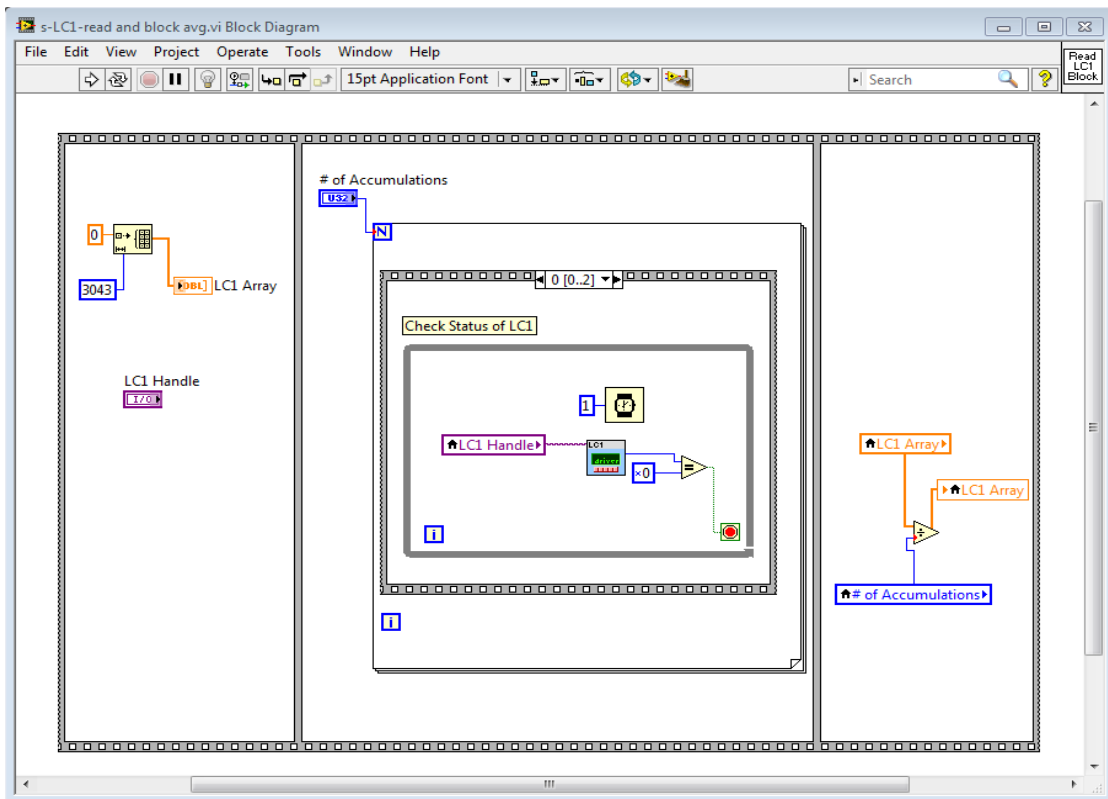


Figure A.7 The first portion of the block diagram associated with the front panel of Figure A.6. The LC1 “Get Device Status.vi” virtual instrument is provided by the supplier of the LC1 camera, Thorlabs, Inc.

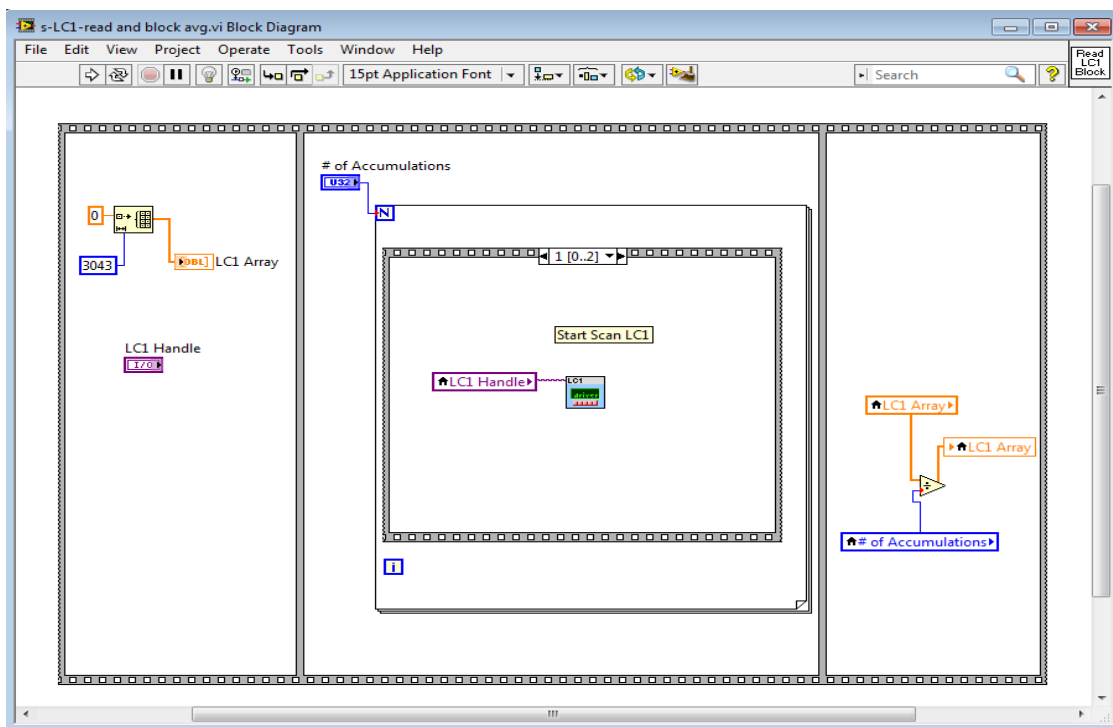


Figure A.8 The second portion of the block diagram associated with the front panel of Figure A.6. The LC1 “Start Scan.vi” virtual instrument is provided by the supplier of the LC1 camera, Thorlabs, Inc.

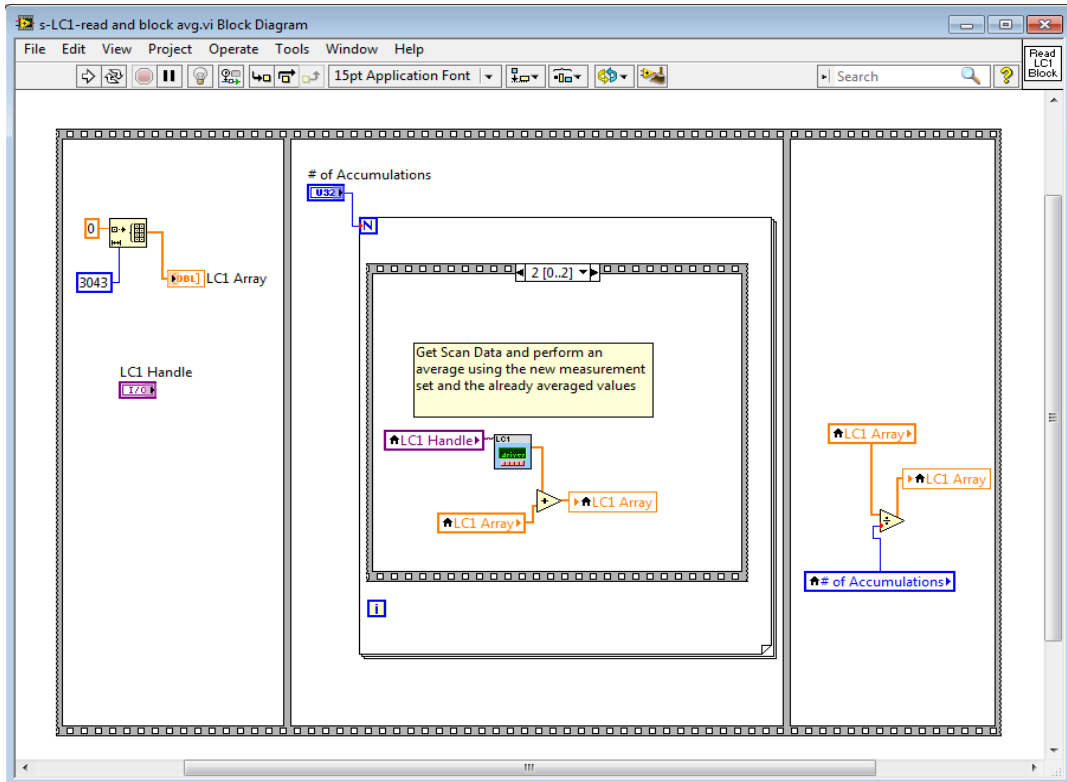


Figure A.9 The third portion of the block diagram associated with the front panel of Figure A.6. The LC1 “Get Scan Data.vi” virtual instrument is provided by the supplier of the LC1 camera, Thorlabs, Inc.

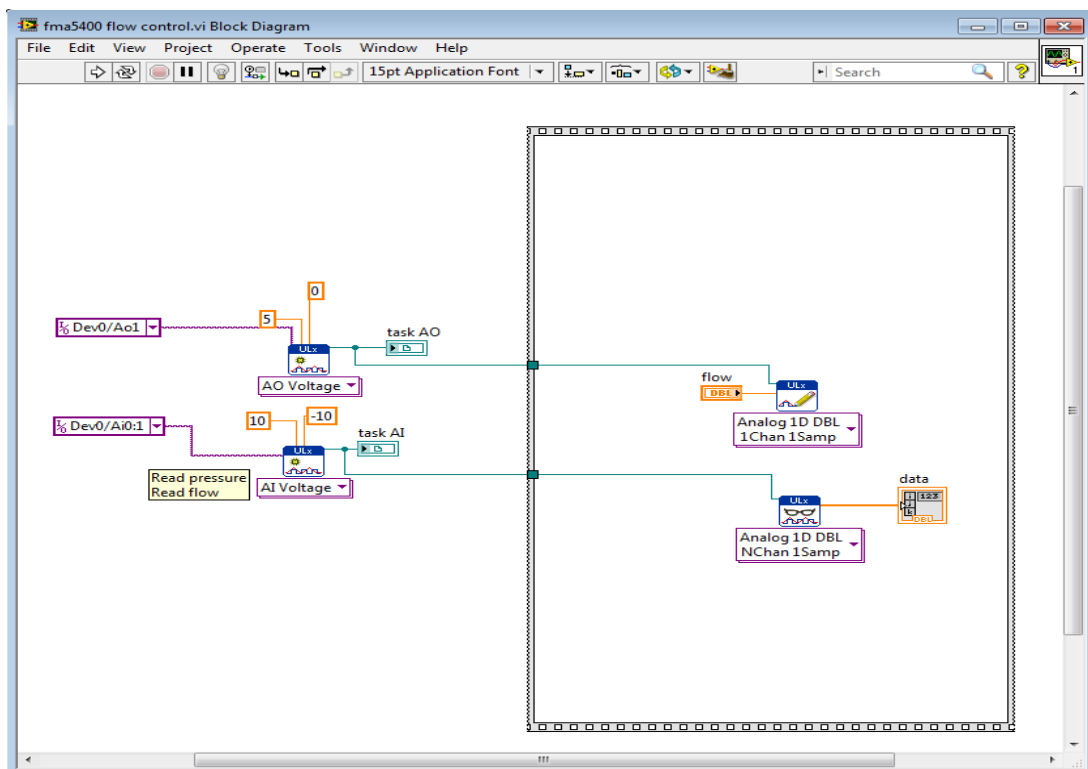


Figure A.10 The block diagram associated with the front panel of Figure 3.7. The ULx virtual instruments are provided by the National Instruments corporation.

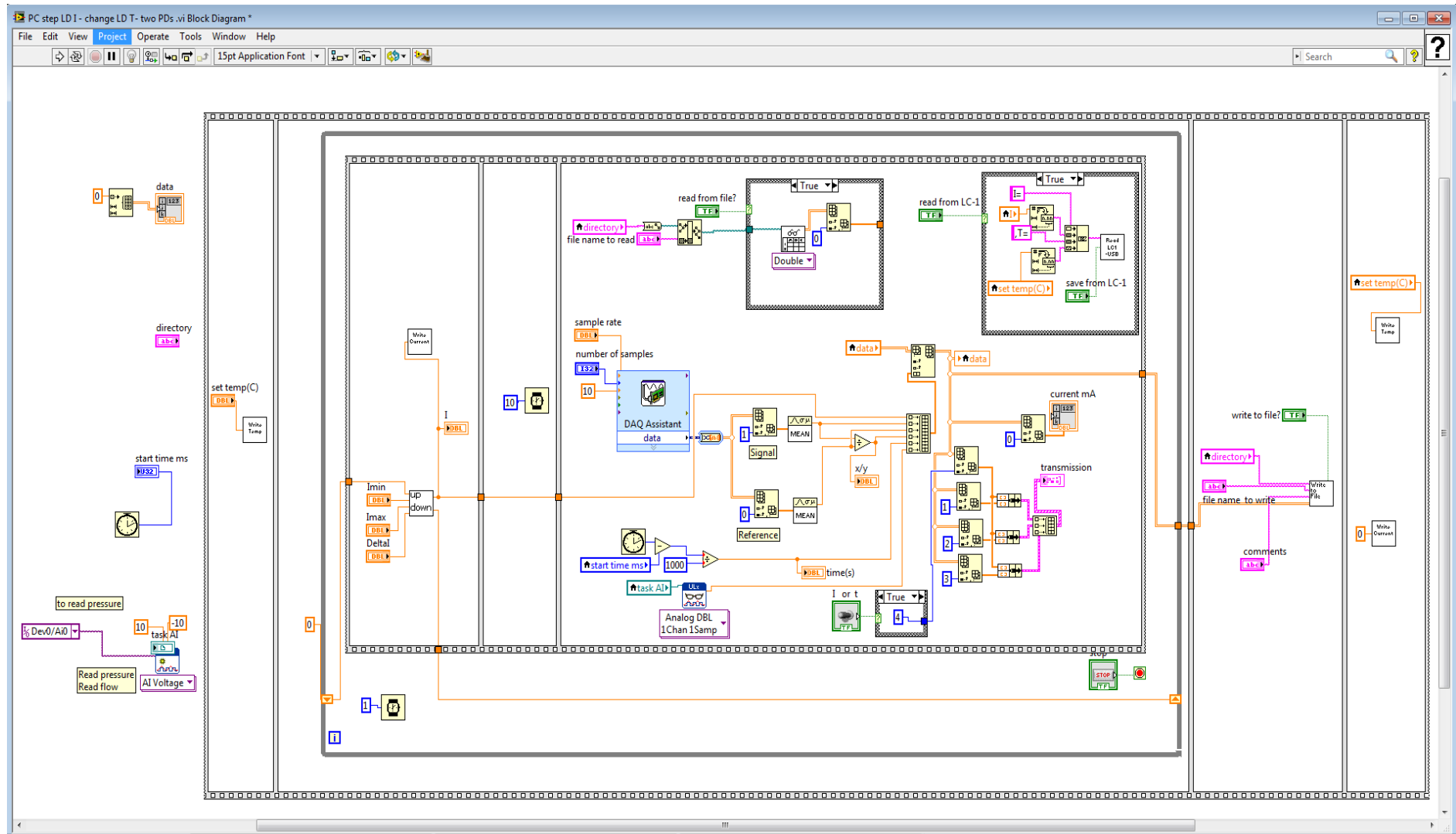


Figure A.11(a) The block diagrams associated with the front panel of Figure 3.8 or 3.9 with different options of the case structures. The front panels and the block diagrams of the virtual instruments “Write Temp”, “Write Current”, “ up/down” and “Write to File” are shown in Figures A.12, A.13, A.14 and A.15, respectively.

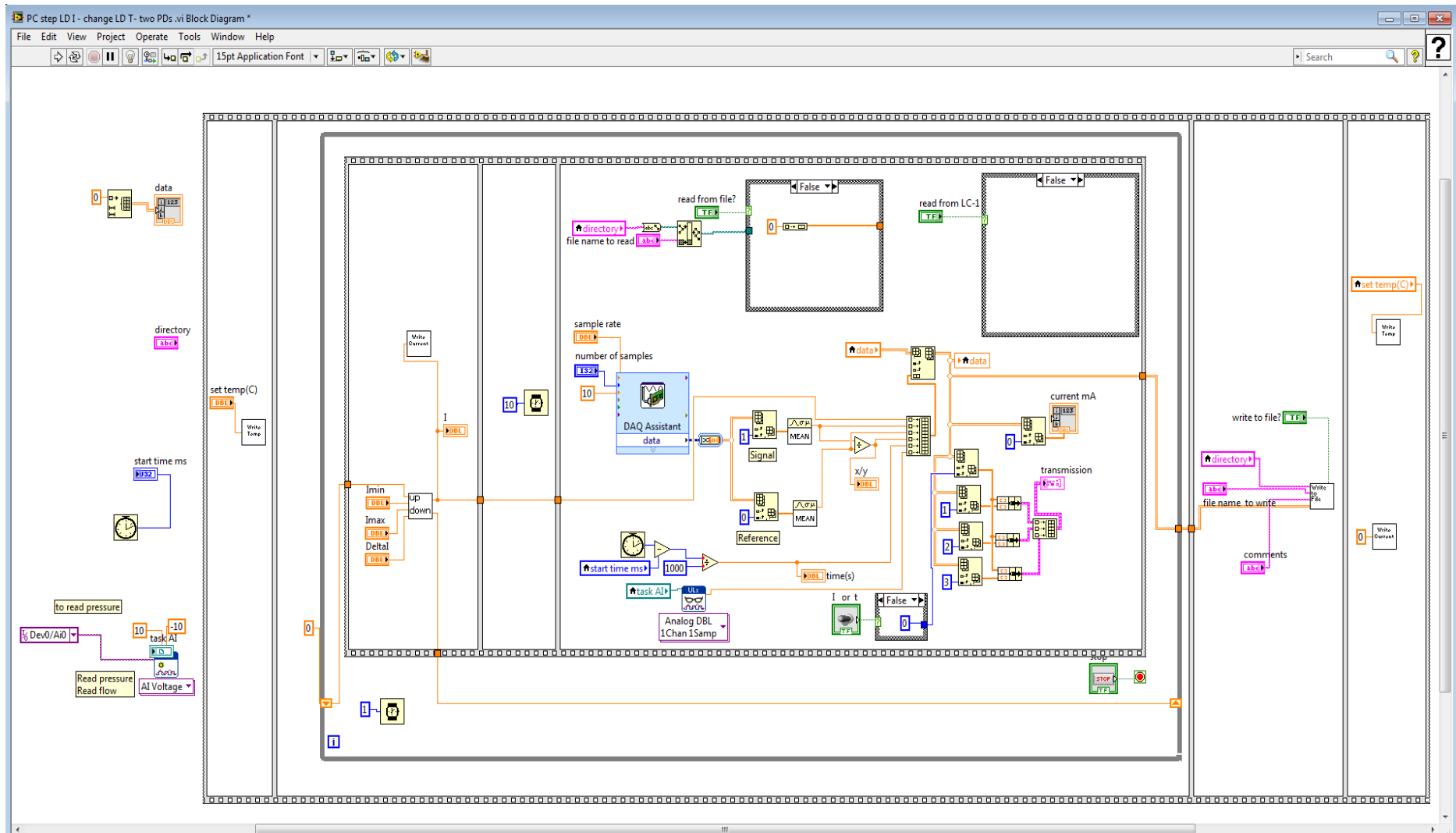


Figure A.11(b) The block diagrams associated with the front panel of Figure 3.8 or 3.9 with different options of the case structures. The front panels and the block diagrams of the virtual instruments “Write Temp”, “Write Current”, “up/down” and “Write to File” are shown in Figures A.12, A.13, A.14 and A.15, respectively.

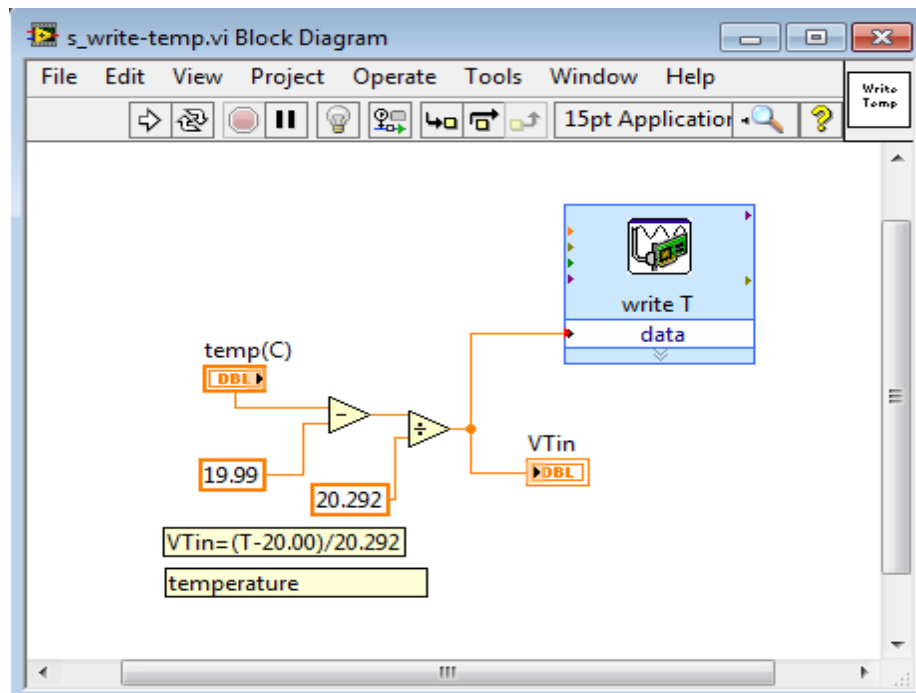
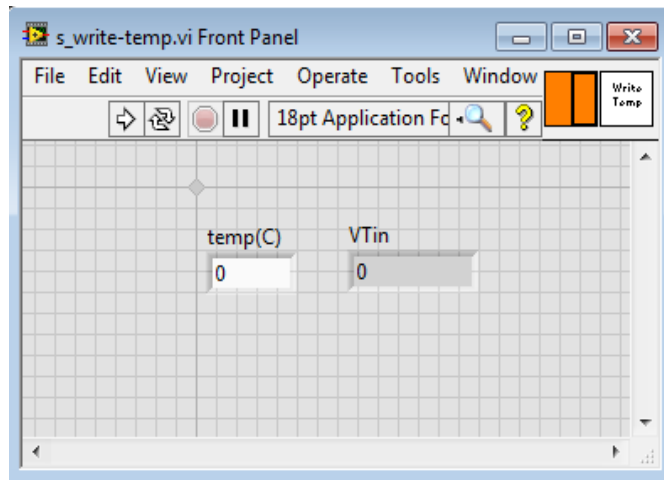


Figure A.12 The front panel and the block diagram for the “Write Temp” virtual instrument used in Figure A.11.

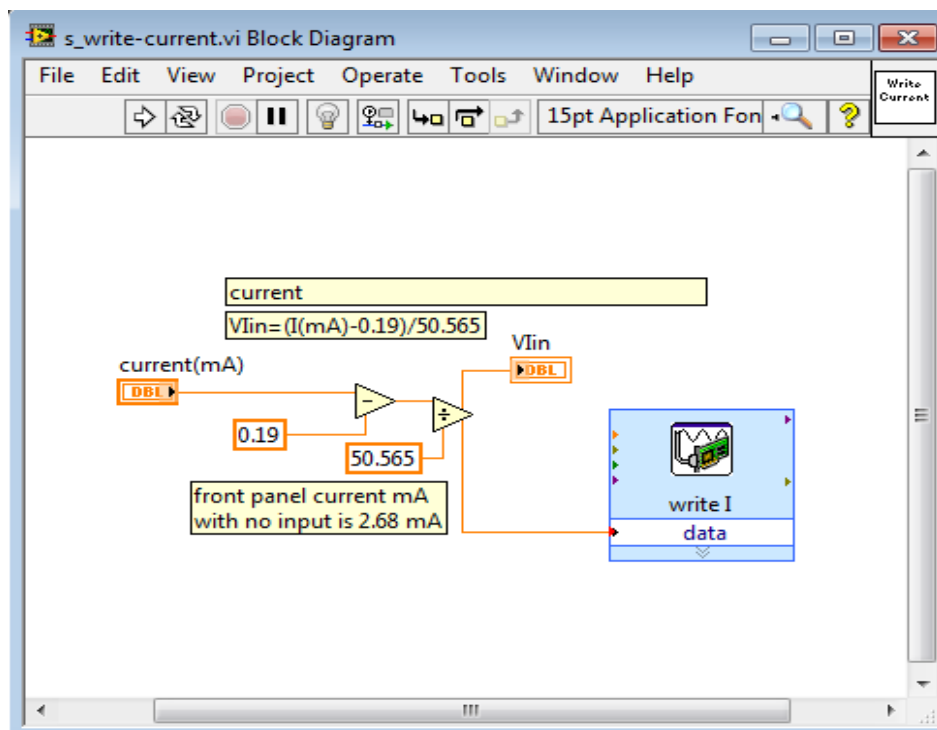
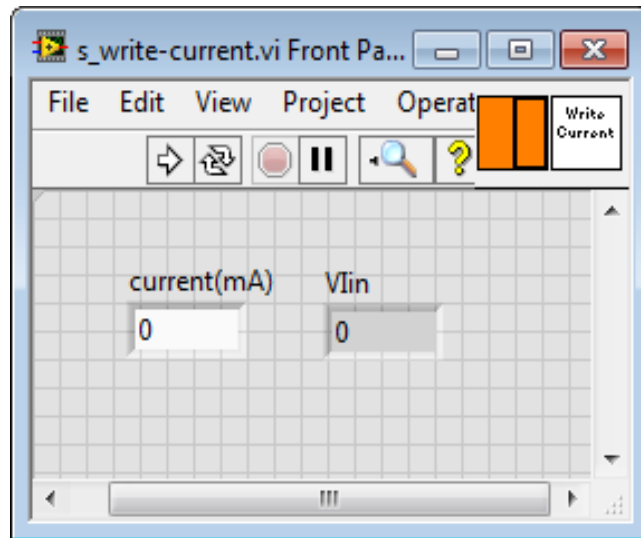


Figure A.13 The front panel and the block diagram for the “Write Current” virtual instrument used in Figure A.11.

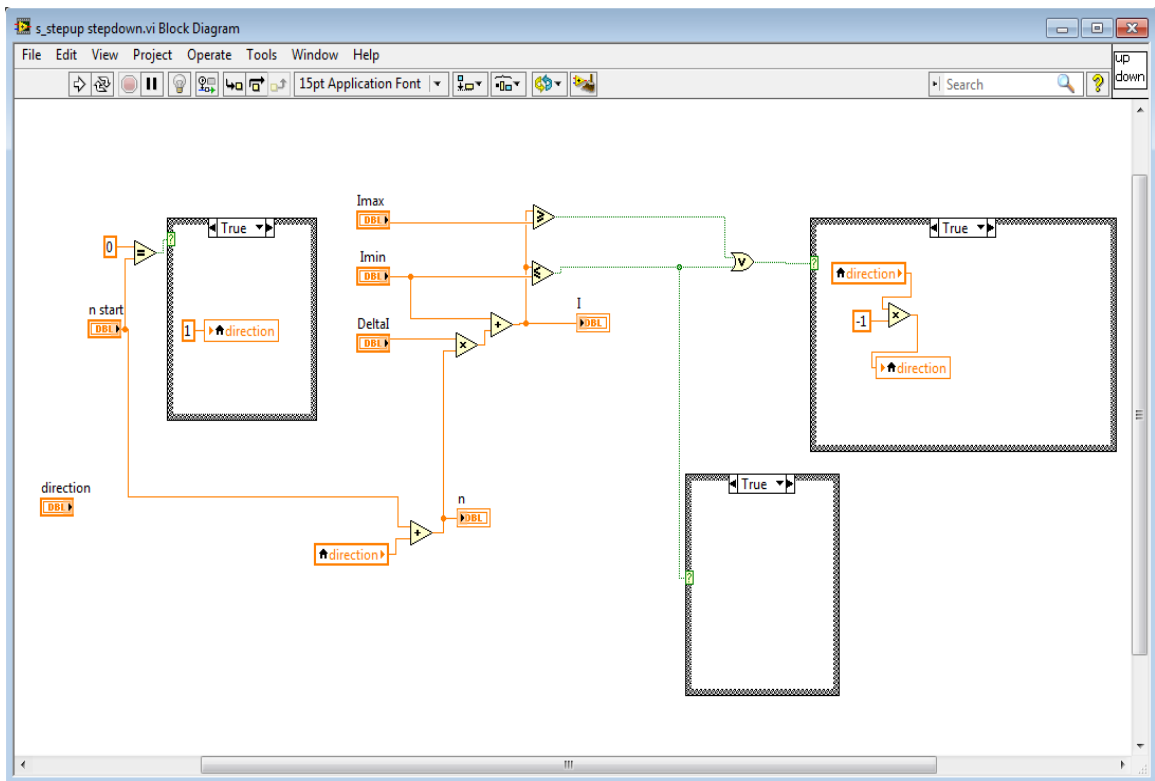
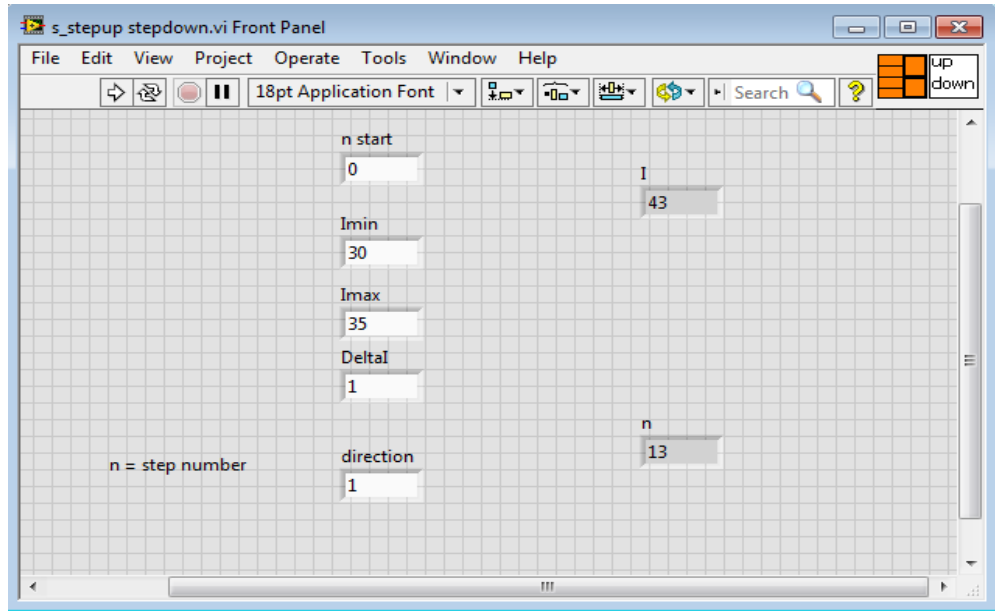


Figure A.14 The front panel and the block diagram for the “ up/down” virtual instrument used in Figure A.11.

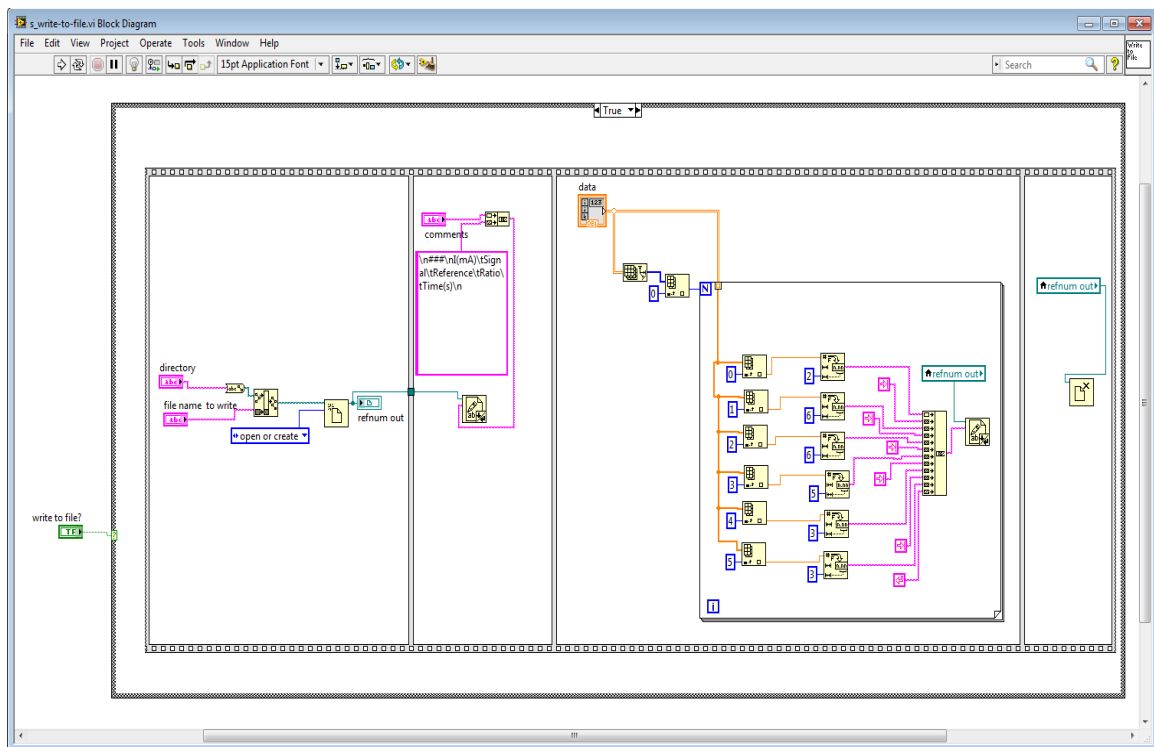
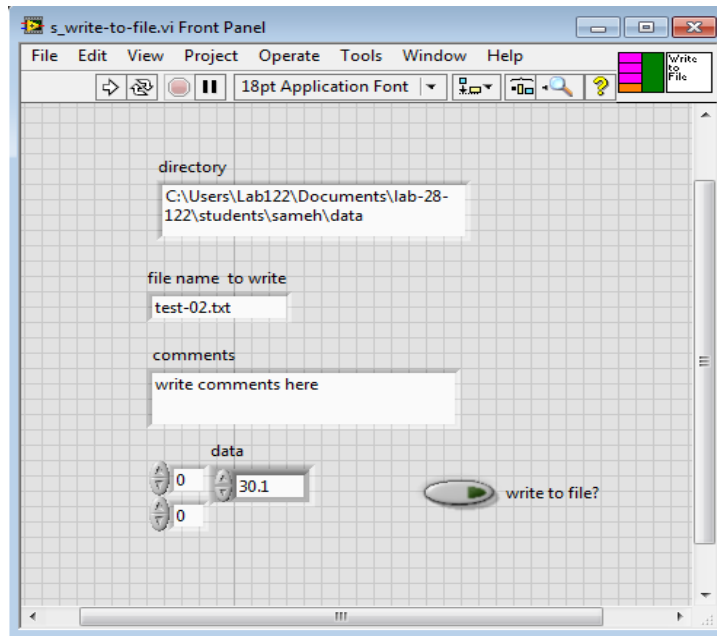


Figure A.1 The front panel and the block diagram for the “Write to File” virtual instrument used in Figure A.11.

Appendix B

Mathematica codes for data analysis

Mathematica computer codes used for analyzing and evaluating the experimental measurements are listed below.

List B.1: A listing of the code for performing simulation calculations


```

(* The brackets along with stars indicates an effectless statement on the
Mathematica evaluation process*)

(* Read cross section. You need this file in the same
directory:"NO2 cross section-1997-yoshino-nm.csv" *)
(*SetDirectory[NotebookDirectory []] sets the current working directory
to NotebookDirectory*)
(*NotebookDirectory [] gives the directory of the current evaluation notebook*)
SetDirectory[NotebookDirectory[]];

(*The cross section  $\sigma$  is in units of  $10^{-18}$  cm2 *)
(*To read the data from the file "NO2 cross section-1997-yoshino-nm.csv"*)
str = OpenRead["NO2 cross section-1997-yoshino-nm.csv"];

(*To read the objects(elements) of record file from the stream file,
untill the end of the file is reached,
with record separators to specify the list of strings to be taken as
delimiters of records *)
lst0 = ReadList[str, {Record, Record}, RecordSeparators -> {"\n", ", "};

(*To close the stream*)
Close[str];

(*ToExpression is to set all the read objects to a specified form,
StringReplace is to replace a string by something else,
we replaced the string exponent E by 10^ everywhere in list lst0*)
lst1 = ToExpression[Table[StringReplace[lst0[[i]], {"E" -> "*10^"}],
{i, 1, Length[lst0]}]];

(* To put the objects(elements) of list in atable form *)
lst $\lambda$  = Table[{lst1[[i, 1]], 1018 lst1[[i, 2]]}, {i, 1, Length[lst0]}];

(*To plot points correspond to a list of values, to unjoin the plotted points,
to color the points, to specify the range of plotting,
to specify tick marks (appear/disappear) for the edges of the plot frame,
to label the axes, to specify the style used in displaying the label-like elements*)
(* cross section versus wavelength *)
plt $\lambda$  = ListPlot[lst $\lambda$ , Joined -> False, PlotStyle -> {Black},
PlotRange -> {{443, 451}, {0, 1}}, Frame -> True,
FrameTicks -> {Automatic, Automatic, None, None},
FrameLabel -> {Wavelength [nm], Cross section[X10-18 cm2]},
LabelStyle -> Directive[Black, Bold]];

```

```

(* TO read file from LC1 camera and return intensity of laser vs wavelength *)
readLvm[f_String] := (
  SetDirectory[NotebookDirectory[]];
  str = OpenRead[f];

  (* read the first line *)
  l1 = Read[str, Record, RecordSeparators -> {"\n", ",", "\t"}];
  l2 = Read[str, Record];

  (* read rest of the first line: current and temperature *)
  lst0 = ReadList[str, Record, RecordSeparators -> {"\n", ",", "\t"}];
  Close[str];
  lst0 = Prepend[lst0, l1];
  lst1 = ToExpression[Table[StringReplace[lst0[[i]], {"E" -> "*10^"}],
    {i, 1, Length[lst0]}]];
  lstWI = Table[{432.474 + 0.0117060 i, lst1[[i]]}, {i, 1, Length[lst0]}];
  (* intensity vesus wavelength *)
  Return[lstWI];
) (*Return is to control the flow of the continuous stream according
to the provided instructions*)
drawRange[λ1_, λ2_, y_, t_] := (
  pltRg = Graphics[Line[{{λ1, y}, {λ2, y}}]];
  (*Graphics represents a two-dimensional graphical image*)
  pltTxt = Graphics[Text["T= " <> ToString[t] <> " °C", {λ1 - .55, y}]];
  (*ToStrings[t] puts the input/output in a string form*)
  Show[pltλ, pltRg, pltTxt]
)

(* To plot spectra, we need to run (Read Cross section for pltλ);
ToString is to give a string to the input/output form of the ith element *)
makeFileName[i_] := "lc1_" <>
  If[i < 10, "00" <> ToString[i],
  If[i < 100, "0" <> ToString[i],
  ToString[i]]] <> ".lvm";
lstS[i_] := readLvm[makeFileName[i]];

(* finding the start and the end of the laser spectra *)
getSpectrum[sNum_] := (
  (*this function get rid of tails *)
  ListPlot[lstS[sNum], PlotRange -> {All, {0, .002}}];
  threshold = 0.003;
  lS[sNum] = Select[lstS[sNum], #[[2]] > threshold &];
  (* lS is a list of the spectra with intensity above threshold *)
  r = .2; (* range before and after threshold in nm *)
  st = First[lS[sNum]][[1]] - r; en = Last[lS[sNum]][[1]] + r;
  lS[sNum] = Select[lstS[sNum], #[[1]] > st && #[[1]] < en &];
  Return[lS[sNum]];)

```

```

(* select the closest wavelength of the cross section vs wavelength data
to the wavelength of the laser intensity vs wavelength data *)
(* then find expected transmittance *)
findTrans[sNum_] := (
  getSpectrum[sNum];
  pNum = Length[LS[sNum]]; (* number of points in laser spectrum *)
  lσ[sNum] = {}; (* list of cross section with wavelength as that of laser *)
  i = 1;
  Table[While[Abs[lstλσ[[i, 1]] - LS[sNum][[j, 1]]] > .001, i = i + 1];
  lσ[sNum] = Append[lσ[sNum], lstλσ[[i]], {j, 1, pNum}];
  (* lσ is list of the selected cross section data that corresponds to
the laser intensity data *)
  IRef = Sum[LS[sNum][[i, 2]], {i, 1, pNum}];
  p = 1.01 × 105;
  kb = 1.38 × 10-23;
  T = 300;
  (*p=atmospheric pressure, kb=Boltzman const., T= room Temperature*)
  n1 = 10-22  $\frac{P}{kb T}$  200 × 10-6 .4; (* cross section in units of 10-18 cm2 *)

  (*Lambert-Beer Law*)
  ISig = Sum[LS[sNum][[i, 2]] * Exp[-lσ[sNum][[i, 2]] * n1], {i, 1, pNum}];
  t[sNum] = ISig / IRef; (*Transmittance*)

  Return[t[sNum]];
)

ticksOld[min_, max_] := (
  tblt = Table[i, {i, If[FractionalPart[min] <= .5, Ceiling[min] - .5, Ceiling[min]],
    If[FractionalPart[max] >= .5, Floor[max] + .5, Floor[max]], .5}];
  (*FractionalPart gives the fractional part of a number*)
  (*Ceiling [min] gives the smallest integer greater than or equal to the minmum*)
  (*Floor[max] gives the greatest integer less than or equal to the maximum*)
  Return[tblt];
)

ticks[min_, max_] := (
  tblt = Table[i, {i, Ceiling[min], Floor[max], 1}];
  Return[tblt];
)

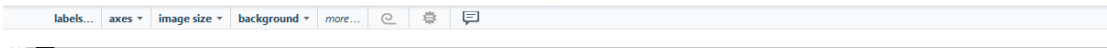
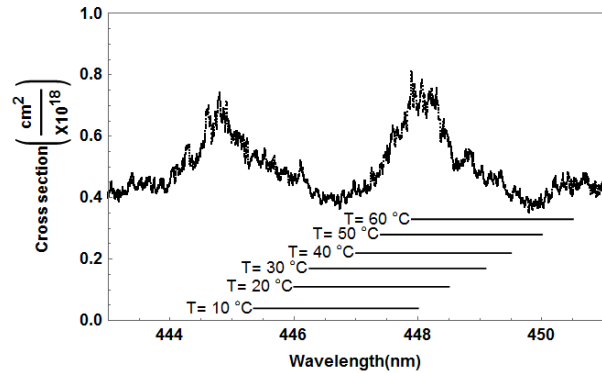
```

```

In[155]= p1 = drawRange[445.35, 448, .04, 10];
          (*0.04,0.11,0.17 ... are related to spacing*)
          p2 = drawRange[446, 448.5, .11, 20];
          p3 = drawRange[446.25, 449.09, .17, 30];
          p4 = drawRange[447, 449.5, .22, 40];
          p5 = drawRange[447.4, 450, .28, 50];
          p6 = drawRange[447.9, 450.5, .33, 60];
          Show[p1, p2, p3, p4, p5, p6]

```

Out[160]=



(* the file Number we start with and that we end up with for the plots of the laser intensity vs its wavelength*)

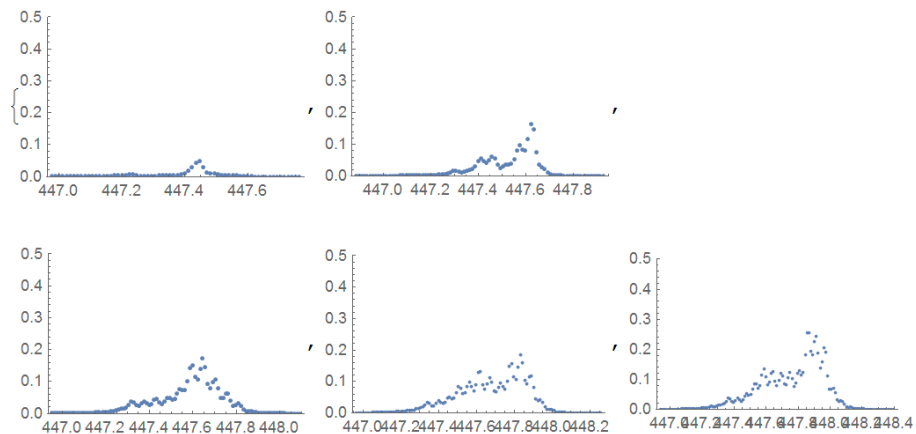
```

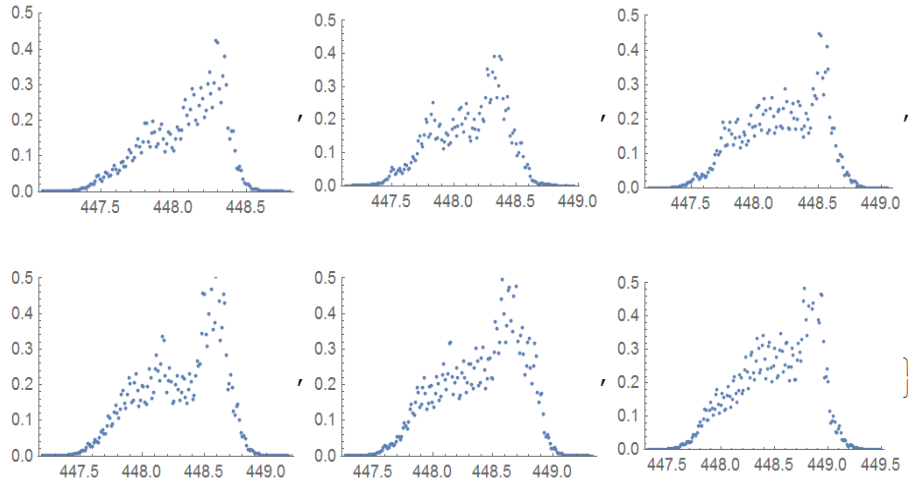
In[127]= fNumSt = 162;
          fNumEn = 175;

          pltS[i_] := ListPlot[getSpectrum[i], Joined -> False, PlotRange -> {All, {0, .5}}];
          tb = Table[Show[pltS[i]], {i, fNumSt, fNumEn}]

```

Out[130]=



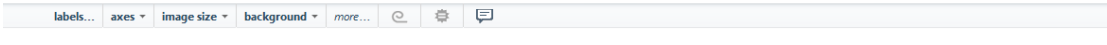
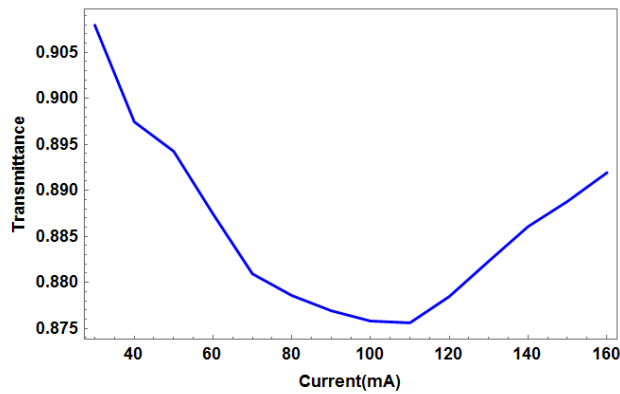


```

lstI = Table[30 + 10 (i - 1), {i, 1, fNumEn - fNumSt + 1}]; (* list currents *)
lstIT1 = Table[{lstI[[i - fNumSt + 1]], findTrans[i]}, {i, fNumSt, fNumEn}];
(* list laser current and transmittance *)
p1 = ListPlot[lstIT1, Joined → False, PlotRange → All, Frame → True,
  FrameTicks → {Automatic, Automatic, None, None},
  FrameLabel → {Current [mA], Transmittance}, LabelStyle → Directive[Black, Bold],
  PlotStyle → {Blue}]

```

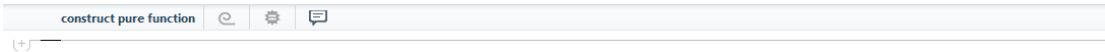
Out[133]=



List B.2: A listing of the code for processing measurement data of the real experiment

Read5 - five Columns

```
(*To read five columns: current, Signal intensity (Is), reference intensity(Ir),  
transmittance (Is/Ir),  
pressure of the detection cell*)  
  
In[14]= read5[f_String] := (  
  SetDirectory[NotebookDirectory[]];  
  str = OpenRead[f];  
  txt = "";  
  While[txt ≠ "####", txt = Read[str, Record]];  
  Read[str, Record];  
  lst0 = ToExpression[ReadList[str, {Record, Record, Record, Record, Record, Record},  
    RecordSeparators → {"\n", ",", "\t"}]];  
  Close[str];  
  Return[lst0];  
)  
  
In[26]= (* Get one scan *)  
  lstS[s_] := (  
    lst1 = Table[{lst[[i, 1]], lst[[i, 4]]}, {i, 1300 (s - 1) + 1, 1300 * s - 1}];  
    (*1 represents the 1st column of the file which is current column and 4  
    represents the 4th column which represents the transmittance*)  
    If[EvenQ[s], lst1 = Reverse[lst1]];  
    (*EvenQ gives True if s is even otherwise gives False,  
    Reverse is to reverse the order of the elements of lst1*)  
    Return[lst1])
```

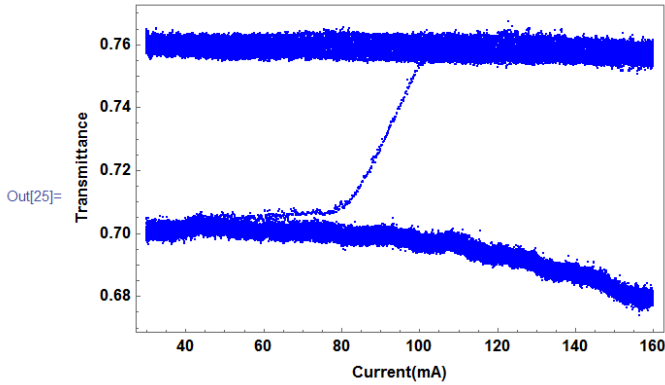


```

In[23]= lst = read5["F:\\data3MayToptica\\tdls-02.txt"]; (* get all data *)
Length[lst]
1299.
there are 1299 steps for 0.1 mA per step from 30 to 160 mA *)
ListPlot[lst[[All, {1, 4}]], PlotRange -> All, Frame -> True,
FrameTicks -> {Automatic, Automatic, None, None}, FrameLabel -> {Current [mA], Transmittance},
LabelStyle -> Directive[Black, Bold], PlotStyle -> {Blue}]

```

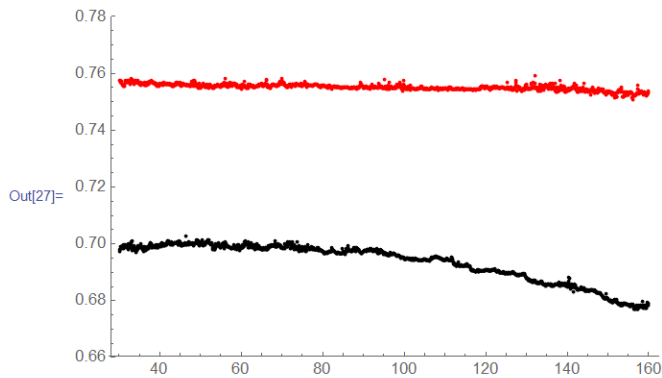
Out[24]= 65.2818



```

In[27]= ListPlot[{lstS[25], lstS[55]}, PlotRange -> {0.66, .78}, PlotStyle -> {Red, Black}]

```

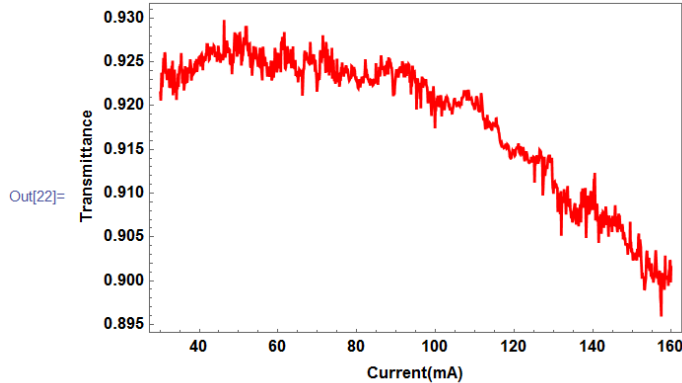


theme... frame... labels... axes... more... [refresh] [settings] [help]

```

In[19]= lstN2 = lstS[25];(* For the 25th (the last) N2 gas flow scanning round *)
lstNO2 = lstS[55];(* For the 50th (the last) NO2/N2 gas flow scanning round*)
(* To have a pure NO2 gas transmittance*)
lstTrans = Table[{{lstN2[[i, 1]],  $\frac{\text{lstNO2}[[i, 2]]}{\text{lstN2}[[i, 2]]}$ }, {i, 1, Length[lstN2]}];
plt7 = ListPlot[lstTrans, PlotRange → All, Joined → True, Frame → True,
  FrameTicks → {Automatic, Automatic, None, None},
  FrameLabel → {Current [mA], Transmittance}, LabelStyle → Directive[Black, Bold],
  PlotStyle → Red]

```

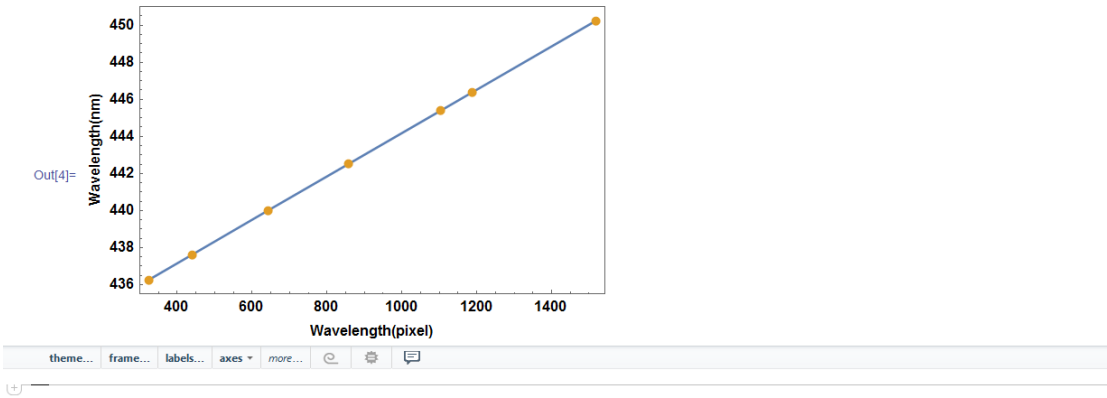


List B.3: A listing of the code for plotting the wavelength of spectral lines of the krypton lamp versus their pixel locations on the CCD camera

```

In[1]= kr = {436.26, 437.61, 440, 442.52, 445.39, 446.37, 450.24};
lst = {{kr[[1]], 324}, {kr[[2]], 439}, {kr[[3]], 642}, {kr[[4]], 858}, {kr[[5]], 1103.5},
  {kr[[6]], 1187}, {kr[[7]], 1518}};
data = Table[{lst[[i, 2]], lst[[i, 1]]}, {i, 1, Length[lst]}]
ListPlot[{data, data}, Joined → {True, False}, Frame → True,
  FrameTicks → {Automatic, Automatic, None, None},
  FrameLabel → {Wavelength [pixel], Wavelength [nm]}, LabelStyle → Directive[Black, Bold]]
Out[3]= {{324, 436.26}, {439, 437.61}, {642, 440},
  {858, 442.52}, {1103.5, 445.39}, {1187, 446.37}, {1518, 450.24}}

```

```
In[5]= line = Fit[data, {1, x}, x]
```

```
Out[5]= 432.474 + 0.011706 x
```

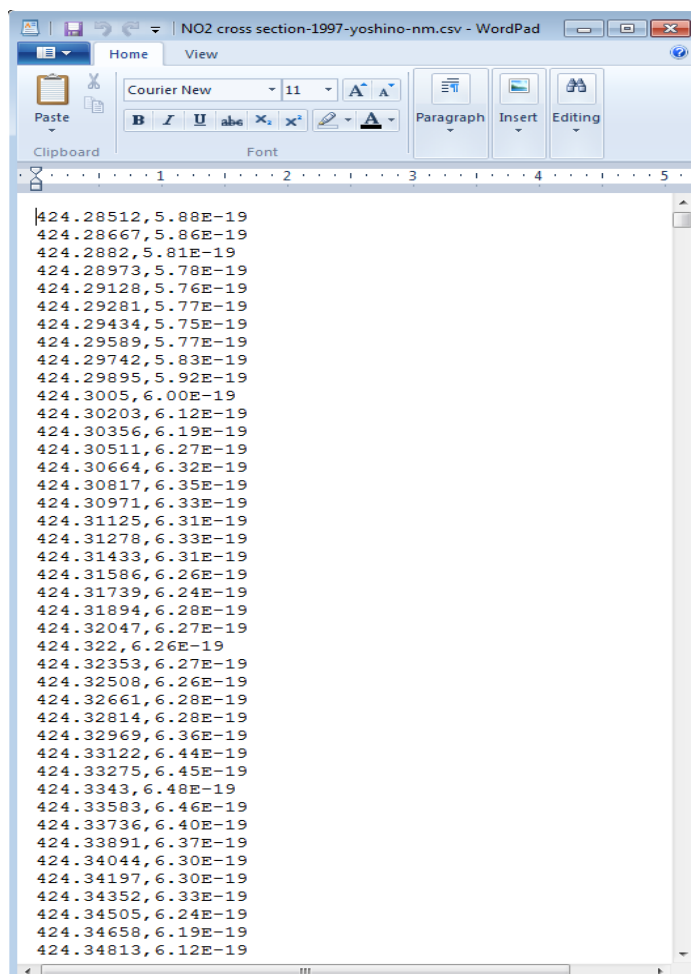
(+)

Appendix C

Formats of measurement data files

Three types of data files are used in this work. All data files are text files and their formats can be inferred from the listing below.

List C.1: A portion of the data file for the NO₂ absorption cross section as a function of wavelength. The first column represents the wavelength in nm and the second column represents the absorption cross section in $cm^2/molecule$.



The image shows a screenshot of a WordPad window titled "NO2 cross section-1997-yoshino-nm.csv - WordPad". The window displays a list of data points in a two-column format. The first column represents wavelength in nm, and the second column represents the absorption cross section in $cm^2/molecule$. The data points are as follows:

424.28512	5.88E-19
424.28667	5.86E-19
424.2882	5.81E-19
424.28973	5.78E-19
424.29128	5.76E-19
424.29281	5.77E-19
424.29434	5.75E-19
424.29589	5.77E-19
424.29742	5.83E-19
424.29895	5.92E-19
424.3005	6.00E-19
424.30203	6.12E-19
424.30356	6.19E-19
424.30511	6.27E-19
424.30664	6.32E-19
424.30817	6.35E-19
424.30971	6.33E-19
424.31125	6.31E-19
424.31278	6.33E-19
424.31433	6.31E-19
424.31586	6.26E-19
424.31739	6.24E-19
424.31894	6.28E-19
424.32047	6.27E-19
424.322	6.26E-19
424.32353	6.27E-19
424.32508	6.26E-19
424.32661	6.28E-19
424.32814	6.28E-19
424.32969	6.36E-19
424.33122	6.44E-19
424.33275	6.45E-19
424.3343	6.48E-19
424.33583	6.46E-19
424.33736	6.40E-19
424.33891	6.37E-19
424.34044	6.30E-19
424.34197	6.30E-19
424.34352	6.33E-19
424.34505	6.24E-19
424.34658	6.19E-19
424.34813	6.12E-19

List C.2: A portion of the data file for measuring the signal-to-reference intensity ratio versus the laser injection current.

T= 20 C |
Flow=600 ml/min
deltaI=0.1 mA

10 min N2 flow,
Then
scanning transition from: N2 -> NO2

P(N2)=1001.9- 1002.6 mbar;
P(NO2)= 1019.5-1002.6 mbar;

```
###  
I(mA)   Signal Int.   Reference Int.   Ratio   Time(s)   Pressure  
30.10   0.046566          0.061143         0.76159 0.205     7.529  
30.20   0.047019          0.061683         0.76226 0.279     7.534  
30.30   0.047399          0.062283         0.76103 0.360     7.529  
30.40   0.047885          0.062894         0.76135 0.432     7.529  
30.50   0.048332          0.063551         0.76053 0.517     7.529  
30.60   0.048847          0.064237         0.76042 0.594     7.534  
30.70   0.049350          0.064894         0.76047 0.673     7.529  
30.80   0.049789          0.065548         0.75958 0.761     7.529  
30.90   0.050407          0.066273         0.76061 0.836     7.529  
31.00   0.050887          0.066928         0.76033 0.913     7.529  
31.10   0.051432          0.067617         0.76064 0.991     7.529  
31.20   0.051928          0.068323         0.76003 1.069     7.529  
31.30   0.052456          0.069000         0.76022 1.148     7.529  
31.40   0.053020          0.069627         0.76149 1.225     7.529
```

List C.3: A portion of the data for measuring the laser spectrum at fixed diode temperature and certain injection current. Each number in the column represents the intensity in each camera pixel.

```
0.000216    I=30.000000,T=10.000000
0.000232
0.000225
0.000220
0.000230
0.000279
0.000289
0.000235
0.000196
0.000197
0.000232
0.000234
0.000220
```

References

- [1] J. Orehek, J. P. Massari, P. Gayraud, C. Grimaud, and J. Charpin, "Effect of short-term, low-level nitrogen dioxide exposure on bronchial sensitivity of asthmatic patients.," *J. Clin. Invest.*, vol. 57, no. 2, pp. 301–7, 1976.
- [2] N. C. Murail, "This electronic theses or dissertation has been downloaded from the King ' s Research Portal at This electronic theses or dissertation has been downloaded from the King ' s Research Portal at Author : Estelle Murail."
- [3] D. R. Tobergte and S. Curtis, "No Title No Title," *J. Chem. Inf. Model.*, vol. 53, no. 9, pp. 1689–1699, 2013.
- [4] I. Courtillot, J. Morville, V. Motto-Ros, and D. Romanini, "Sub-ppb NO₂ detection by optical feedback cavity-enhanced absorption spectroscopy with a blue diode laser," *Appl. Phys. B Lasers Opt.*, vol. 85, no. 2–3, pp. 407–412, 2006.
- [5] B. Brunekreef and S. T. Holgate, "Air pollution and health," *Lancet*, vol. 360, no. 9341, pp. 1233–1242, 2002.
- [6] H. Mori, T. Nayuki, N. Cao, T. Fukuchi, T. Fujii, K. Nemoto, and N. Takeuchi, "Development of a Laser Radar Using LDS Dye and Sum Frequency Generation for NO₂ Measurement," vol. 144, no. 2, pp. 1727–1733, 2003.
- [7] T. Laurila, J. Saarela, T. Sorvaj, and J. Toivonen, "Phase-sensitive method for background-compensated photoacoustic detection of NO₂ using high-power LEDs," vol. 19, no. 2, pp. 561–566, 2011.
- [8] K. Hdlc, Z. Beleck, J. Wojtas, P. Perlin, J. Goss, A. Czyzewski, F. Magryta, and T. Stacewicz, "Blue laser diodes for trace matter detection," *Opt. Appl.*, vol. 40, no. 3, pp. 641–651, 2010.
- [9] S. Voigt, J. Orphal, and J. P. Burrows, "The temperature and pressure dependence of the absorption cross-sections of NO₂ in the 250-800 nm region measured by Fourier-transform spectroscopy," *J. Photochem. Photobiol. A Chem.*, vol. 149, no. 1–3, pp. 1–7, 2002.
- [10] S.Beirle, U.Platt, M.Wenig, and T.Wagner, "Weekly cycle of NO₂ by GOME measurements: a signature of anthropogenic sources," *Atmos. Chem. Phys.*, vol. 3, no. 2, pp. 2225–2232, 2003.
- [11] J. L. Peel, R. Haeuber, V. Garcia, A. G. Russell, and L. Neas, "Impact of nitrogen and climate change interactions on ambient air pollution and human health," *Biogeochemistry*, vol. 114, no. 1–3, pp. 121–134, 2013.

- [12] P. C. Moonen, J. N. Cape, and R. Mccolm, "Measurement of the $\text{NO} + \text{O}_3$ Reaction Rate at Atmospheric Pressure Using Realistic Mixing Ratios," no. 2, pp. 299–314, 1998.
- [13] K. W. Scholtens, B. M. Messer, C. D. Cappa, and M. J. Elrod, "Kinetics of the $\text{CH}_3\text{O}_2 + \text{NO}$ Reaction: Temperature Dependence of the Overall Rate Constant and an Improved Upper Limit for the CH_3ONO_2 Branching Channel," no. 2, pp. 4378–4384, 1999.
- [14] O. B. Gadzhiev, S. K. Ignatov, S. Gangopadhyay, E. Masunov, and A. I. Petrov, "Mechanism of Nitric Oxide Oxidation Reaction ($2\text{NO} + \text{O}_2 \rightarrow 2\text{NO}_2$) Revisited," *J. Chem. Theory Comput.*, vol. 7, pp. 2021–2024, 2011.
- [15] E. S. P. B. V, "Formation and control of nitrogen oxides," *Catal. Today*, vol. 2, pp. 369–379, 1988.
- [16] A. G. Russell, G. J. Mcrae, and G. R. Cassx, "THE DYNAMICS OF NITRIC ACID PRODUCTION AND."
- [17] F. Lin, Z. Wang, Q. Ma, Y. He, R. Whiddon, Y. Zhu, and J. Liu, " N_2O_5 Formation Mechanism during the Ozone-Based Low-Temperature Oxidation deNO_x Process," *Energy and Fuels*, vol. 30, no. 6, pp. 5101–5107, 2016.
- [18] G. G. Gimmestad, D. Tan, and D. W. Roberts, "Development of a differential absorption lidar for NO_2 monitoring," no. 2, pp. 1–4.
- [19] V. Spagnolo, "Quartz-enhanced photoacoustic spectroscopy: a review," *Sensors (Basel)*, vol. 14, no. 4, pp. 6165–6206, 2014.
- [20] H. Fuchs, W. P. Dub??, B. M. Lerner, N. L. Wagner, E. J. Williams, and S. S. Brown, "A sensitive and versatile detector for atmospheric NO_2 and NO_x based on blue diode laser cavity ring-down spectroscopy," *Environ. Sci. Technol.*, vol. 43, no. 20, pp. 7831–7836, 2009.
- [21] J. Wojtas, J. Mikołajczyk, M. Nowakowski, B. Rutecka, R. Medrzycki, and Z. Bielecki, "Applying CEAS method to UV, VIS, and IR spectroscopy sensors," *Bull. Polish Acad. Sci. Tech. Sci.*, vol. 59, no. 4, pp. 415–418, 2011.
- [22] A. M. Winer and H. W. Biermann, "Long Pathlength Differential Optical-Absorption Spectroscopy (Doas) Measurements of Gaseous Hono, NO_2 and Hcho in the California South Coast Air Basin," *Res. Chem. Intermed.*, vol. 20, no. 3–5, pp. 423–445, 1994.

- [23] G. Hönninger, C. von Friedeburg, and U. Platt, “Multi Axis Differential Optical Absorption Spectroscopy (MAX-DOAS),” *Atmos. Chem. Phys. Discuss.*, vol. 3, no. 6, pp. 5595–5658, 2003.
- [24] Y. Matsumi, F. Taketani, K. Takahashi, T. Nakayama, M. Kawai, and Y. Miyao, “Fluorescence detection of atmospheric nitrogen dioxide using a blue light-emitting diode as an excitation source,” *Appl. Opt.*, vol. 49, no. 19, pp. 3762–3767, 2010.
- [25] J. Parra and L. a George, “Development of an ambient pressure laser-induced fluorescence instrument for nitrogen dioxide,” *Appl. Opt.*, vol. 48, no. 18, pp. 3355–3361, 2009.
- [26] J. Peltola, T. Hieta, and M. Vainio, “Parts-per-trillion-level detection of nitrogen dioxide by cantilever-enhanced photo-acoustic spectroscopy,” *Opt. Lett.*, vol. 40, no. 13, p. 2933, 2015.
- [27] J. Kalkman and H. W. Van Kesteren, “Relaxation effects and high sensitivity photoacoustic detection of NO₂ with a blue laser diode,” *Appl. Phys. B Lasers Opt.*, vol. 90, no. 2, pp. 197–200, 2008.
- [28] Y. Yang, Z. Gao, D. Zhong, and W. Lin, “Detection of nitrogen dioxide using an external modulation diode laser,” *Appl. Opt.*, vol. 52, no. 13, pp. 3027–3030, 2013.
- [29] P. Werle, “Laser excess noise and interferometric effects in frequency-modulated diode-laser spectrometers,” *Appl. Phys. B Lasers Opt.*, vol. 60, no. 6, pp. 499–506, 1995.
- [30] J. Wojtas, J. Mikolajczyk, and Z. Bielecki, “Aspects of the application of cavity enhanced spectroscopy to nitrogen oxides detection,” *Sensors (Basel)*, vol. 13, no. 6, pp. 7570–7598, 2013.
- [31] J. a. Thornton, P. J. Wooldridge, and R. C. Cohen, “Atmospheric NO₂: in situ laser-induced fluorescence detection at parts per trillion mixing ratios,” *Anal. Chem.*, vol. 72, no. 2, pp. 528–39, 2000.
- [32] M. Bruns, “NO₂ Profile Retrieval using Airborne Multiaxis Differential Optical Absorption Spectrometer (AMAXDOAS) data,” *Structure*, no. 2, 2004.
- [33] J. P. Malhado, M. Tavares, and M. N. Berberan-santos, “Study of a Reversible Gas Phase Reaction : An Integrated Physical Chemistry Project,” *Chem. Educ.*, vol. 2, no. 2, pp. 32–38, 2004.
- [34] “lines_form @ physics.nist.gov. |

Vitae

Name :{SAMEH M. A. ALTANANY |

Nationality :{Palestinian |

Date of Birth :{11/17/1989|

Email :{sameh_tanani@hotmail.com|

Address :{Beit Hanoun-Gaza-Palestine|

Academic Background :{ Education: B.Sc degree in Physics, Al-Azhar University-Gaza, Palestine, 2011. M.Sc degree in Physics, The Islamic University of Gaza (IUG), Palestine, 2016. Title of thesis: Modeling of Newly Multilayer Waveguide Structure Containing Diamond-Like Carbon, Porous Silicon and Left-Handed Materials. Academic experience: Physics Lab Instructor, Department of Physics, Al-Azhar University-Gaza, Palestine, 2012- 2013. Physics Lab Instructor, Department of Physics, King Fahd University of Petroleum and Minerals, Saudi Arabia, 2014- 2016. Selected publications: 1. Ubeid, M. F., Shabat, M. M., & Altanany, S. M. (2017). Low reflection and high transmission by a layered structure containing diamond-like carbon, porous silicon, and left-handed material. *Superlattices and Microstructure*, 103, 85–92.3. 2. Abdulaziz Aljalal, Sameh Altanany, Khaled Gasmi, Watheq Al-Basheer, Morad Hamad, “Detection of trace amount of NO₂ gas using tunable blue laser diode”, *Proc. SPIE 10231, Optical Sensors 2017,102311E* (May 16, 2017); doi:10.1117/12.2264513.}